

**DOT/FAA/TC-22/2**

Federal Aviation Administration  
William J. Hughes Technical Center  
Aviation Research Division  
Atlantic City International Airport  
New Jersey 08405

# **Rotorcraft Strike Avoidance System Using Airborne Avian Radar**

June 2022

Final report



U.S. Department of Transportation  
**Federal Aviation Administration**

## NOTICE

This document is disseminated under the sponsorship of the U.S. Department of Transportation in the interest of information exchange. The U.S. Government assumes no liability for the contents or use thereof. The U.S. Government does not endorse products or manufacturers. Trade or manufacturers' names appear herein solely because they are considered essential to the objective of this report. The findings and conclusions in this report are those of the author(s) and do not necessarily represent the views of the funding agency. This document does not constitute FAA policy. Consult the FAA sponsoring organization listed on the Technical Documentation page as to its use.

This report is available at the Federal Aviation Administration William J. Hughes Technical Center's Full-Text Technical Reports page: [actlibrary.tc.faa.gov](http://actlibrary.tc.faa.gov) in Adobe Acrobat portable document format (PDF).

**Form DOT F 1700.7** (8-72)

Reproduction of completed page authorized

1. Report No. DOT/FAA/TC-22/2		2. Government Accession No.		3. Recipient's Catalog No.	
4. Title and Subtitle Rotorcraft Strike Avoidance System Using Airborne Avian Radar				5. Report Date June 2022	
				6. Performing Organization Code ANG-E271	
7. Author(s) Greg Piesinger <sup>1</sup> and Dave Vandebout <sup>2</sup>				8. Performing Organization Report No.	
9. Performing Organization Name and Address  <sup>1</sup> Origo Corporation 6225 E. Saguaro Vista CT. Cave Creek, AZ 85331  <sup>2</sup> XESS Corp. (consultant to Origo) 2608 Sweetgum Drive Apex, NC 27539				10. Work Unit No. (TRAIS)	
				11. Contract or Grant No. DTFACT-17-C-00007	
12. Sponsoring Agency Name and Address Federal Aviation Administration William J. Hughes Technical Center Aviation Research Division Atlantic City International Airport New Jersey 08405				13. Type of Report and Period Covered Final Report October 2017 - May 2019	
				14. Sponsoring Agency Code AIR-600	
15. Supplementary Notes The Federal Aviation Administration William J. Hughes Technical Center Aviation Research Division CORs: Paul Swindell and Traci Stadtmueller (alternate).					
16. Abstract  A research and development (R&D) proof-of-concept airborne avian radar to detect birds and other targets ahead of a rotorcraft was designed, constructed, and ground tested. The radar was designed to provide collision warning out to 1500 meters day or night in haze, fog, or rain. Its principal of operation was to use a single forward-looking antenna to measure target intensity and Doppler velocity as the rotorcraft approached the target. A constant target intensity and Doppler velocity during the approach indicated that the target was on a collision course with the rotorcraft and flight deviation was recommended. A coherent segmented binary pseudo noise PN-coded radar was designed to simultaneously display and track multiple targets at different ranges or Doppler velocities. Using available components, the radar was designed as a software defined radar composed of a RF receive/transmit unit, an analog to digital sampling board, a field programmable gate array (FPGA) processing board, and a personal computer (PC) running Matlab for processing and display. The radar was extensively ground tested on road traffic and drone flights, which verified its ability to detect and simultaneously measure the range and Doppler velocity of multiple targets.					
17. Key Words Airborne avian radar, Bird strike avoidance, Rotorcraft, Software defined radar, Pulse compression radar				18. Distribution Statement  This document is available to the U.S. public through the National Technical Information Service (NTIS), Springfield, Virginia 22161. This document is also available from the Federal Aviation Administration William J. Hughes Technical Center at <a href="http://actlibrary.tc.faa.gov">actlibrary.tc.faa.gov</a> .	
19. Security Classif. (of this report) Unclassified		20. Security Classif. (of this page) Unclassified		21. No. of Pages 117	19. Security Classif. (of this report) Unclassified

## Contents

<b>1</b>	<b>Introduction.....</b>	<b>1</b>
<b>2</b>	<b>Rotorcraft avian radar solution.....</b>	<b>1</b>
<b>3</b>	<b>Radar implementation considerations .....</b>	<b>1</b>
<b>4</b>	<b>Radar fundamentals .....</b>	<b>2</b>
4.1	Radar target detection .....	2
4.2	Radar cross section (RCS) .....	3
4.3	Radar cross section of real targets .....	4
4.4	Radar range equation .....	5
4.5	Antenna gain .....	6
4.6	Radar frequency selection.....	7
4.7	Available federal frequency.....	8
<b>5</b>	<b>Single antenna solution.....</b>	<b>9</b>
5.1	Simplest solution.....	9
5.2	Simulated Simple Solution Performance .....	11
<b>6</b>	<b>Ground clutter.....</b>	<b>15</b>
6.1	Characteristics of ground clutter .....	16
6.2	Simulated simple solution performance on ground clutter .....	18
<b>7</b>	<b>Enhanced techniques .....</b>	<b>25</b>
7.1	Yagi antenna .....	25
7.2	Bird strike avoidance .....	26
<b>8</b>	<b>Radar signals .....</b>	<b>27</b>
8.1	Radar signal ambiguity function.....	27
8.2	Pulse compression.....	29
8.3	Segmented PN coded pulse compression .....	30
<b>9</b>	<b>Avian radar block diagrams .....</b>	<b>31</b>
9.1	Top level block diagram .....	32

9.2	RTA block diagram.....	33
9.3	Software processing block diagram .....	34
9.4	Range filter block diagram.....	35
9.5	Doppler filter block diagram.....	36
<b>10</b>	<b>Projected radar range performance.....</b>	<b>37</b>
<b>11</b>	<b>Radar insulation on S76 helicopter .....</b>	<b>39</b>
<b>12</b>	<b>Radar hardware .....</b>	<b>42</b>
12.1	Radar hardware block diagram .....	42
12.2	RTA hardware.....	43
12.3	ADC/FPGA enclosure .....	44
12.4	Overall radar hardware setup .....	45
12.5	Flat plate antenna .....	46
<b>13</b>	<b>Radar display &amp; control.....</b>	<b>47</b>
<b>14</b>	<b>Radar performance.....</b>	<b>50</b>
14.1	Ground traffic test.....	50
14.2	Drone & conductive balloon test .....	57
14.3	Drone tests .....	59
14.4	S76 Flight tests.....	61
<b>15</b>	<b>Conclusions.....</b>	<b>61</b>
<b>16</b>	<b>Lessons learned .....</b>	<b>63</b>
<b>17</b>	<b>Path to production .....</b>	<b>64</b>
<b>18</b>	<b>References.....</b>	<b>65</b>
<b>A</b>	<b>Appendices.....</b>	<b>A-1</b>
	A.2.3. FPGA radar processor parameters .....	A-26
	A.3. MATLAB radar processing .....	A-29
	A.3.1. Script Processing.....	A-29

## Figures

Figure 1. Radar detection.....	3
Figure 2. Radar cross section.....	4
Figure 3. Aircraft cross section.....	4
Figure 4. Radar range equation.....	5
Figure 5. Relative antenna gain.....	6
Figure 6. Beam width and gain tradeoff.....	6
Figure 7. RCS radar wavelength.....	7
Figure 8. Target regions versus target size.....	8
Figure 9. 2400 MHz to 2500 MHz ISM band frequency.....	9
Figure 10. Simplest solutions.....	10
Figure 11. Boresight and off boresight target.....	11
Figure 12. Side view of horn 3D antenna pattern.....	12
Figure 13. Simple solution performance at a 10m target offset.....	13
Figure 14. Simple solution performance at a 200M target offset.....	14
Figure 15. Simple solution performance at a 400 m target offset.....	15
Figure 16. Ground clutter area versus pulse width.....	16
Figure 17. Ground clutter RCS versus grazing angle.....	17
Figure 18. Ground clutter RCS versus grazing angle and terrain.....	18
Figure 19. Ground clutter amplitude and Doppler at 100 knots & 500 feet.....	19
Figure 20. Pilot reaction time at 100 knots in Figure 19.....	20
Figure 21. Ground clutter amplitude and Doppler at 100 knots & 1000 feet.....	21
Figure 22. Ground clutter amplitude and Doppler at 100 knots & 2000 feet.....	22
Figure 23. Ground clutter RCS in 3D at 100 knots & 500 feet.....	23
Figure 24. Ground clutter RCS in 2D at 100 knots & 500 feet.....	24
Figure 25. Yagi antenna.....	25
Figure 26. Evasion techniques.....	26
Figure 27. Common radar waveforms ambiguity functions.....	28
Figure 28. Coherent PN-coded radar I & Q components.....	29
Figure 29. Sin x/x rolloff.....	30
Figure 30. Segmented coherent PN-coded radar I & Q components.....	31
Figure 31. Avian radar block diagram.....	32
Figure 32. Range/Doppler bins (indicate time axis).....	33
Figure 33. RTA hardware block diagram.....	34

Figure 34. Processing block diagram.....	35
Figure 35. Range filter .....	36
Figure 36. Doppler filter .....	37
Figure 37. Calculated avian radar range .....	38
Figure 38. Primus P650 side view .....	40
Figure 39. Primus P650 mount view.....	41
Figure 40. Avian radar block diagram .....	42
Figure 41. RTA stackup.....	43
Figure 42. RTA .....	44
Figure 43. ADC/FPGA enclosure .....	45
Figure 44. Avian radar setup.....	46
Figure 45. Alfa flat plate antenna .....	47
Figure 46. Range/Doppler display .....	48
Figure 47. Display control panel.....	49
Figure 48. STC visualization panel.....	50
Figure 49. Traffic sequence 1 .....	51
Figure 50. Traffic sequence 2 .....	52
Figure 51. Traffic sequence 3 .....	53
Figure 52. Traffic sequence 4 .....	54
Figure 53. Traffic sequence 5 .....	55
Figure 54. Traffic sequence 6 .....	56
Figure 55. Drone & balloon sequence 1 .....	57
Figure 56. Drone & balloon sequence 2 .....	58
Figure 57. Drone & balloon sequence 3 .....	59
Figure 58. Drone target.....	60

## Acronyms

Acronym	Definition
2D	Two Dimension
3D	Three Dimension
AC	Alternating Current
A/D	Analog to Digital
ADC	Analog to Digital
ANT	Antenna
CW	Continuous Wave
dB	Decibel
DC	Direct Current
EFIS	Electronic Flight Instrument System
FAA	Federal Aviation Administration
FPGA	Field Programmable Gate Array
GHz	Gigahertz
HPA	High Power Amplifier
I	In-Phase
ISM	Industrial, Scientific, and Medical
KTS	Knots
MDS	Minimum Detectable Signal
MFD	Multifunction Display
MHz	Megahertz
MPH	Miles per hour
PC	Personal computer
PN	Pseudo noise
PRF	Pulse repetition frequency
PWB	Printed wiring board
Q	Quadrature phase
R&D	Research and development
RAM	Random access memory
RCS	Radar cross section
RF	Radio frequency
RT	Receiver transmitter



<b>Acronym</b>	<b>Definition</b>
RTA	Receiver transmitter antenna
RX	Receiver
S76	Sikorsky S-76 helicopter
S-BAND	Designation for 2 to 4 gigahertz band
SDR	Software defined radar
STC	Sensitivity time control
TX	Transmitter
TYPE-N	RF connector type
VAC	Alternating current voltage
VDC	Direct current voltage
VHDL	VHSIC hardware description language
VHSIC	Very high speed integrated circuit
VNE	Never exceed speed

## **Executive summary**

Bird strikes to aircraft are a huge problem. Annually, bird strikes cause \$1.2 billion in damages and other costs. The bird strike problem is also increasing due to the increasing population of large birds, quieter engines, and an increase in the number of flights. Going forward, strikes from small drones will further increase these statistics.

Bird strike avoidance is the only practical approach for preventing aircraft damage and serious accidents. Large commercial jet engines and transport category airframes have to tolerate eight (8) pound bird impacts. For business jet engines, the tolerance is four pounds. However, during the past 30 years, there has been a four-fold increase in the populations of nearly all bird species having average weights greater than eight pounds. Many species have average body weights of 15 to 20 pounds or more.

Bird strikes to rotorcraft pose a major threat. Not only does a bird strike have the potential to cause significant and costly damage to the aircraft itself, but the potential for human injury or death is a risk as well. At present time, manufacturers of rotary-wing aircraft must assume that birds will strike the vehicle while in flight at speeds up to and including VNE (never exceed speed).

The purpose of this project was to investigate potential solutions that will mitigate bird strikes with rotorcraft. Avian radar is one of the main technologies that can provide the required performance and can operate in day, night, haze, fog, or rain. The purpose of avian radar is to detect birds, drones, and other non-cooperative airborne hazards ahead of the rotorcraft and provide timely warnings to the pilot.

This project studied various radar approaches that would lead to a practical avian radar solution that could be applied to a rotorcraft. The solution was designed to provide collision warning out to 1500 meters and provide an approximately 5 to 15 second warning time of an imminent bird strike. This warning time is similar to the five second warning provided by current wind shear avoidance systems and is enough time for a pilot to take evasive action to prevent a collision.

A prototype avian radar was constructed and extensively tested on ground targets and airborne drone targets to verify its ability to detect and measure the range, velocity, and collision threat of multiple simultaneous targets.

# 1 Introduction

There are currently no airborne aircraft avian radars due to the impracticability of installing traditional scanning radar antennas, such as those used for weather radar. Implementing avian radar on rotorcraft is even more difficult due to their small frontal cross section, which excludes the possibility of implementing target triangulation techniques by using widely spaced antennas.

This is in contrast to large winged aircraft, such as airliners, in which multiple widely spaced antennas can be mounted near the wingtips and on the tail. Target triangulation techniques can then be used to indicate the target range and position (left, right, above, or below) with respect to the aircraft.

To obtain a practical radar solution, a single small non-scanning antenna is used to monitor the airspace in front of the aircraft and provide an approximately 5 to 15 second warning time of an imminent bird strike.

## 2 Rotorcraft avian radar solution

The primary solution philosophy for bird strike mitigation on rotorcraft using avian radar is summarized below. This philosophy is because rotorcraft generally fly slower than 100 knots and are quite agile.

- Only required to monitor immediate airspace in front of rotorcraft.
- Require 5 to 15 second warning time (0.26 to 0.77 kilometer range at 100 knots).
- Avoidance by minor altitude or course correction (approximately one hundred feet is sufficient to prevent strike).

Detection of any short-range target directly ahead of the aircraft is potentially a threat.

Although longer warning times are preferred, even reliable short-range avian radar detection performance is useful. Especially for helicopters that generally fly fairly low and slow. The avian radar described in this report is designed to detect bird size targets out to a maximum range of 1500 meters.

## 3 Radar implementation considerations

Any radar implementation involves a tradeoff between multiple factors such as available placement, antenna size, frequency, power, etc. This rotorcraft application was designed to be

tested on the FAA's S76 test helicopter. The most important considerations for this application are listed below.

- All aircraft radar implementations are a compromise between airframe-antenna placement restrictions and performance capabilities.
- The transmitter frequency, power, bandwidth, and modulation allocations available for this application.
- Experimental antenna size, mounting location, and form factor on the S75 for performance test flights.
- Threat evasion maneuvers based on range and threat performance compromises.
- Use only off-the-shelf components.

This research and development (R&D) project was scheduled and budgeted to design and implement a proof-of-concept avian radar for testing on the S76 helicopter. Therefore, only readily available off-the-shelf components could be used in its implementation. That is, the time and budget was not available to design and build custom parts such as transmitter power amplifiers, antennas, or radiofrequency (RF) components

## 4 Radar fundamentals

This section explores some of the fundamental principles and techniques of radar that must be considered in making the tradeoff choices listed in bullet points of section 3. They are presented here as general radar background information.

### 4.1 Radar target detection

Radar detection is illustrated in Figure 1. A radar antenna transmits a RF signal towards a distant object and receives the reflected RF signal from the object. Based on the time delay between the transmission and reception, the object is both detected and its range determined.

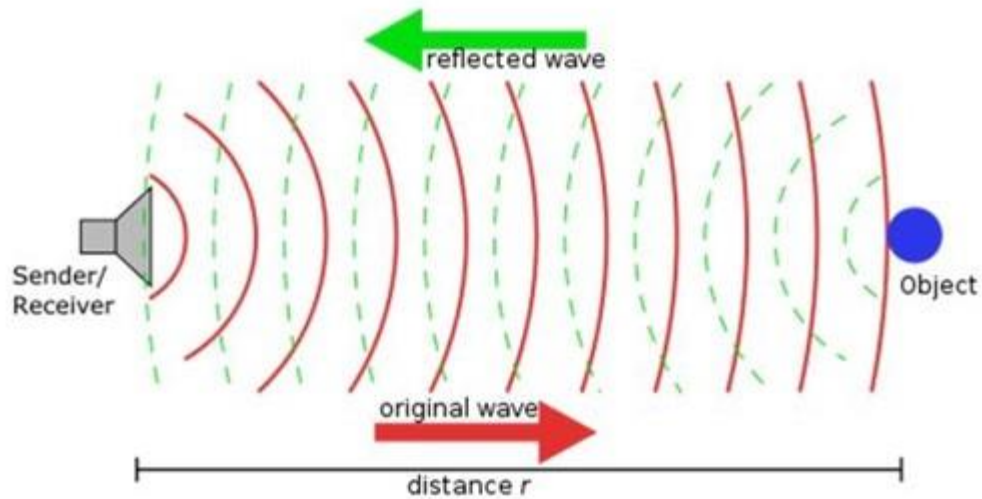


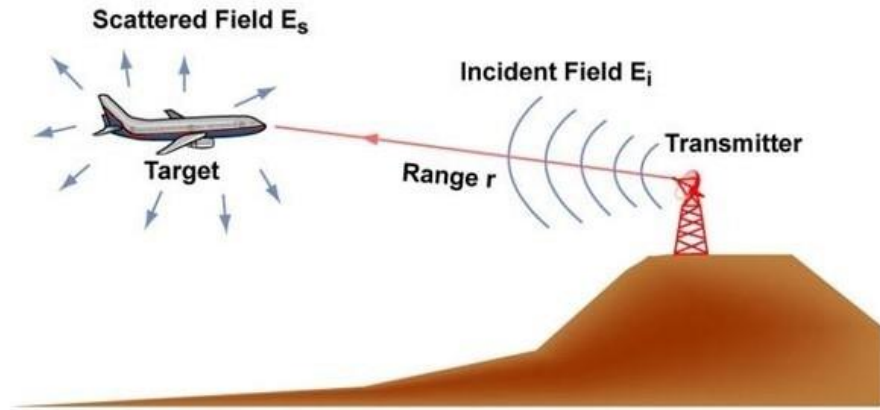
Figure 1. Radar detection

## 4.2 Radar cross section (RCS)

The power reflected by the distant target is a function of the RCS of the object, along with its distance and many other radar properties. RCS is illustrated in Figure 2. The target RCS is a convenient measure of the reflected power of various targets detected using a particular radar.

RCS is typically indicated as the target cross section illuminated by the radar signal measured in meters squared, irrespective of the objects actual physical cross section. For example, the RCS of a 1.13-meter diameter sphere is one square meter, independent of frequency. The RCS of a 1-meter rectangular flat plate normal to the radar signal is 835 square meters at 2450 megahertz (MHz).

This difference occurs because most of the radar signal from the sphere is reflected in directions away from the radar. In contrast, the flat plate acts like a mirror in that the entire radar signal is reflected back towards the radar.



**Radar Cross Section (RCS)** is the hypothetical area, that would intercept the incident power at the target, which if scattered isotropically, would produce the same echo power at the radar, as the actual target.

Figure 2. Radar cross section

### 4.3 Radar cross section of real targets

For complex targets, like an aircraft in Figure 3, the RCS is statistical depending on its physical cross section orientation with respect to the radar illumination signal. In weather radar, the instantaneous pulse-to-pulse reflected radar signal from trillions of raindrops could vary over a 40-decibel (dB) power range.

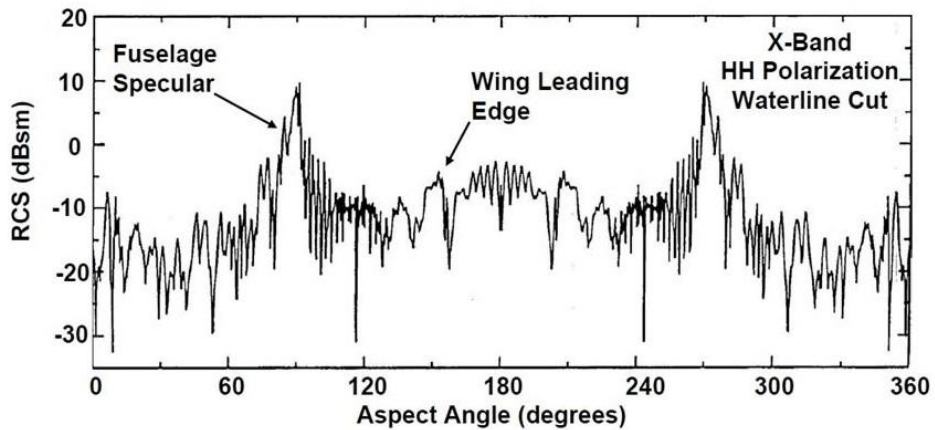


Figure 3. Aircraft cross section

Therefore, to determine meaningful target detection, the power of multiple reflected radar pulses must be processed. This processing is important to minimize the target detection false alarm rate

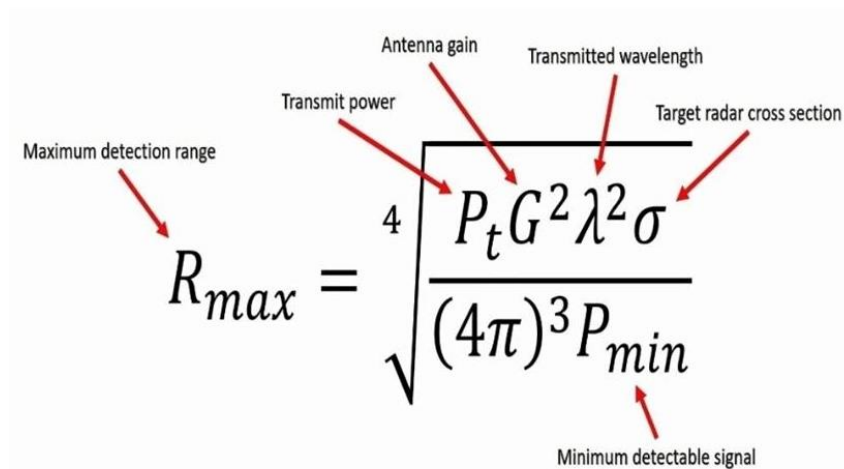
The average RCS is about 0.01 m<sup>2</sup> for a pigeon, 0.1 m<sup>2</sup> for a large bird, and 1 m<sup>2</sup> for a light aircraft.

#### 4.4 Radar range equation

The radar range equation predicts the maximum range at which a target can be detected based on radar properties, target range, and target cross section. Target properties include the radar transmit power, antenna gain, frequency, and minimum detectable signal (MDS).

The radar range equation is illustrated in Figure 4. For a given radar frequency, the parameter that has the most effect on maximum range is antenna gain. Assuming the same antenna is used for both the transmitter and receiver (the normal case), increasing the antenna gain by 10 dB results in a 20 dB increase in reflected signal power.

In contrast, to obtain this same increase in reflected signal power would require a 10-watt transmitter's power level to be increased to 1000 watts.



The diagram shows the radar range equation with red arrows pointing from text labels to the corresponding variables in the equation. The labels are: 'Maximum detection range' pointing to  $R_{max}$ ; 'Transmit power' pointing to  $P_t$ ; 'Antenna gain' pointing to  $G^2$ ; 'Transmitted wavelength' pointing to  $\lambda^2$ ; 'Target radar cross section' pointing to  $\sigma$ ; and 'Minimum detectable signal' pointing to  $P_{min}$ .

$$R_{max} = \sqrt[4]{\frac{P_t G^2 \lambda^2 \sigma}{(4\pi)^3 P_{min}}}$$

Figure 4. Radar range equation

## 4.5 Antenna gain

Antenna gain of a particular antenna is defined as its peak directional gain with respect to an isotropic antenna (whose gain is uniform in all directions and equal to 1.0). The tradeoff for higher gain in a particular direction is lower gain in other directions as illustrated in Figure 5.

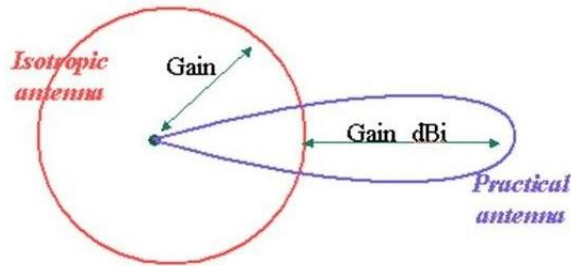


Figure 5. Relative antenna gain

The tradeoff between beam width and gain is illustrated in Figure 6. For this avian radar, the antenna only needs to point in the direction of travel as helicopters only run into birds. It would be very unusual for a bird to fly into the side or back of a helicopter.

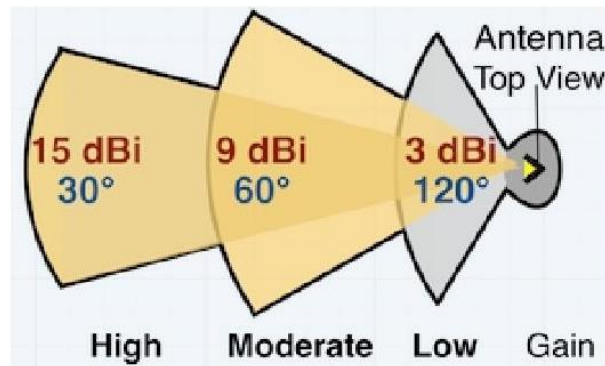


Figure 6. Beam width and gain tradeoff

There is an operational tradeoff between gain and beam width for this avian radar application. A high antenna gain is desired to maximize range and minimize transmitter power. However, a too narrow beam width might miss close targets converging on the aircraft. An antenna gain of around 15 dB appears optimum, as it will provide an approximately 30-degree detection cone ahead of the helicopter along with a 30 dB two-way antenna gain.



## 4.6 Radar frequency selection

Radar frequency selection is primarily dictated by governmental frequency allocations of which there are a few potential radar bands available at widely different frequencies. Some radar frequencies are much better for this application than others are. The tradeoffs are between antenna size, signal propagation attenuation, transmitter cost, and radar cross section of intended targets.

Figure 9 illustrates the effect of frequency on target RCS as a function of target size. As the target circumference increases with respect to the radar wavelength, the RCS increases. Therefore, the RCS of birds is much greater than the RCS of insects and raindrops. This is desirable in that using larger wavelengths (lower frequencies) insects and raindrops will not be detected.

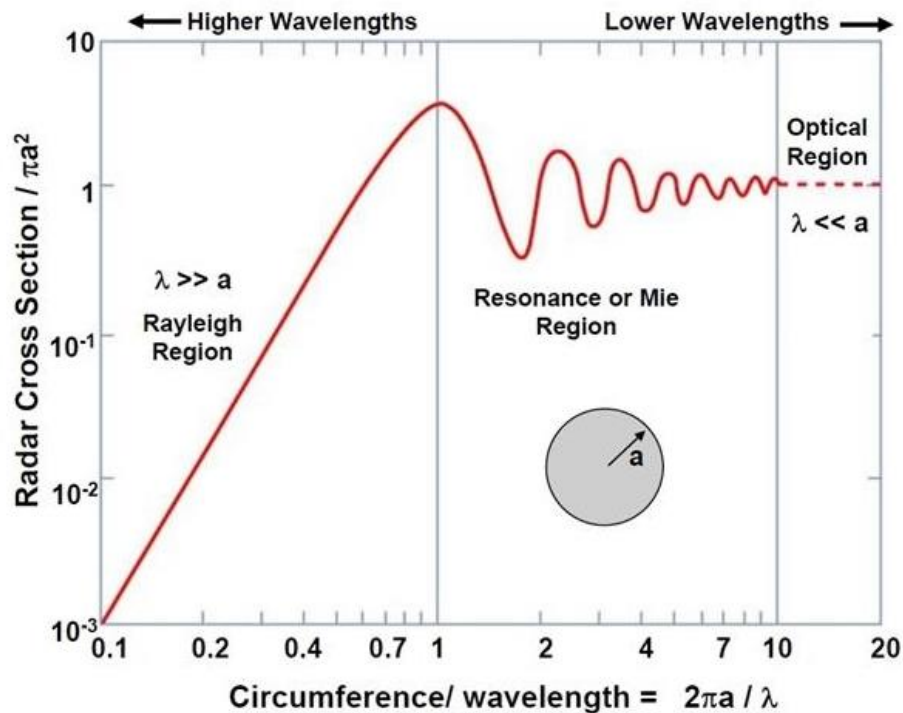


Figure 7. RCS radar wavelength

Figure 8 illustrates that birds fall in the upper Rayleigh region (higher RCS in Figure 7) at a frequency of 3 gigahertz (GHz) while raindrops and insects fall in the lower Rayleigh region (lower RCS in Figure 7). Since the RCS is linear in the Rayleigh region, the larger the target, the higher the RCS, and therefore the greater the detection range. The RCS is not linear in the Mie region.

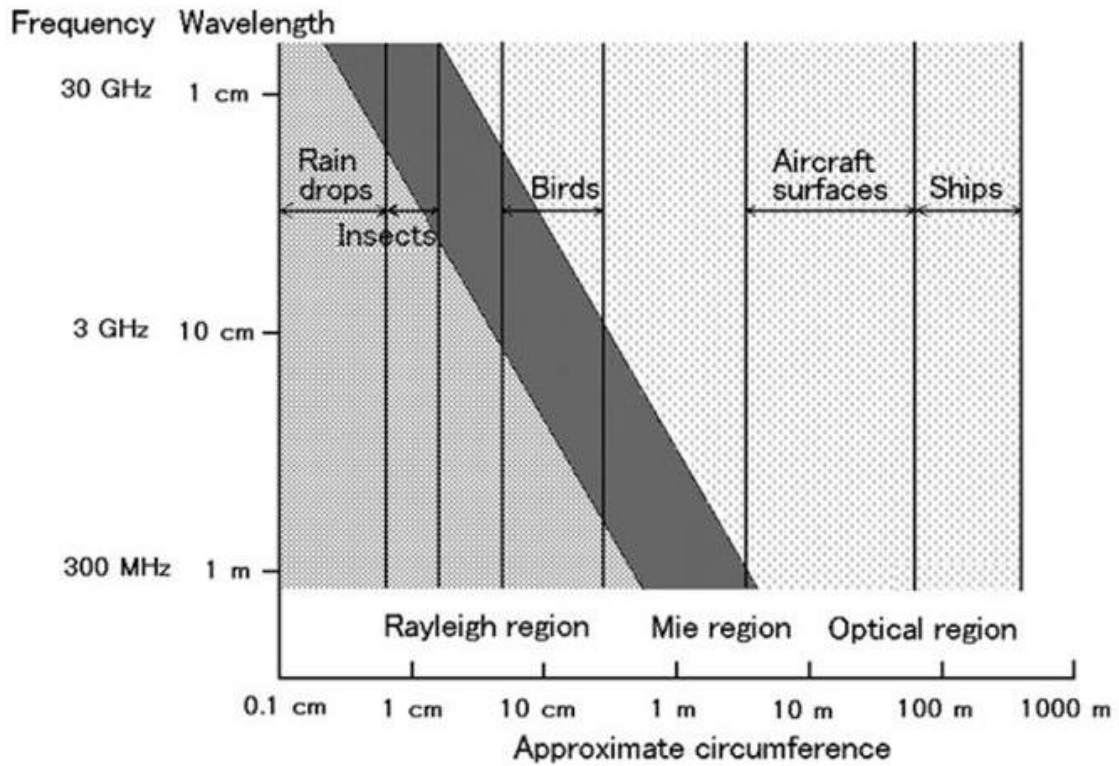


Figure 8. Target regions versus target size

#### 4.7 Available federal frequency

As all frequencies below 10 GHz are already allocated for numerous purposes, the first task of this avian radar project was to search for a frequency that was already allocated and available.

Fortunately, the 2400 MHz to 2500 MHz ISM band frequency was available and was in the desired Rayleigh region. Microwave ovens, WiFi, and Bluetooth equipment operate in this band.

Figure 9 states the rules regarding the 2400 MHz to 2500 MHz (industrial, scientific, and medical) ISM band for Federal uses. For this FAA radar project, the only restriction is that the radar emissions do not fall outside the 100 MHz band centered at 2450 MHz.

## MANUAL OF REGULATIONS AND PROCEDURES FOR FEDERAL RADIO FREQUENCY MANAGEMENT

- Without further authority from the Assistant Secretary, ISM equipment may be operated under the conditions specified in this part for particular categories of equipment or types of operations.
- Frequency: 2450 MHz    Bandwidth:  $\pm 50.0$  MHz
- Miscellaneous ISM equipment may be operated on the designated ISM frequencies without regard to the type or power of emissions being radiated, provided any harmonic or other spurious radiation outside the frequency limits specified in this section is suppressed.

Figure 9. 2400 MHz to 2500 MHz ISM band frequency

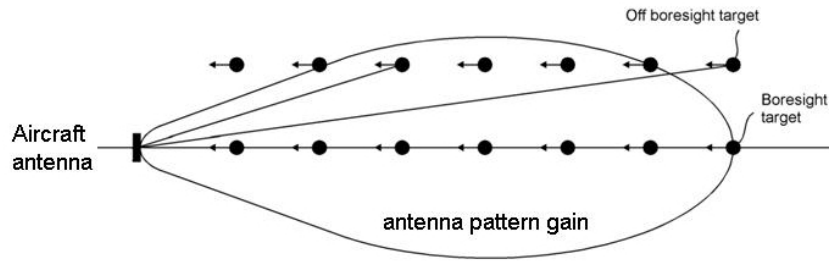
### 5    Single antenna solution

As explained previously, avian radar implementations are essentially restricted to a single forward-looking antenna due to their narrow frontal cross section. Therefore, an avian radar solution using a single antenna is required.

#### 5.1    Simplest solution

Using a coherent radar, the three most common target properties that can be measured are target amplitude, range, and Doppler velocity. Figure 10 illustrates how these three target properties can be used to mitigate bird strikes.

The gain of most airborne antenna patterns are as illustrated in Figure 10. If the target is approaching the aircraft along the antenna boresight, the antenna gain is constant for all target ranges. To keep the reflected radar target signal constant versus range, a radar can implement sensitivity time control (STC), which reduces the radar receiver gain as the target range decreases. Therefore, the amplitude of the reflected target signal is constant for any target approaching along antenna boresight.



- Single forward looking antenna. Monitor target range, amplitude, and Doppler as aircraft approaches target.
- On boresight, normalized (STC) target amplitude and Doppler are constant.
- Off boresight, both amplitude and Doppler decrease.
- Evasion is to simply alter heading sufficient to cause approaching target amplitude and Doppler to decrease. After 10 to 15 seconds, return to previous heading and course.

Figure 10. Simplest solutions

For targets approaching off boresight, the STC target amplitude decreases with range due to the reduced antenna pattern gain as seen in Figure 10.

Additionally, along boresight the target Doppler velocity is greatest and constant. Off boresight, Doppler velocity decreases with range and drops to zero when the target is perpendicular to the radar antenna.

Therefore, by monitoring target amplitude and Doppler velocity, the pilot can determine if the target is on a collision course with the aircraft or if it will pass off to the side of the aircraft's line of flight. Using a single antenna, the pilot cannot determine if the target is above, below, left, or right of the aircraft. However, by making a slight course change, the target's amplitude and Doppler velocity will also change which will indicate if the maneuver was away from or towards the target.

Alternatively, to prevent a collision with a boresight target, the pilot can simply alter heading for 10 or 15 seconds so the target will pass harmlessly off to the side.

The STC processed amplitude and Doppler velocity of an on-boresight and off-boresight target is illustrated in Figure 11. Note that both the amplitude and Doppler are constant for an on-boresight target and both decrease for an off-boresight target.

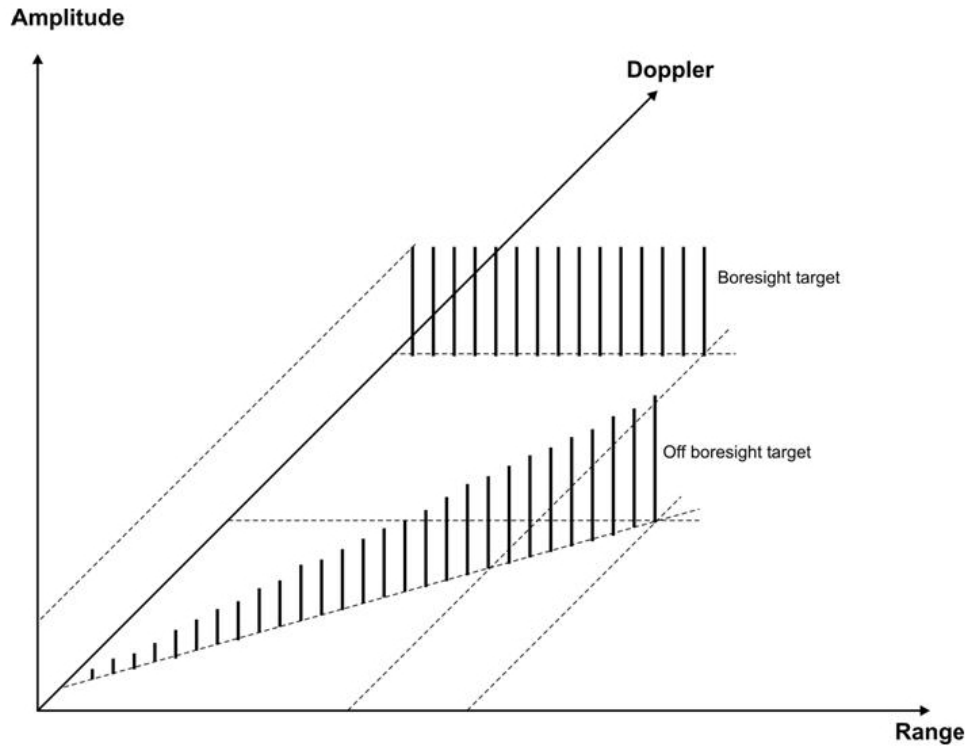


Figure 11. Boresight and off boresight target

## 5.2 Simulated Simple Solution Performance

The gain pattern of a typical horn antenna versus aircraft offset from boresight is illustrated in Figure 12.

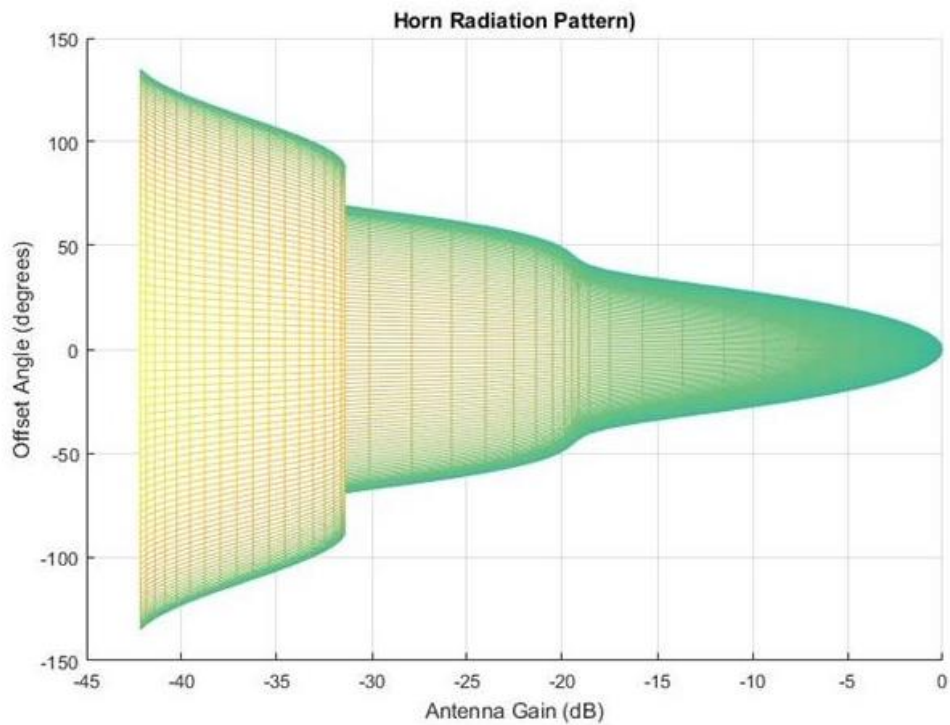


Figure 12. Side view of horn 3D antenna pattern

Figure 13 illustrates the calculated antenna pattern gain in dB (and thus STC target amplitude) and Doppler velocity in knots versus target range for an aircraft to target closing velocity of 100 knots. The target offset from boresight is 10 meters.

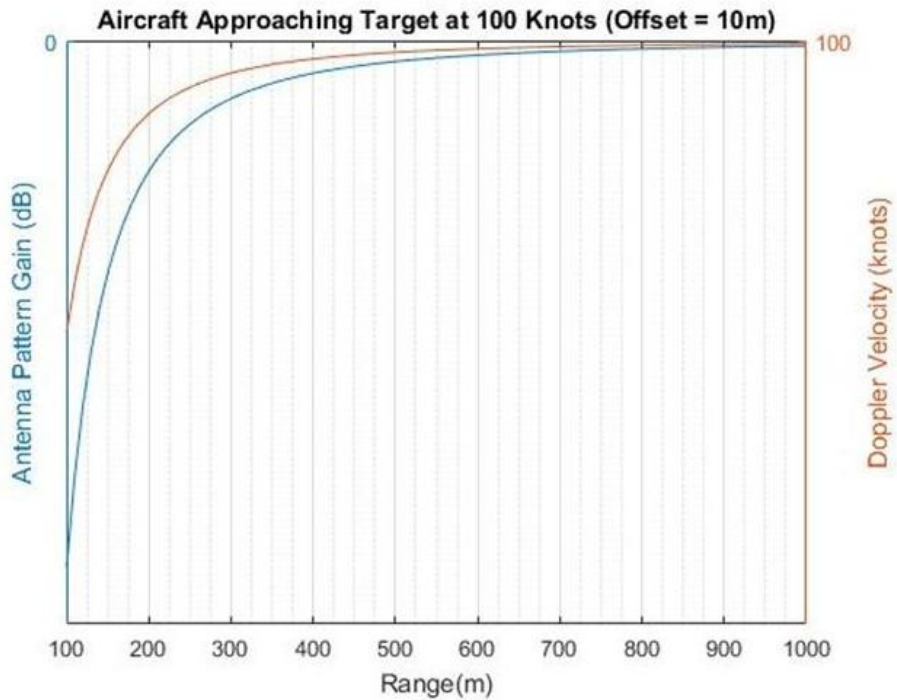


Figure 13. Simple solution performance at a 10m target offset

Note that for a target closing close to boresight, both the target amplitude and Doppler velocity are nearly constant. This will alert the pilot that a target has been detected ahead of the aircraft and that the aircraft is on a collision course with the target. Therefore, a course deviation is required.

The calculated target amplitude in dB and Doppler velocity in knots versus target range for a aircraft to target closing velocity of 100 knots at a target offset from boresight of 200 meters is illustrated in Figure 14.

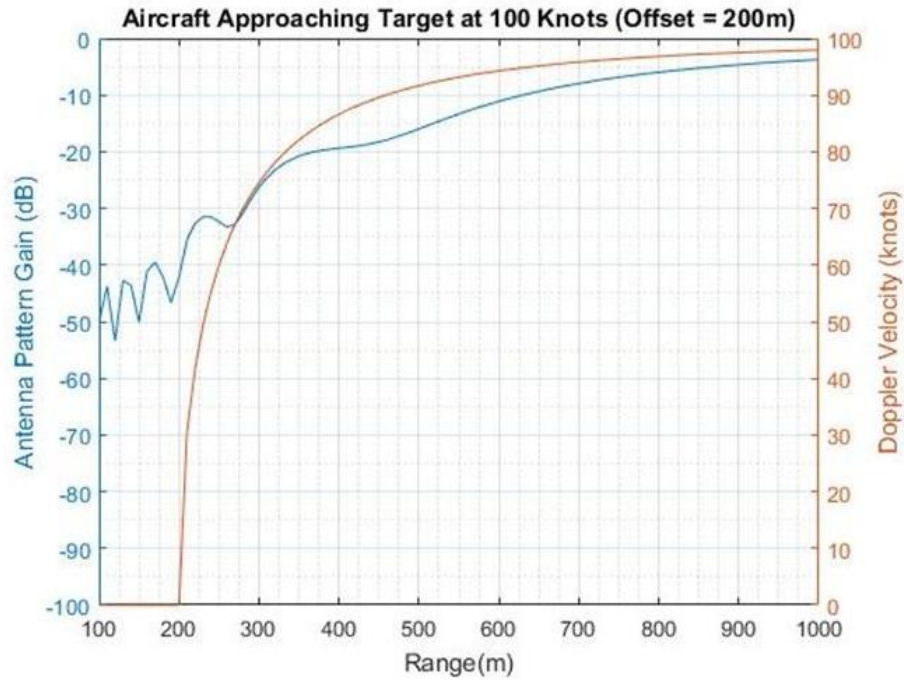


Figure 14. Simple solution performance at a 200M target offset

For a large target offset, the pilot should carefully monitor the radar as the aircraft approaches the target. The pilot might be well advised to make a slight course correction and monitor if the correction was either away from or towards the target.

The calculated target amplitude in dB and Doppler velocity in knots versus target range for an aircraft to target closing velocity of 100 knots at a target offset from boresight of 400 meters is illustrated in Figure 15.



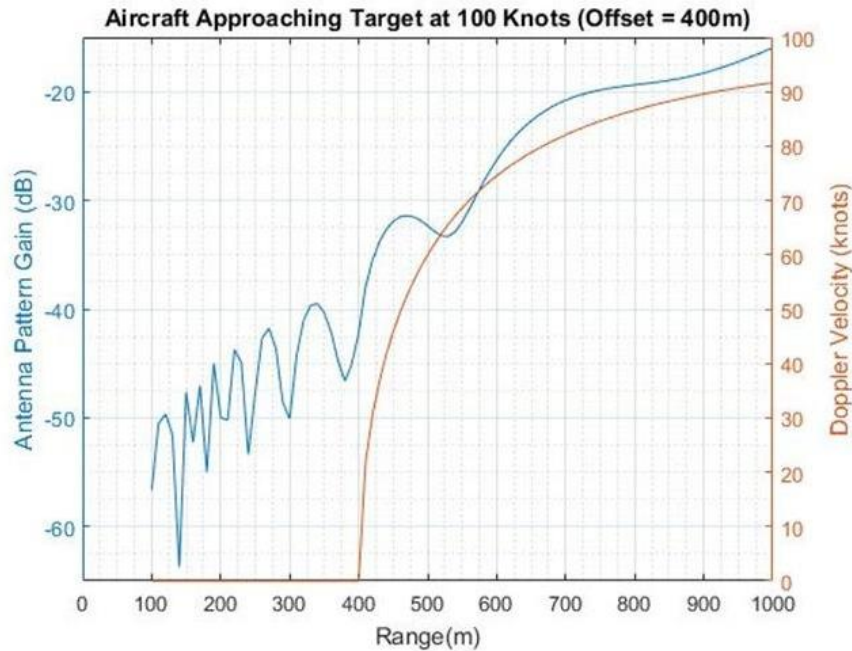


Figure 15. Simple solution performance at a 400 m target offset

For a large target offset, the radar processing could automatically determine that the target would harmlessly pass off to the side of the aircraft. For this situation, the radar could be programmed to select either to issue an advisory to the pilot or to ignore the target.

In general, any target detected ahead of the aircraft is cause for concern as the target might suddenly alter course and pass closer to the aircraft.

## 6 Ground clutter

When flying at high altitudes, any avian radar targets detected are airborne targets. However, at low altitudes the bottom of the antenna beam will strike the ground at long ranges. This is a normal issue for any airborne radar such as aircraft weather radars. The normal solution for weather radar is to tilt the antenna down until the antenna beam just touches the ground at the maximum displayed range. In this way, any targets closer on the display are weather targets.

Unfortunately, most rotorcraft fly at low altitudes so ground clutter is more of a problem. When flying over cities, many strong ground targets will always be either present or will appear shortly due to mirror-like flat objects, which have a very high RCS when pointing at the radar antenna as was explained earlier.

It is anticipated that most of the ground clutter can be eliminated using processing which ignores targets that do not have the consistency and track of normal airborne targets.

This section explores the expected level of ground clutter as a function of aircraft altitude.

## 6.1 Characteristics of ground clutter

The magnitude of ground clutter radar returns is a function of the antenna beamwidth, pulsewidth, and grazing angle as illustrated in Figure 16. That is, antenna beam footprint on the ground defines the area of the ground intersected, and thus the ground target size. The wider the beamwidth, the longer the pulsewidth, and the steeper the grazing angle, the greater the area of ground illuminated by the antenna beam. They are presented here as general clutter background information.

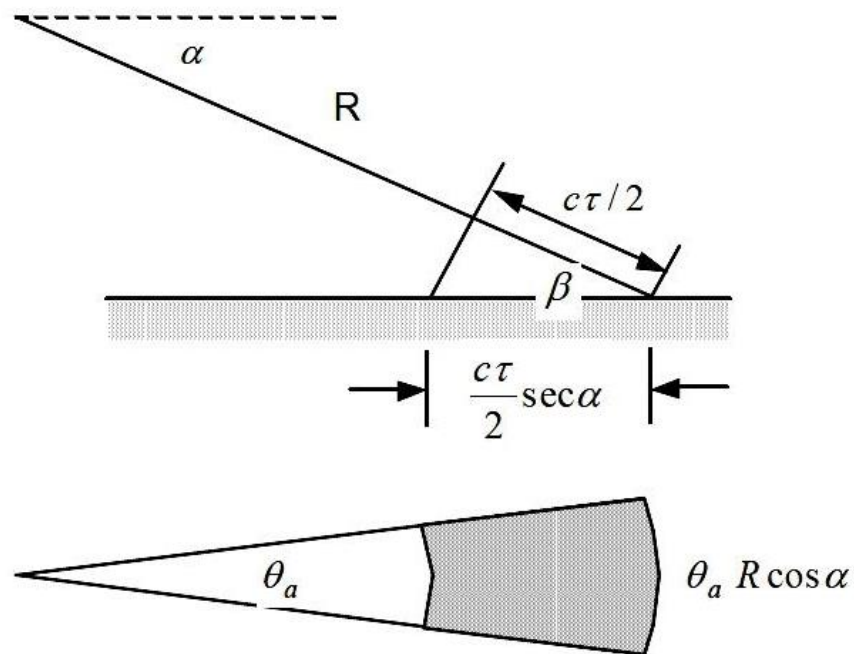


Figure 16. Ground clutter area versus pulse width

In general, the RCS of the illuminated ground clutter is a function of the antenna beam-grazing angle as illustrated in Figure 17. At low grazing angles, the RCS is low and is greatest when the beam is pointing directly at the ground.

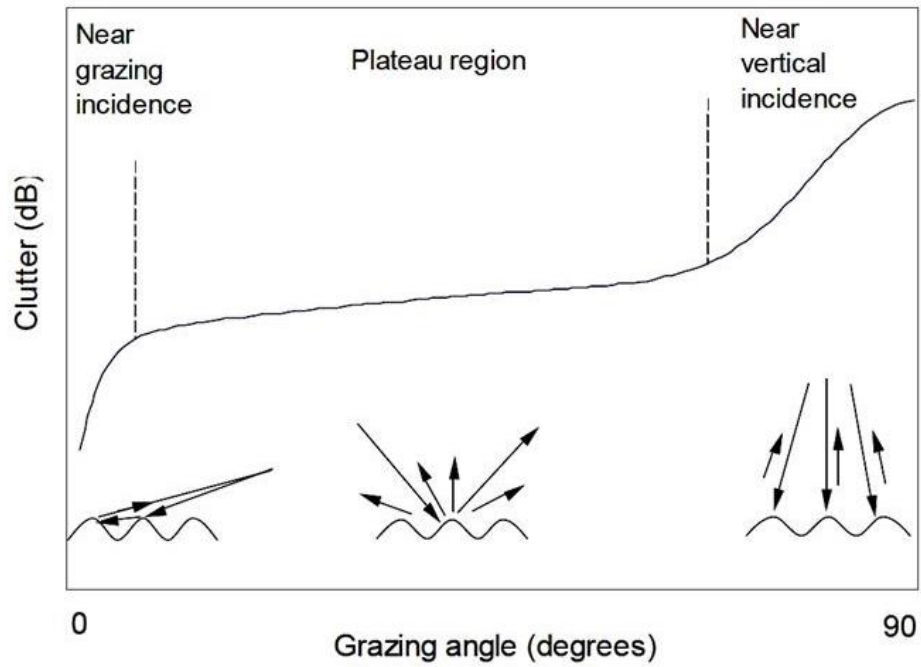


Figure 17. Ground clutter RCS versus grazing angle

In addition to grazing angle, the ground clutter RCS is also a function of the type of terrain being illuminated as illustrated in Figure 18. RCS is lowest when flying over flat desert and largest when objects on the ground have a large vertical dimension, such as mountains or cities with many tall buildings.

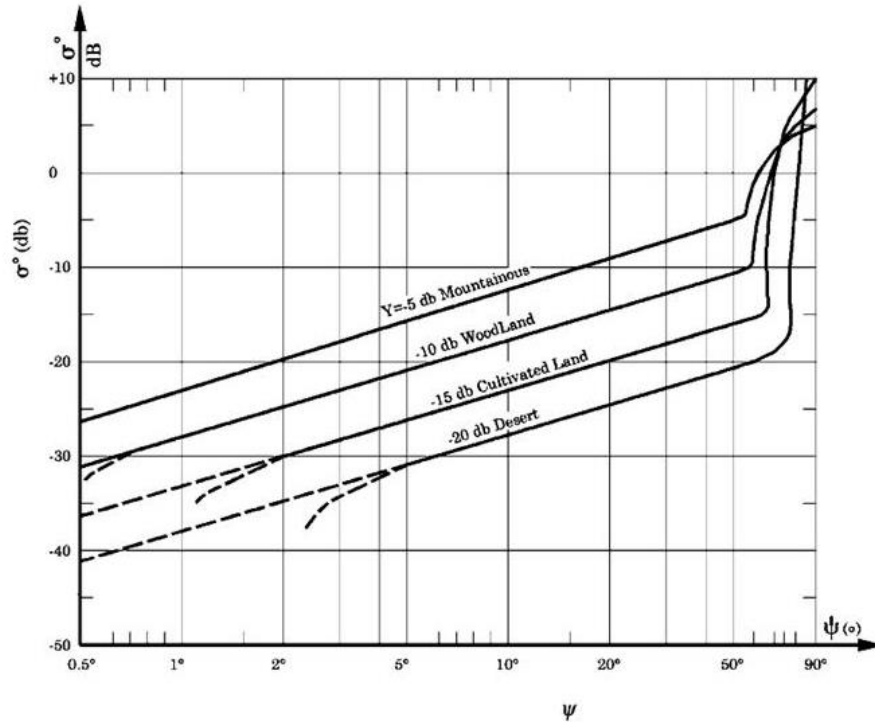


Figure 18. Ground clutter RCS versus grazing angle and terrain

## 6.2 Simulated simple solution performance on ground clutter

An aircraft flying over constant terrain with the antenna pointing along the direction of flight (no antenna tilt) will observe ground clutter as a function of range on the radar display. The magnitude of clutter will be greatest at maximum displayed range since the highest gain portion of the antenna beam will be striking the ground.

However, at the closest displayed range, the ground clutter will be zero as long as the aircraft altitude is greater than the displayed range. That is, if the aircraft is flying at 500 meters, no ground clutter will be displayed closer than 500 meters since the ground terrain is further away than 500 meters.

In the following simulations, the antenna pattern gain in dB (and thus STC clutter amplitude) and clutter Doppler velocity in knots versus range on the radar display for an aircraft flying at 100 knots at a particular altitude are calculated. The Doppler velocity is independent of terrain but the clutter amplitude is dependent on the type of terrain.

The terrain is unspecified and constant in all simulations, as the purpose of this simulation is to obtain a general idea of clutter characteristics as a function of altitude. The horn antenna pattern gain illustrated in Figure 12 is used.

The clutter amplitude and Doppler versus displayed range for an aircraft at 500 feet altitude and velocity of 100 knots is illustrated in Figure 19.

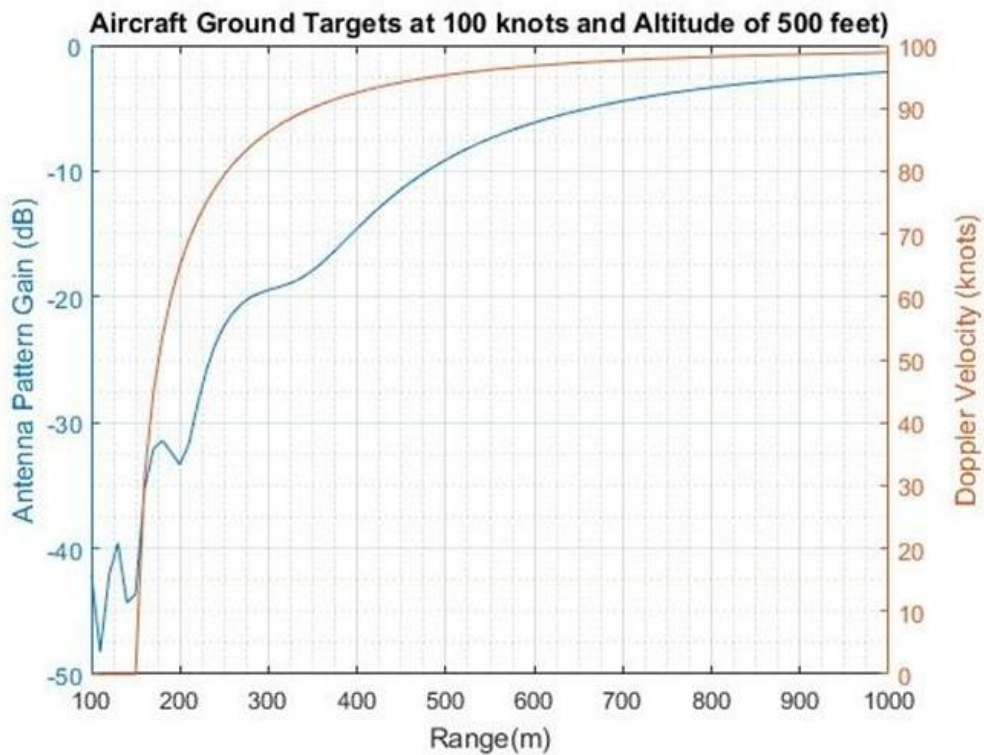


Figure 19. Ground clutter amplitude and Doppler at 100 knots & 500 feet

Note that ground clutter occurs essentially at the aircraft velocity at long range. The range at which the Doppler velocity drops to zero indicates the altitude of the aircraft. However, this graph does not contain any information on the amplitude of the ground clutter.

The clutter amplitude and Doppler versus time to target for the clutter illustrated in Figure 19 is depicted in Figure 20.

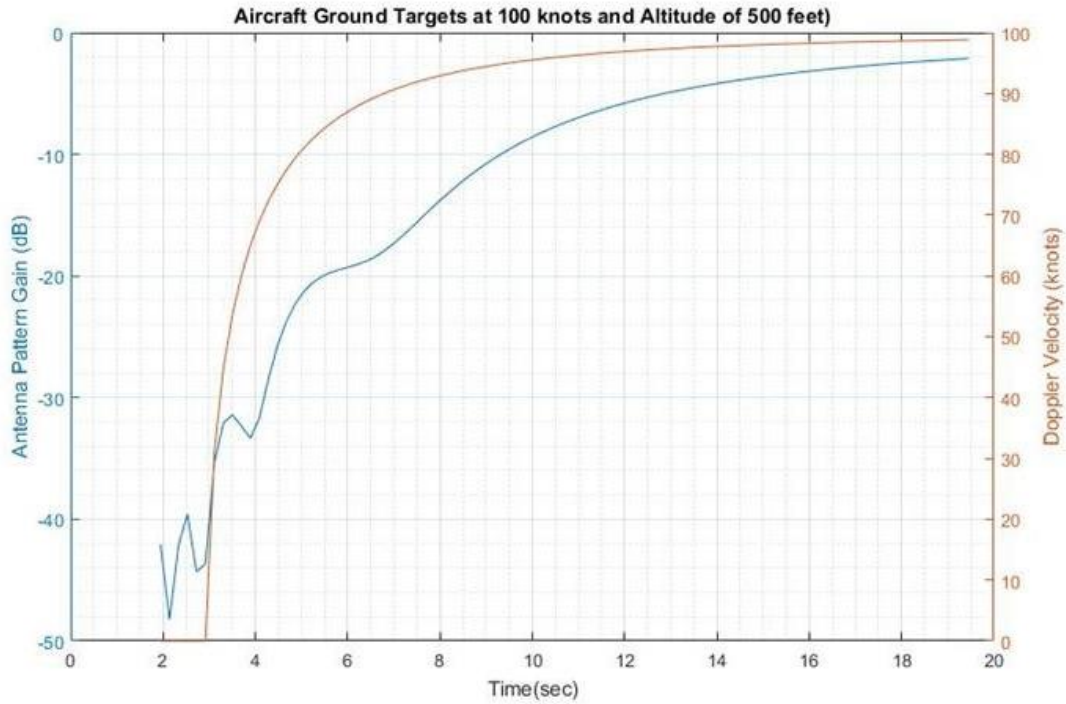


Figure 20. Pilot reaction time at 100 knots in Figure 19

If an airborne target clears ground clutter at a range of 500 meters, the avoidance reaction time is approximately 10 seconds.

The clutter amplitude and Doppler versus displayed range for an aircraft at 1000 feet altitude and velocity of 100 knots is illustrated in Figure 21.

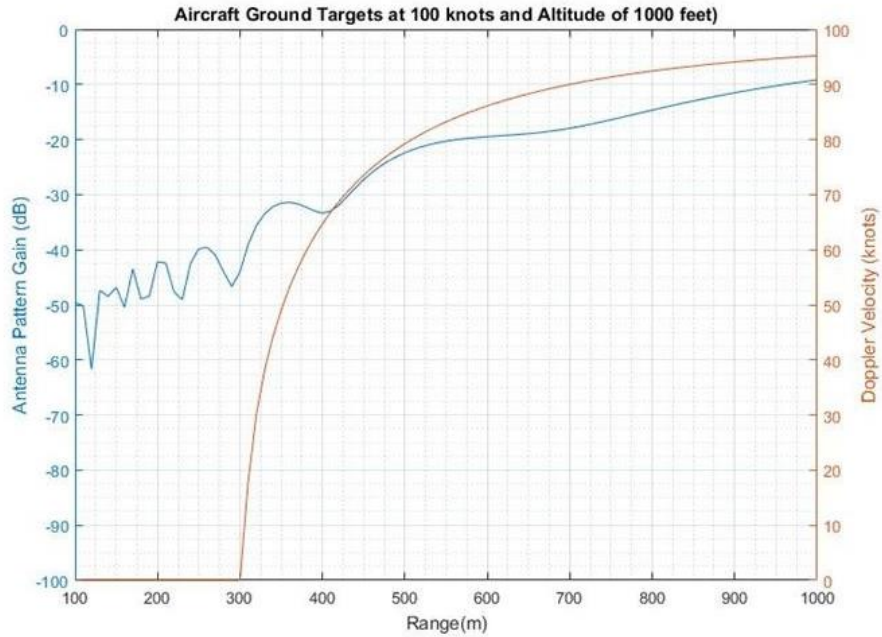


Figure 21. Ground clutter amplitude and Doppler at 100 knots & 1000 feet

Note that at higher altitudes, airborne targets can be reliably detected at longer ranges since the faster Doppler velocity of boresight targets will quickly separate from the slower ground clutter.

The clutter amplitude and Doppler versus displayed range for an aircraft at 2000 feet altitude and velocity of 100 knots is illustrated in Figure 22.

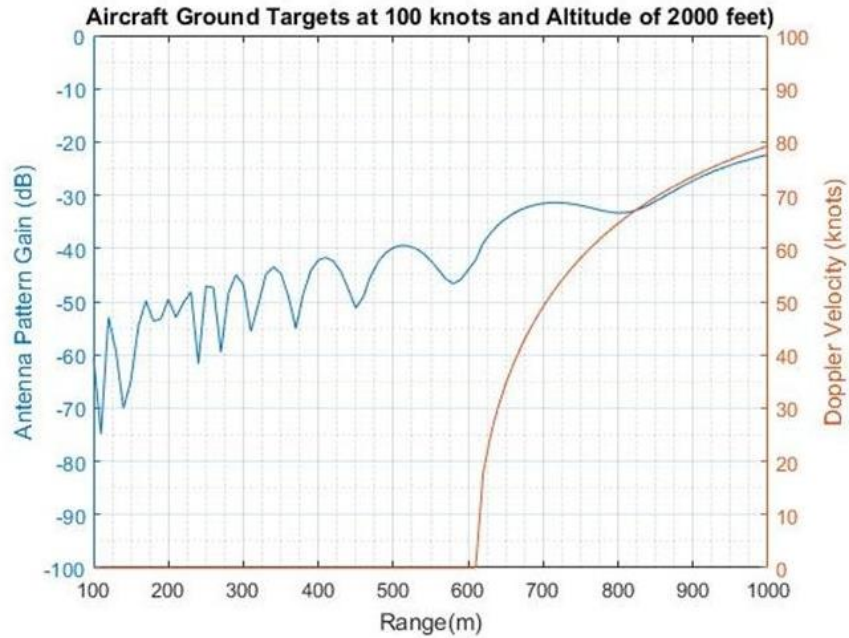


Figure 22. Ground clutter amplitude and Doppler at 100 knots & 2000 feet

The higher the altitude, the less effect ground clutter has on avian radar. If the avian radar is designed to operate out to 1500 meters, then no ground clutter will ever be observed when flying higher than 1500 meters (4921 feet).

In Figure 23, the clutter RCS is simulated for a 3D radar display for an aircraft at 500 feet altitude and velocity of 100 knots. For this display, range is displayed in range bins where the width of each range bin is 15 meters. Each Doppler velocity bin represents 1 knot.



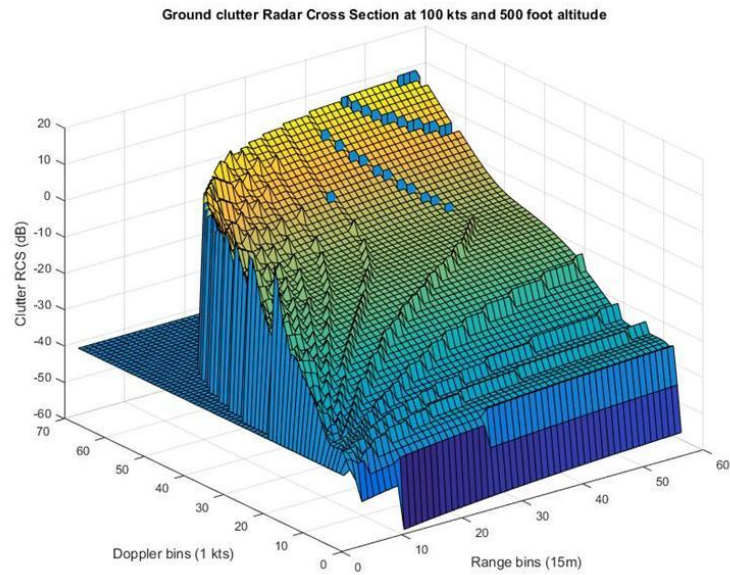


Figure 23. Ground clutter RCS in 3D at 100 knots & 500 feet

Note in Figure 23, that no clutter exists at ranges less than 500 feet. High clutter RCS occurs at high Doppler velocity which means that this clutter is being received at near boresight antenna angles. That is, the closing velocity of the clutter is close to the aircraft velocity.

In Figure 24, the RCS simulated in Figure 23 is displayed in 2D (Range/Doppler).

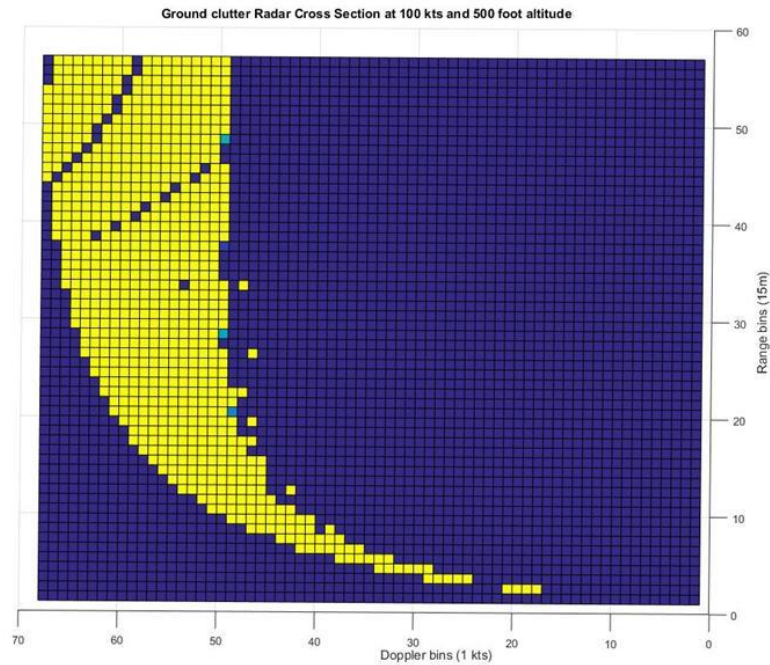


Figure 24. Ground clutter RCS in 2D at 100 knots & 500 feet

Figure 24 indicates areas in which airborne targets are free from ground clutter. A boresight target whose closing speed is either greater than 70 knots or less than 45 knots is free from clutter. Therefore, a dangerous boresight target closing close to the aircraft speed of 100 knots can be detected at any range since its Doppler velocity is greater than any ground clutter.

For range/Doppler areas where ground clutter exists, airborne targets may still be detected depending on the RCS of the target and the RCS of the terrain ground clutter. The probability of detecting airborne targets is higher over desert terrain than over cities or mountains as indicated previously in Figure 18.

## 7 Enhanced techniques

### 7.1 Yagi antenna

The simulations of the last section indicate that ground clutter may not be as serious a problem as initially suspected. This is especially true if target track pattern behavior processing is implemented. An airborne target will have a smooth display update-to-update amplitude and Doppler velocity as it closes on the aircraft. In contrast, ground clutter will have a much more random pattern with aircraft movement. Therefore, it should be possible to separate clutter returns from airborne target returns by further processing of range/Doppler bins.

Another clutter reduction tool is to use a Yagi antenna as illustrated in Figure 25. A Yagi antenna has a small frontal cross section, is lightweight, low cost, and has high gain. They are available either with or without a radome sleeve. As such, one or more could be easily mounted on a rotorcraft. If implemented with automatic tilt capability, it could be tilted up slightly at lower altitudes to reduce the illumination of ground targets.

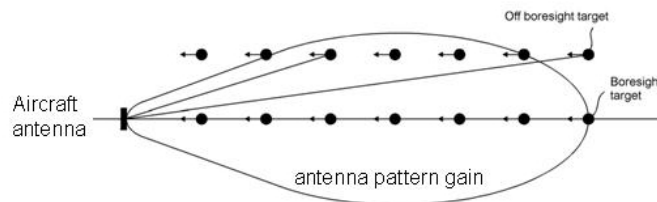


Figure 25. Yagi antenna

Modern airborne weather radars already use this technique to tilt automatically their flat plate antennas up during descent to restrict ground clutter to a narrow band near maximum range on the display. Instead of tilt capability, a couple of Yagi antennas could be used with different tilt angles and the tilted up Yagi used below a certain altitude.

## 7.2 Bird strike avoidance

A summary of the bird-strike avoidance technique is illustrated in Figure 26.



- Assume a 3D antenna beam pattern of adequate beamwidth is pointing directly ahead of the rotorcraft.
- Assume target processing determines if the target is approaching on or off boresight, but cannot determine which side of boresight (above, below, left, or right).
- By yawing the rotorcraft a few degrees, the pilot can determine if the yaw direction points away from a potential bird strike. If so, a slight course deviation in the yaw direction is made for a few seconds before returning to the previous heading.
- An alternate evasion technique is to simply turn 30 degrees left or right for 15 seconds upon receiving a bird strike alert before returning to the previous course.
- Fly as high as possible to reduce ground clutter. No clutter above 1500 meters.

Figure 26. Evasion techniques

Currently, aircraft and rotorcraft have no bird-strike avoidance tools other than visually seeing and avoiding a bird, drone, aircraft, paratrooper, or other hazard directly ahead. However, simulation indicates a small single non-scanning antenna avian radar has the ability to detect targets ahead of the aircraft day or night, and in haze, fog, snow, or rain.

Coherent Doppler radar has the ability to determine accurately the range, amplitude, and Doppler velocity of any detectable targets. By monitoring the closing target's amplitude and Doppler Velocity, software processing or the pilot attention can determine either if the target is a potential collision threat or if it will pass harmlessly to the side.

By using advanced processing during target closure with the aircraft, it should be possible to mitigate most ground clutter over most portions of the target closure period.

A slight evasion maneuver should be sufficient to avoid a collision as bird strikes are already statistically rare with respect to the miles traveled. A conservative pilot can make a course

correction early in a target detection alert to move well out of danger long before a target reaches the aircraft.

## 8 Radar signals

Radar signals are designed and chosen both for target detection and to determine target properties. If only target detection is desired, without any regard to range precision or velocity, than any type of transmit signal can be used. However, if any properties of the target are desired (range, velocity, polarization, etc.), then a specific radar signal must be designed and used.

### 8.1 Radar signal ambiguity function

A radar signal's range and Doppler velocity precision is defined by its ambiguity function as summarized in Figure 28. The ambiguity function defines and illustrates the radar's ability to measure target range and Doppler velocity.

- Radar detection is a function of transmit energy, irrespective of the transmit signal waveform design.
- Range and Doppler resolution are determined by the radar-signal ambiguity function.
- The radar ambiguity function is simply the cross correlation between the transmit pulse and its range and Doppler shifted versions.
- CW radar using a PN coded pulse compression waveform has both high range and Doppler resolution.

The ambiguity function for some common radars are illustrated in Figure 27.

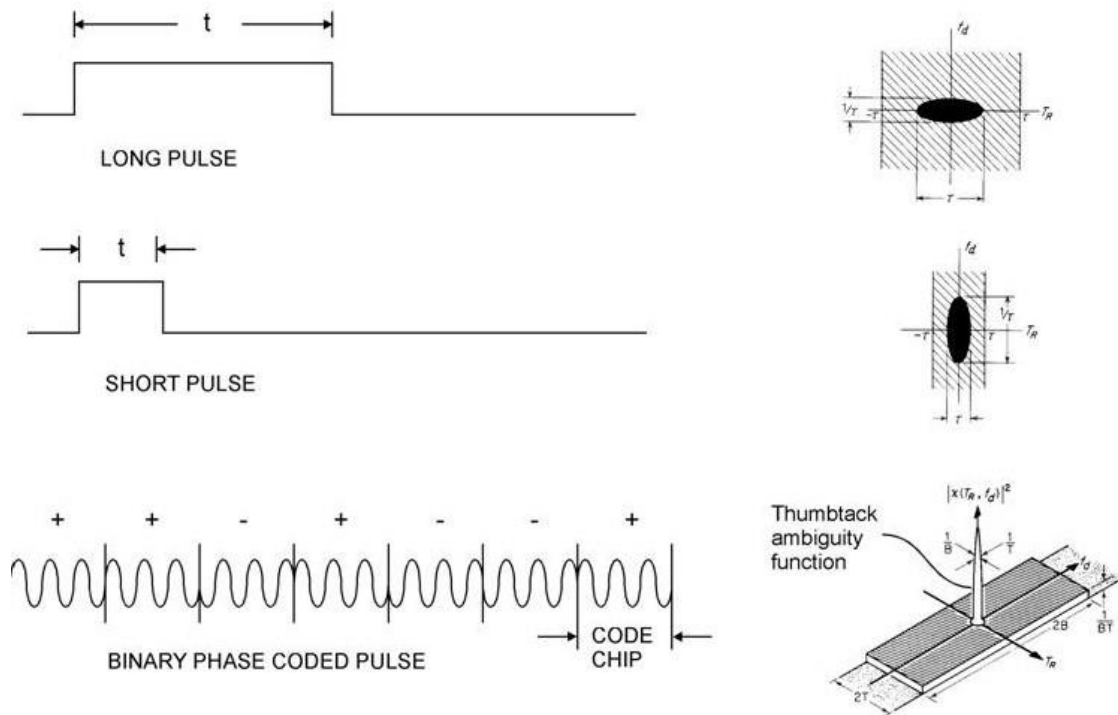


Figure 27. Common radar waveforms ambiguity functions

The most common radar signal is simply a RF pulse at a particular frequency and duration. For a particular radar transmitter power, a long pulse has the advantage of good target detection due to its high pulse energy. A long pulse also has good Doppler resolution as indicated by its narrow ambiguity width in frequency. That is, the radar has good target velocity resolution. However, its range resolution is very poor as indicated by its wide ambiguity width in range.

A short pulse is just the opposite in that it has high range resolution as indicated by its narrow ambiguity width in range, but poor Doppler resolution as indicated by its wide ambiguity width in frequency.

Pulse compression radars were invented to simultaneously obtain both good range and Doppler resolution. Pulse compression operates by modulating the transmit pulse to spread its energy over a wide bandwidth. The modulated target reflection signal is then demodulated which integrates its energy over its long pulse width into an energy spike.

The binary phase coded pulse illustrated in Figure 27 is one form of a pulse compression waveform. Its ambiguity function is narrow in both range and Doppler and resembles a "thumbtack" as illustrated.

## 8.2 Pulse compression

Coherent binary pseudo noise (PN) coded pulse compression is an optimum radar signal for this avian radar since it has both superior range and Doppler resolution. This allows the radar to simultaneously separate and display multiple targets of different ranges and Doppler velocities.

Figure 28 illustrates the demodulated in-phase (I) and quadrature-phase (Q) components of a long binary PN coded pulse from a moving target.

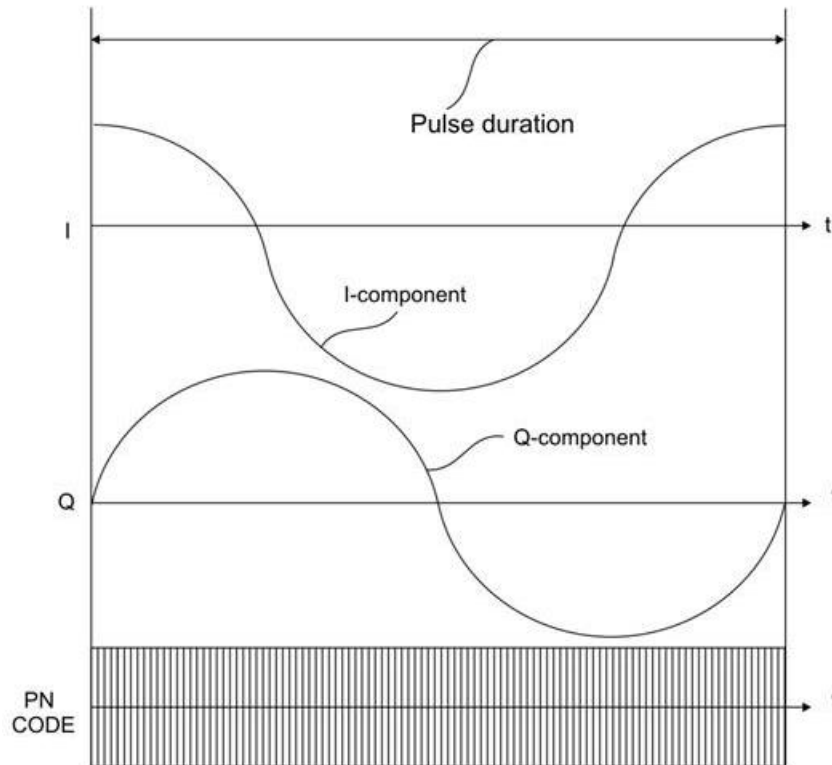


Figure 28. Coherent PN-coded radar I & Q components

Figure 28 assumes the target is moving at a velocity such that the coherent I & Q components of the downconverted reflected target signal forms a single sine wave over the duration of the transmitted PN code pulse. When passed through I & Q matched filters of the same frequency and combined, the output will be maximum.

However, when passed through matched filters of other frequencies, their outputs will fall off in a  $\sin x/x$  fashion as illustrated in Figure 29. By implementing a band of matched filters and selecting the maximum output, the target Doppler velocity will be accurately displayed.

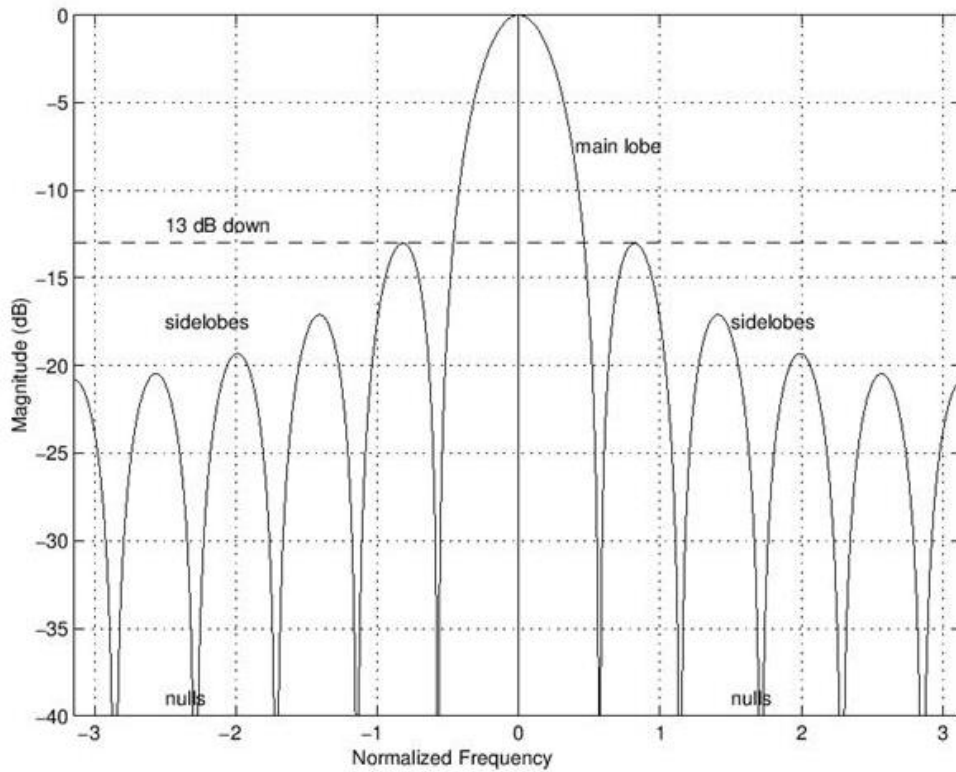


Figure 29. Sin x/x rolloff

### 8.3 Segmented PN coded pulse compression

The problem with the technique illustrated in Figure 28 is that to obtain high Doppler resolution, very high microwave frequencies or very long PN code sequences must be used. Piesinger teaches a technique designed to overcome this problem with a method for independently setting range & Doppler resolution along with processing gain (U.S. Patent No. 7382310, 2008).

High Doppler resolution can be achieved by transmitting and receiving a short PN coded signal in segments spread out over a longer period. This increases the processing dwell time on the target, which then increases the effective processing Doppler shift of the target and thus provides a higher Doppler resolution. This technique is illustrated in Figure 30. This technique is the key innovation that makes this avian radar possible.



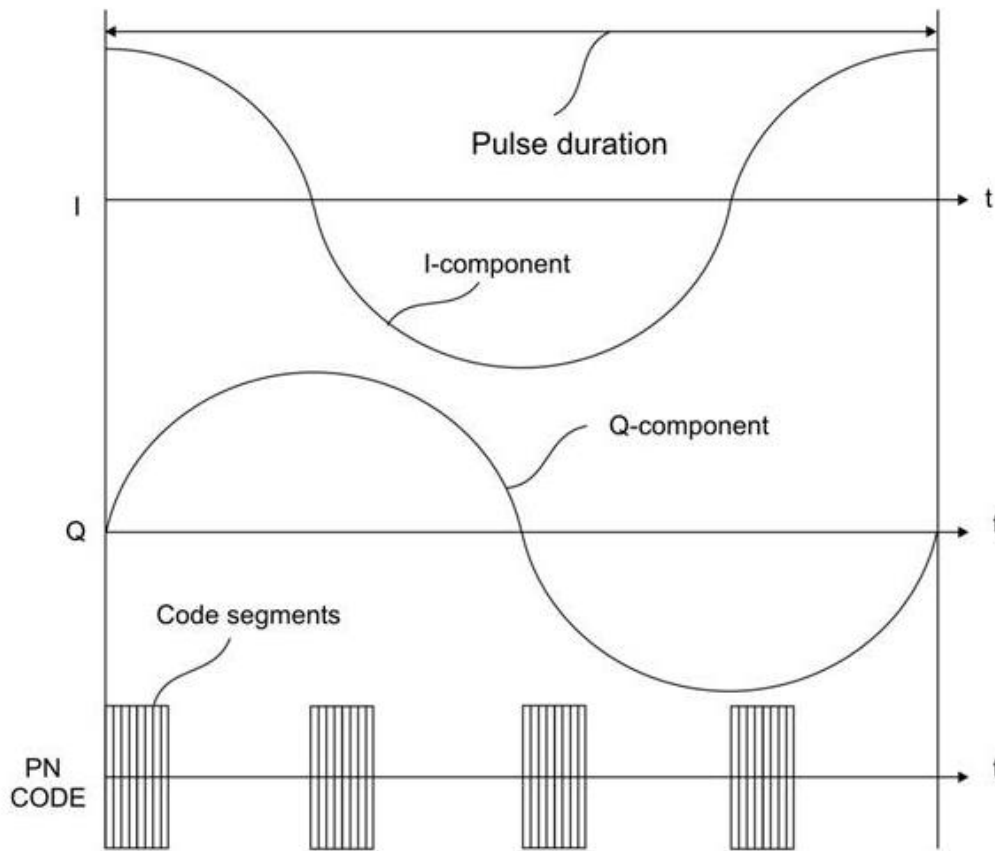


Figure 30. Segmented coherent PN-coded radar I & Q components

For this avian radar, each transmission is coded with a sequential PN code chip from a 10-bit binary PN code. The transmission of all 1023-code chips constitutes a single radar radial.

## 9 Avian radar block diagrams

This avian radar design is based on implementing the coherent segmented binary PN-coded radar described in the section 8.2. The block diagrams presented here are "functional" block diagrams that describe the processing required to implement the radar.

As this is a software-defined radar (SDR), the required processing is split between the field programmable gate array (FPGA) code and the Matlab code. In some cases, a particular described function in a block diagram is partially coded in the FPGA and partially coded in Matlab. Appendix A describes where and how each function is coded.

## 9.1 Top level block diagram

Figure 31 illustrates the avian radar overall top-level block diagram. The RTA creates a 392 MHz clock, trigger pulse, and target RF signal. The 392 MHz clock is the master clock for the entire radar. This clock is processed in both the RTA FPGA and signal processing FPGA to define the transmit pulsewidth, pulse repetition frequency (PRF), range bins, analog to digital (ADC) sampling, and main FPGA clock.

Radar-target reflection signals at RF are digitized in the (ADC), processed in the FPGA, and sent to the personal computer (PC) for further processing and display in Matlab. A trigger pulse from the RTA defines the start of each transmit pulse. Ping/pong memory in the FPGA allows target data from the preceding transmit pulse to be processed while saving data from the current transmit pulse.

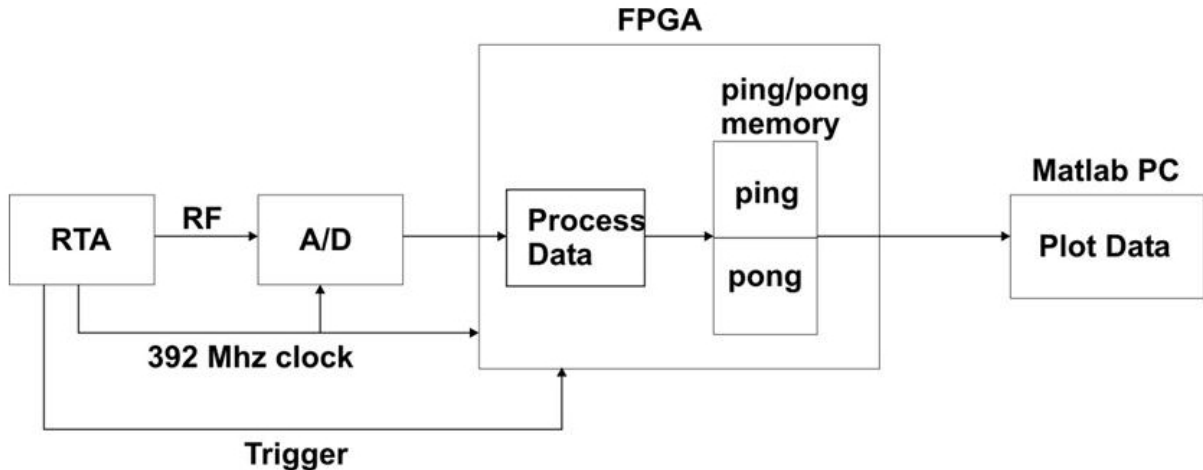


Figure 31. Avian radar block diagram

Radar data is processed to create 192 range bins and 160 Doppler bins using a 50ns pulsewidth, which are displayed as, illustrated in Figure 32. Each X,Y display update processes a radar radial that is processed from 1023 binary PN coded transmit pulses.

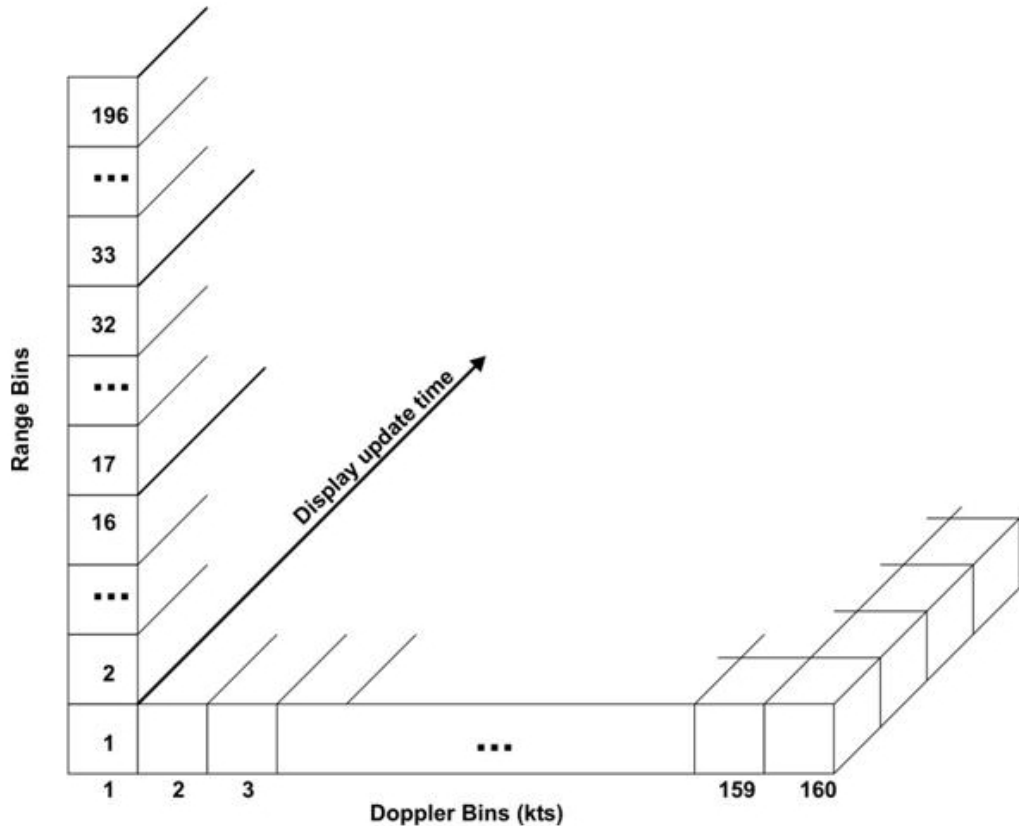


Figure 32. Range/Doppler bins (indicate time axis)

Each radar radial processing update sends the latest 196 range bins by 160 Doppler bins to the PC Matlab Range/Doppler display when in high-resolution 50ns pulsewidth mode.

The avian radar supports four range resolutions using transmit pulsewidths of 50, 100, 200, and 400ns. The high-resolution 50ns pulsewidth mode creates 196 range bins. The number of range bins are divided by two each time the pulsewidth is doubled. The number of Doppler bins is constant. The maximum radar range is 1500 meters for all four pulsewidths.

## 9.2 RTA block diagram

A block diagram of the RTA is illustrated in Figure 33. The RTA is fully coherent in that all frequencies and timing are derived from the 2450 MHz oscillator, which defines the transmit pulse frequency. This frequency is split into in-phase and quadrature-phase components in the 180-degree power splitter.

The PN code switch binary-phase modulates the 2450 MHz transmit signal as commanded by the PN code from the FPGA. The TX pulse modulator sets the transmit pulsewidth as commanded

by the TX pulsewidth from the FPGA. Its output signal is amplified in the high power amplifier (HPA) and transmitted. The FPGA defines the transmit period, pulsewidth, and PN code.

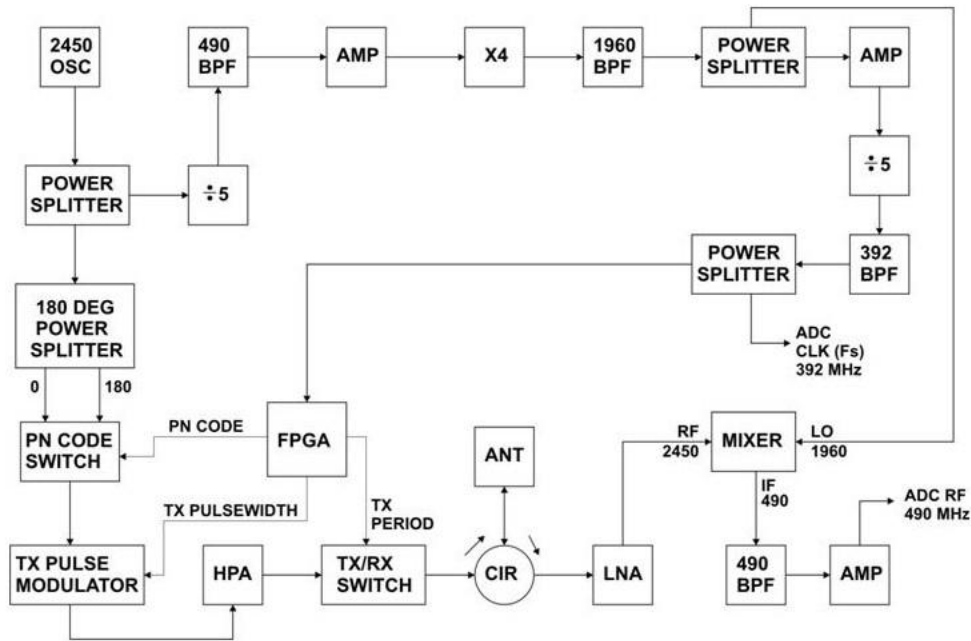


Figure 33. RTA hardware block diagram

The 2450 MHz clock is divided by 5 and multiplied by 4 to create a 1960 MHz LO signal. Target return signals at 2450 MHz are downconverted to 490 MHz in the mixer to create a 490 MHz IF frequency. The 392 MHz master clock frequency is created by dividing the LO frequency by five. The 490 MHz IF signal is downconverted to baseband in the ADC by harmonic sampling at RF using the 392 MHz master clock.

As this avian radar proof-of-concept project could only use off-the-shelf parts, a 10 watt continuous wave (CW) HPA was selected, as non-custom pulse amplifiers were not available. During testing, the high noise figure of the HPA during the radar receive period required the installation of the TX/RX switch which isolates the HPA from the circulator during the RX period. In any production version, this switch will be eliminated as the HPA will be replaced by a pulsed amplifier, which is turned off by definition between transmit pulses.

### 9.3 Software processing block diagram

The overall processing block diagram is illustrated in Figure 34. ADC samples from the RTA RF signal are first processed in the range filter to create the in-phase (I) and quadrature-phase (Q) components of the range bins. These samples are buffered in the I-PRF & Q-PRF RAMs for

further processing by the Doppler filters. The output of the Doppler filters are converted to radar target intensities and sent to the PC for Matlab display.

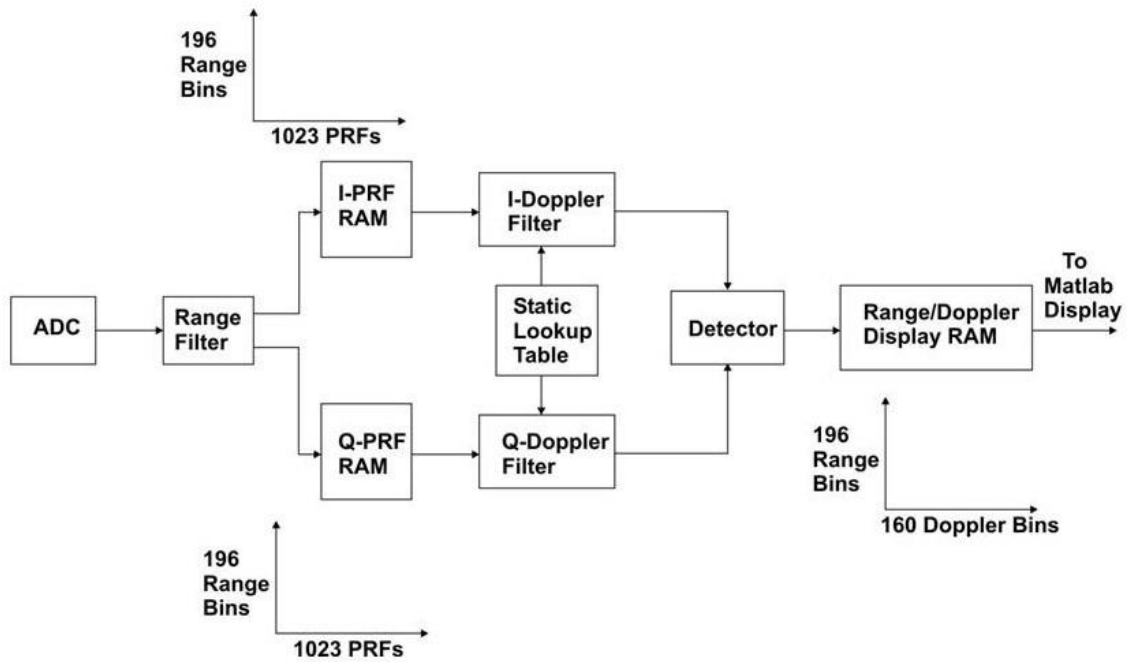


Figure 34. Processing block diagram

#### 9.4 Range filter block diagram

The range filter is illustrated in Figure 35, which processes data from the ADC to create range bins. For the 50ns high resolution pulsewidth, 20 ADC samples are processed in the range filter to create 196 I & Q range bins, 40 samples on 100ns resolution for 98 range bins, 80 samples on 200ns resolution for 49 range bins, and 160 samples on 400ns resolution for 24 range bins.

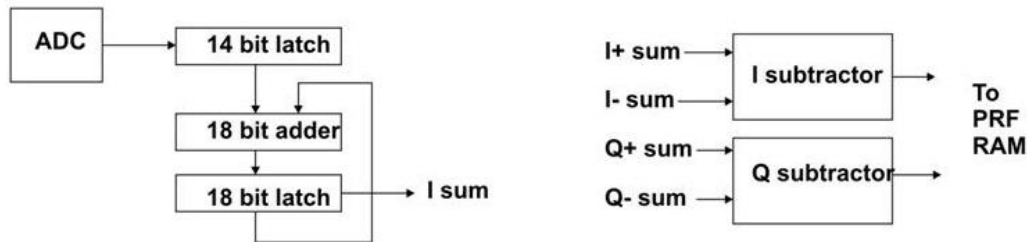
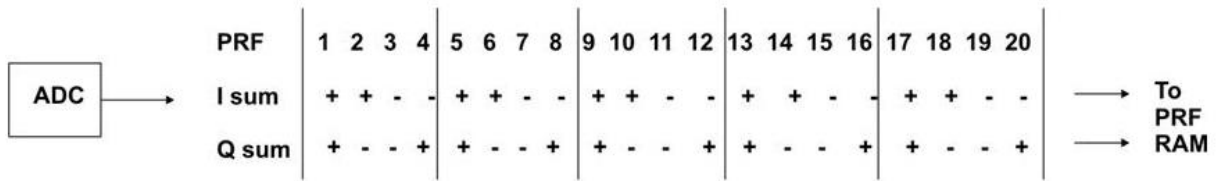


Figure 35. Range filter

Sequential ADC samples at the 392 MHz sample rate are added and/or subtracted in a repeating "+ + - -" fashion to create the in-phase component and in a "+ - - +" fashion to create the quadrature component.

There are many software choices for implementing the range filter. A single four-sample adder/subtractor could be used to create an intermediate sum followed by a second adder that accumulated five of these intermediate sums for the highest resolution range. Individual adders could add only the "+" samples and another only the "-" samples. A following subtractor would then subtract the -sum from the +sum. Refer to the Appendix for the actual software implementation.

## 9.5 Doppler filter block diagram

The Doppler Filter illustrated in Figure 36 processes data from the range filter. For the 50ns high resolution, 196-range bin I & Q components from the range filter are processed for 1023 Pulse Repetition Frequency (PRF) transmissions that constitute a radar radial.

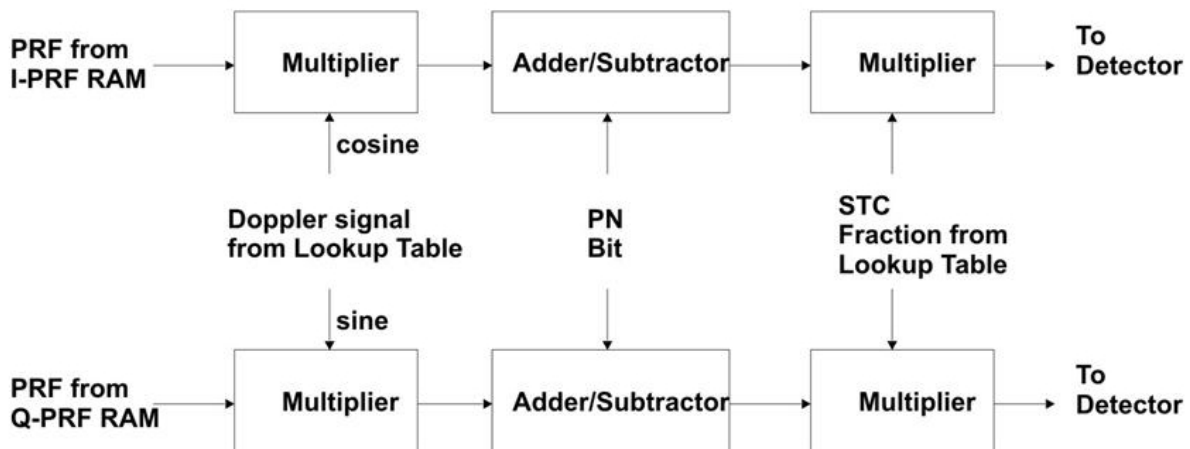


Figure 36. Doppler filter

Each quadrature Doppler filter (0 to 160 knots) reads sequential stored 1023 PRFs words in a range bin row from the PRF RAMs. Each PRF word from the I-PRF random access memory (RAM) and Q-PRF RAM is multiplied by a cosine/sine frequency sample from either a lookup table or a FPGA DCM as illustrated in Figure 36.

The cosine/sine frequency sample used is that of the implemented Doppler Bin filter frequency. This multiplied value is either added or subtracted in the adder/subtractor depending on the polarity of the PN code bit for that PRF transmission. After all 1023 PRF transmissions of the range bin row have been accumulated, the result is multiplied by a fraction value from the STC lookup table radial.

In the final implementation, STC was implemented in the PC Matlab code so its slope could be adjusted by the radar operator.

## 10 Projected radar range performance

Performing a more complete version of the radar range equation in Figure 6, the projected avian radar was calculated for the 50ns high-resolution pulsewidth based on the RCS of a pigeon and a four-pound bird.

As the RCS of any target is statistical, the values listed below are typical values reported in references. The RCS spread between a small bird (pigeon) and a four-pound bird is 10 dB.

- RCS of pigeon and other small birds is 0.01 square meters (-20 dB).

- RCS of flock of small birds or single four-pound bird is 0.1 square meters (-10 db)
- In the following range chart, PR(R) is radar return power for small bird. PR\_flock(R) is for flock of small birds or single four-pound bird. Flock of large birds may be 10 dB larger than PR\_flock(R).

The pigeon radar return versus range is plotted by the green line and the four-pound.bird by the brown line in Figure 37.

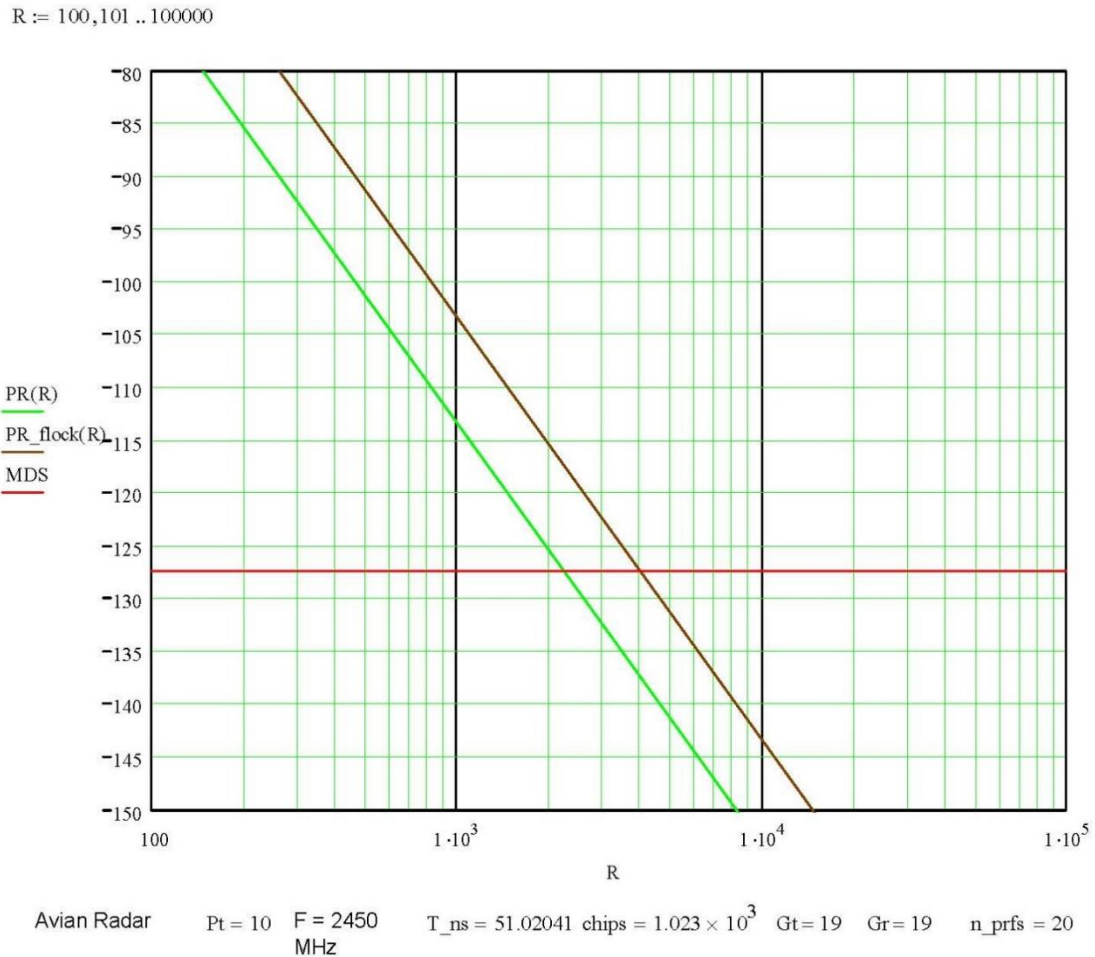


Figure 37. Calculated avian radar range

The key factors are the antenna gain, frequency, pulsewidth, pulse power, and processing gain. The 19 dB Alfa antenna (illustrated later) 2-way antenna gain of 38 dB and the 1023 PN-coded transmission gain of 30 dB are the greatest range performance drivers.



The calculations assume a 10 watt pulse HPA and no TX/RX switch. In the current proof-of-concept prototype implementation, these components result in about a 6 dB lower performance due to the switch and additional cabling losses.

Using a custom designed HPA in a production radar would add at least 10 dB higher performance than calculated and presented in Figure 37 as it is anticipated the HPA power would be increased from 10 watts to 100 watts.

As the current CW amplifier must be on continuously, its direct current (DC) power consumption is about 66 watts even though the average transmitted RF power is approximately 50 mw. The power consumption of a production radar 100 watt pulsed HPA would be a small fraction of the current CW HPA.

As the transmit energy doubles each time the duration of the pulsewidth doubles, the 400ns pulsewidth would increase the transmit energy by 9 dB. Using the Alfa antenna with the low loss antenna cable, the prototype avian radar sensitivity is about 6 dB lower than plotted. That is equivalent to simply increasing the red MDS line by 6 dB to -121 dBm.

## 11 Radar insulation on S76 helicopter

The initial plan for mounting an antenna in the FAA S76 helicopter is as follows:

- Place RTA in S76 radome.
- Remove Primus P650 weather radar to make room for avian radar antenna during flight test phase of the project.
- Mount avian radar antenna on bulkhead using existing fastener locations.
- Avian radar antenna can be flat panel, helix, horn, yagi, etc.
- Radome transmissivity is less at S-band than X-band.

The RTA packaging, using an array antenna, was initially chosen based in the current P650 weather-radar installation drawings illustrated in Figure 38 & Figure 39.

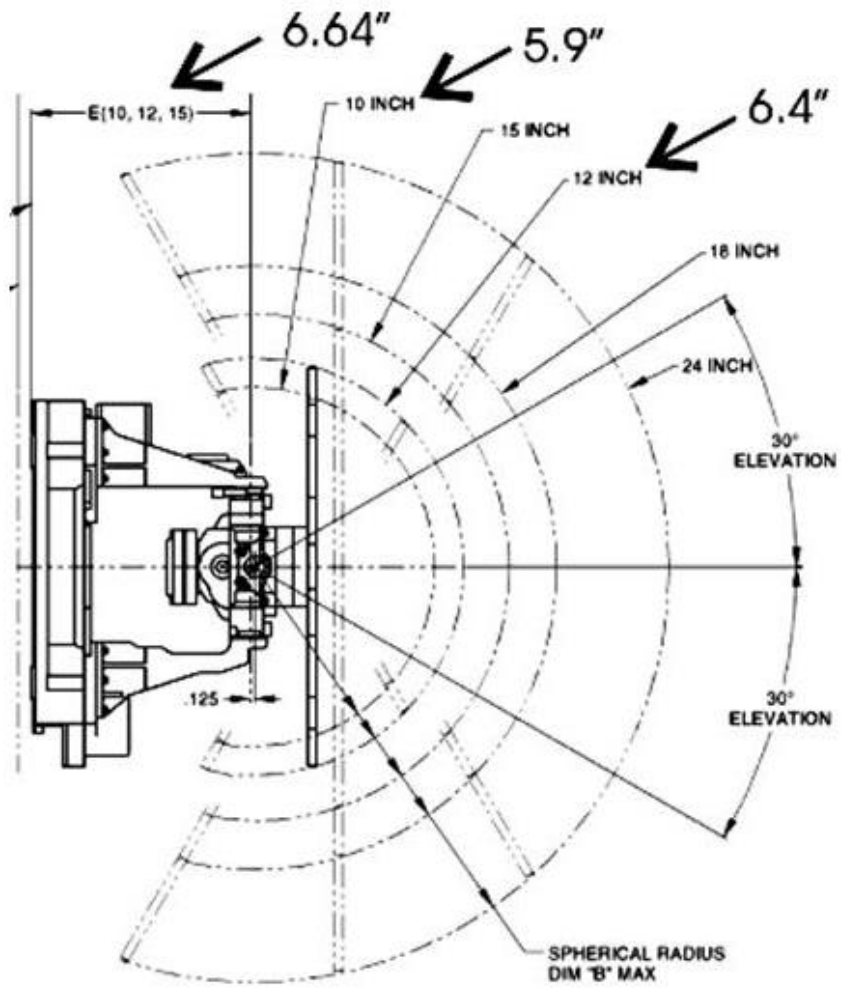


Figure 38. Primus P650 side view

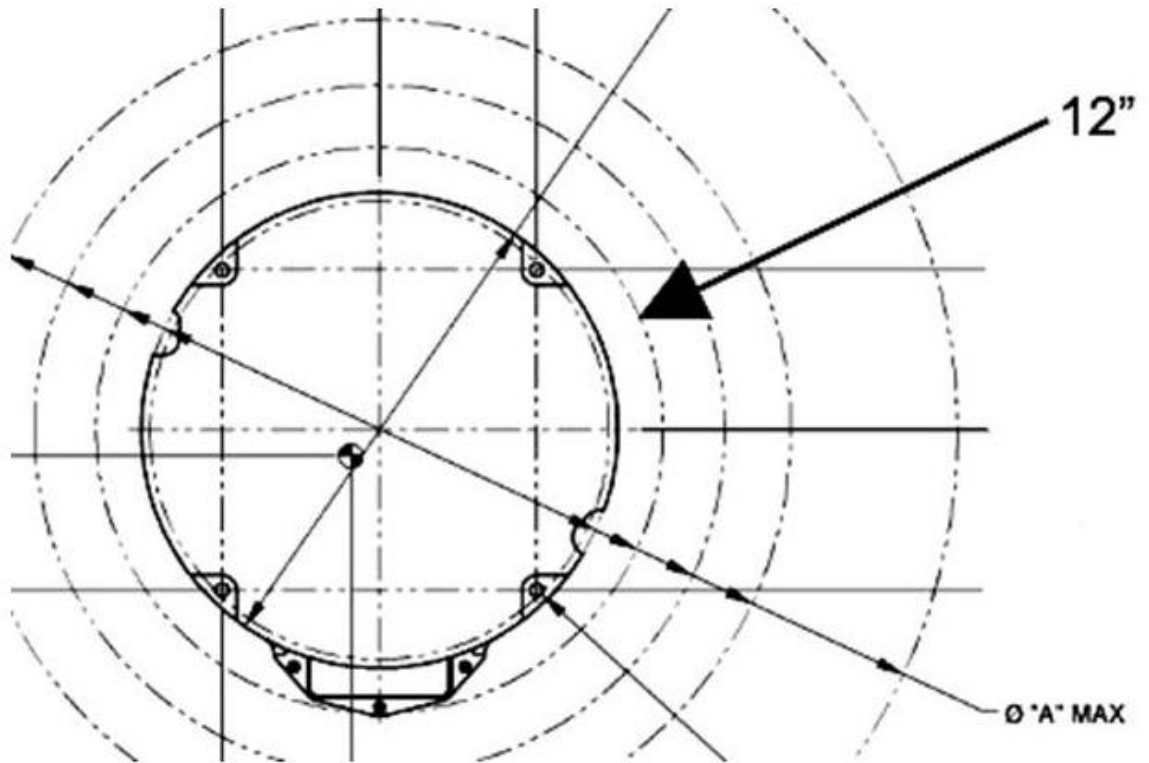


Figure 39. Primus P650 mount view

Unfortunately, late in the implementation it was discovered that the available space indicated in the installation drawings was no longer available due to the many modifications made to this test helicopter over the years.

As the RTA was already constructed, the decision was made to mount the RTA in the cabin and run a RF cable to the antenna mounted in the radome. The two main disadvantages of separating the RTA and antenna is the 2-way antenna cable loss and a larger minimum range dead-zone due to antenna return loss.

Low loss antenna cable could be obtained but its physical diameter was too large and the cable too stiff to install. However, all this became a moot point as the S76 was reassigned and no longer available for flight-testing this avian radar.

## 12 Radar hardware

This avian radar was specifically implemented to mount the RTA in the S76 radome and place the signal processing ADC, FPGA, and PC in the S76 cabin. As indicated, late in the project the RTA (minus the antenna) was also to be placed in the cabin and the antenna only placed in the radome.

### 12.1 Radar hardware block diagram

The overall avian radar block diagram is illustrated in Figure 40. As only off-the-shelf components could be used, commercial ADC & FPGA evaluation boards were used, which were placed in the ADC/FPGA enclosure. These two evaluation boards required a specific power-up sequence to prevent applying signals to the FPGA board prior to powering it up.

To prevent powering up incorrectly, the 24 direct current voltage (VDC) to the system was passed through a 24-volt relay that was activated by the 120 alternating current voltage (VAC) power supplied to the FPGA board. In this way, if the AC power to the FPGA was lost, the 24 VDC would be shut off.

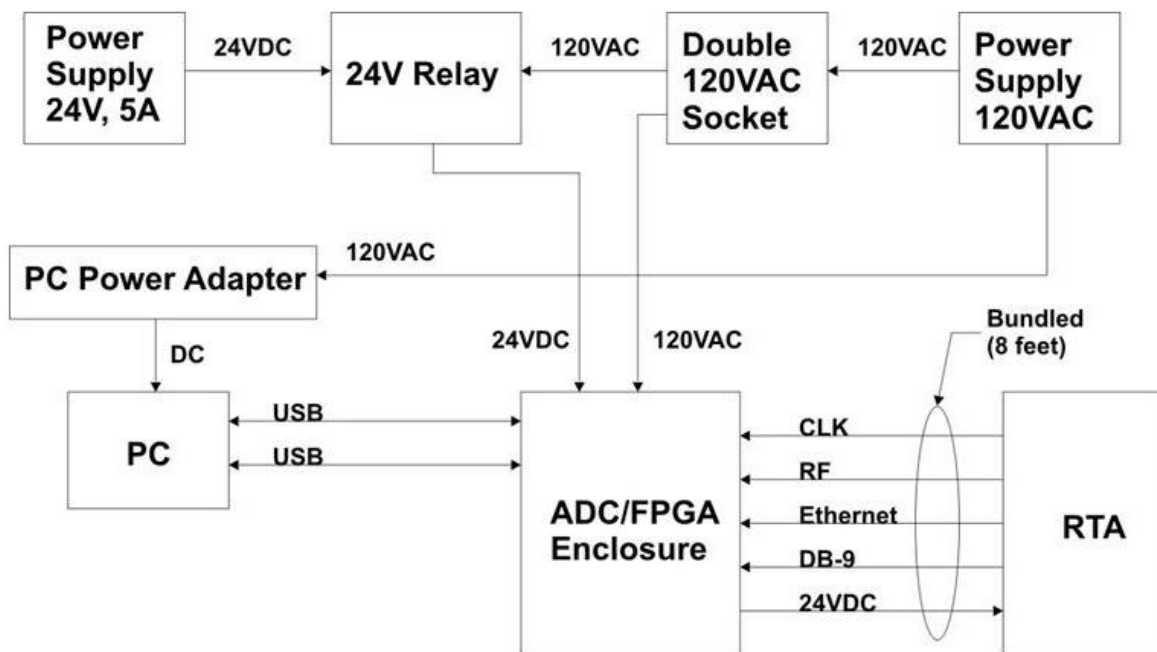


Figure 40. Avian radar block diagram

The ADC/FPGA enclosure is the center of the radar setup. The enclosure contains user switches, which allow the RTA and ADC to be powered on, the pulsewidth resolution to be selected, and the transmitter to be turned on. Not shown is the RTA to radome-mounted antenna and its RF cable.

## 12.2 RTA hardware

The RTA mechanical stackup is illustrated in Figure 41 as initially designed for placement in the radome using its RTA mounted array antenna. For cabin mounting, the array antenna was removed from the RTA and a type N RF connector installed in its place. The mounting rubber vibration isolators were left on the RTA and the RTA was mounted in a Hardigg case.

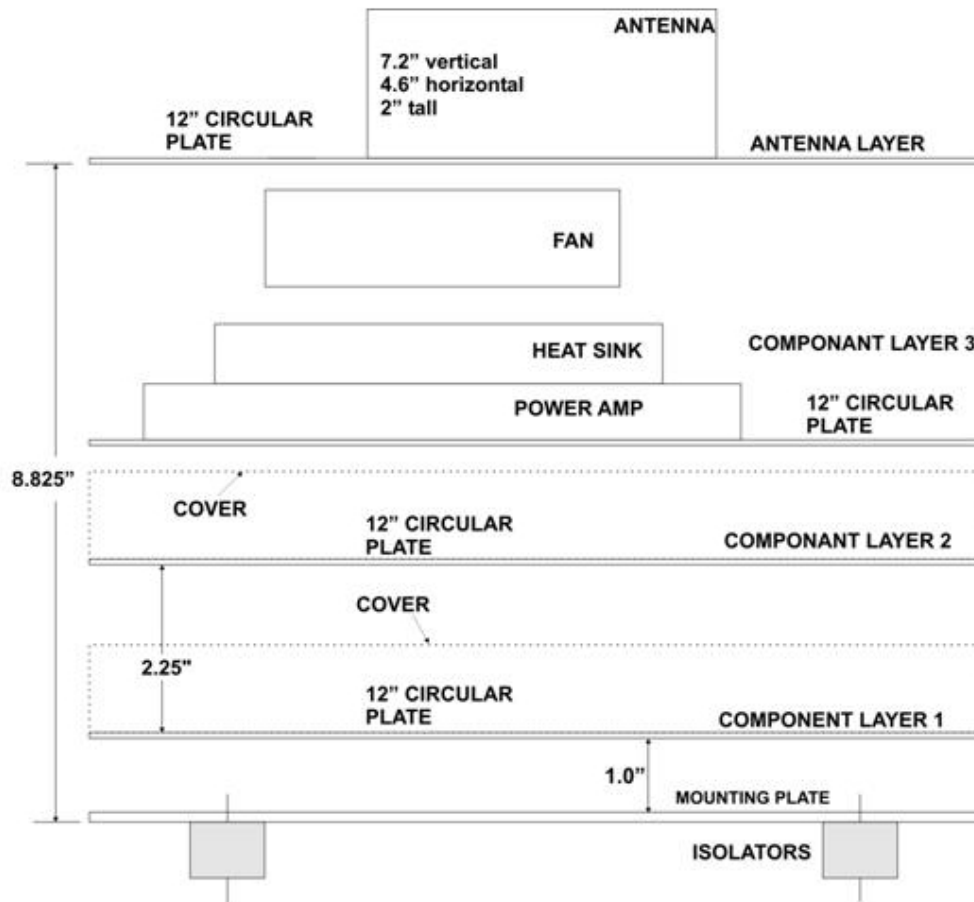


Figure 41. RTA stackup

The actual RTA is illustrated in Figure 42 (prior to removing the array antenna). A fan and large heat sink is mounted on the HPA to ensure its temperature would not exceed its automatic thermal shutdown. Most of the RF components of RTA block diagram in Figure 36 are mounted in the circular enclosures.



Figure 42. RTA

### 12.3 ADC/FPGA enclosure

The ADC/FPGA enclosure is illustrated in Figure 43. The switches and turn-on instructions are mounted near the top.



Figure 43. ADC/FPGA enclosure

A hinged clear cover is implemented so the operator can view the FPGA evaluation board (main green board) LEDs and power it on. However, it is safest to leave the FPGA board power switch on all the time, so it will be automatically powered up when 120 VAC power is supplied to the entire radar setup.

The red board is the ADC evaluation board. The white breadboard implements a few low voltage DC power supplies for the ADC board.

The enclosure top row of user switches allow the various components to be energized and the resolution pulsewidth to be selected.

## 12.4 Overall radar hardware setup

The final avian radar hardware setup is illustrated in Figure 44. The RTA is vibration mounted in the blue Hardigg case. Note the type N connector in place of the original array antenna.



Figure 44. Avian radar setup

The long vertical silver enclosure between the PC and the ADC/FPGA enclosure is the auxiliary enclosure. It contains the 24VDC power relay along with RF amplifiers and filters connected in line between the RTA RF output and the ADC RF input. The gain and filter bandwidth were selected as a performance optimization compromise that would work best for the currently implemented pulsewidths.

## 12.5 Flat plate antenna

The Alfa flat plate antenna selected for this avian radar is illustrated in Figure 45. It is very thin and lightweight with high gain. In the ground tests that follow, a six foot very low-loss coax was used to connect this antenna to the RTA.





Figure 45. Alfa flat plate antenna

## 13 Radar display & control

The avian radar data is displayed on the PC using Matlab. The display update rate is about three updates per second on the high-resolution 50ns setting. The update rate doubles for each lower resolution as the number of range bins are halved at each wider pulsewidth. The range/Doppler display is illustrated in Figure 46. The range is in meters and the Doppler velocity is in knots. Maximum range is 1500 meters and maximum Doppler is 160 knots.

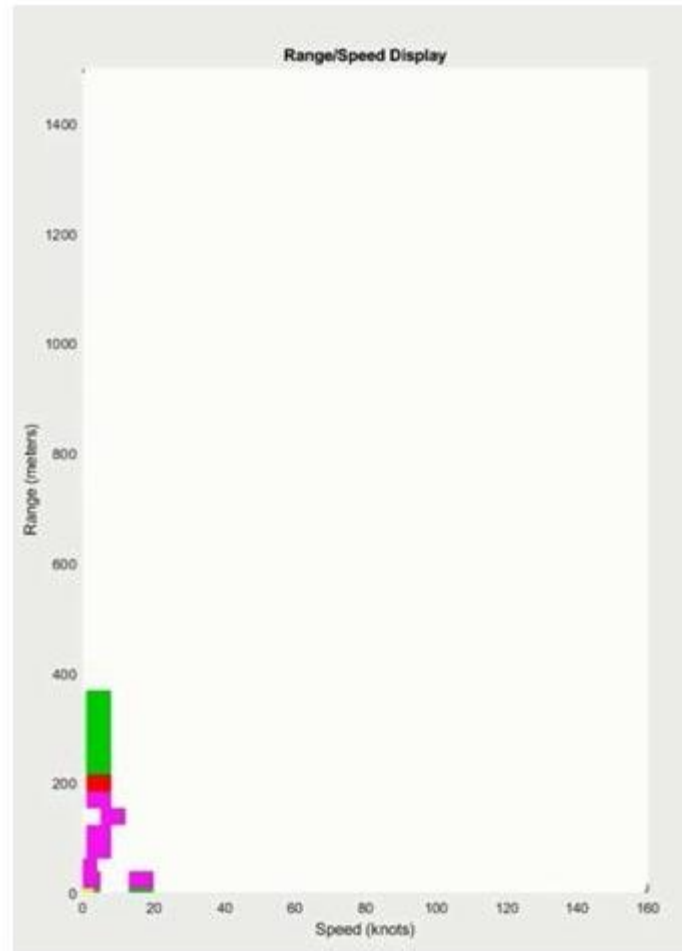


Figure 46. Range/Doppler display

Target intensity is color coded as white, green, yellow, red, and magenta where white is no target and magenta is maximum intensity. This is the same color scheme used on most airborne weather radars, which with pilots are already familiar.

Any square portion of the display can be expanded simply by clicking and dragging the mouse. On ground tests, the high intensity near the origin is due to close static ground clutter.

The control panel for the radar is illustrated in Figure 47. The Data control is no longer used. The green threshold is normally set to zero. Radar gain increases the target sensitivity of the radar. The STC slope is used to lower the radar gain on near targets. STC cutoff sets the range at which STC gain reduction is removed.

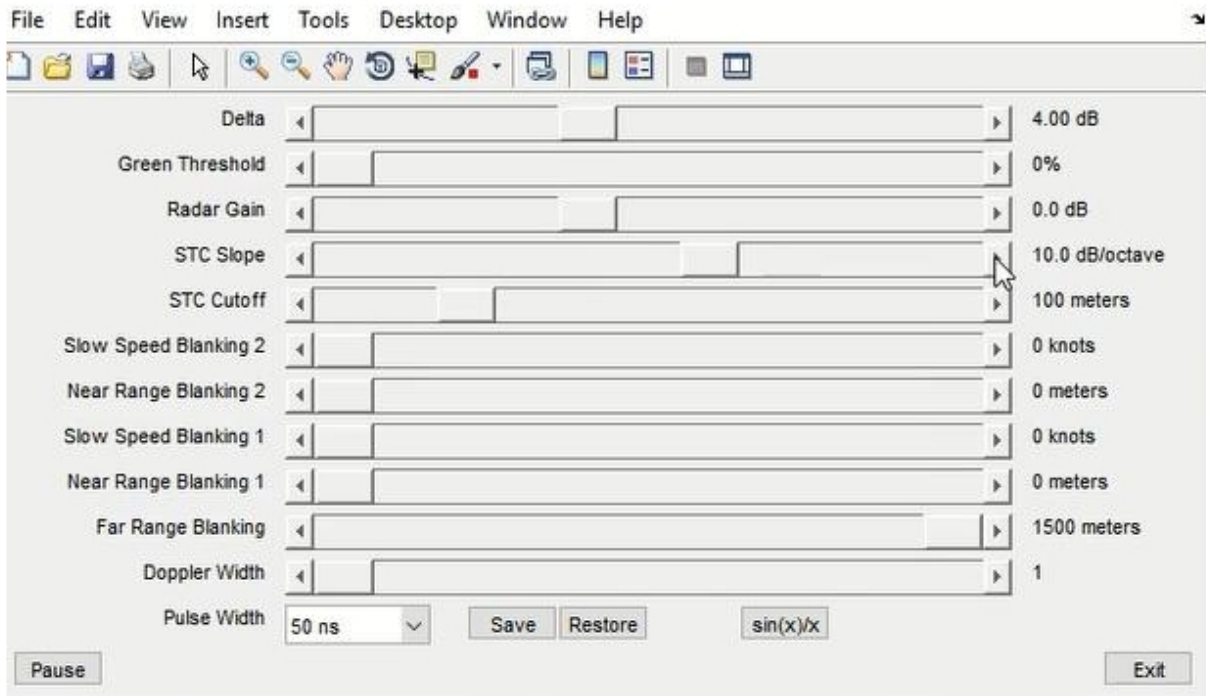


Figure 47. Display control panel

The four blanking sliders allow two independent blanking regions to be set which can be used to eliminate either range or Doppler ground targets. Far range blanking sets a blanking region starting at 1500 meters (maximum range) to eliminate end of display ground clutter.

The Doppler width slider allows the width of Doppler targets to be increased. This is useful on the low-resolution settings since displayed targets are tall in range but thin in Doppler. Increasing the Doppler width makes the target color more visible.

The last settings select the pulsewidth, save or recall control panel setup settings, and display the peak Doppler  $\sin x/x$  value. Without this setting, strong target  $\sin x/x$  Doppler rolloff is distracting.

The STC visualization panel shown in Figure 48 allows the operator to visualize STC control panel settings. This panel indicates the radar gain (horizontal line), STC slope (slope line), and STC cutoff range (straight/slope point).

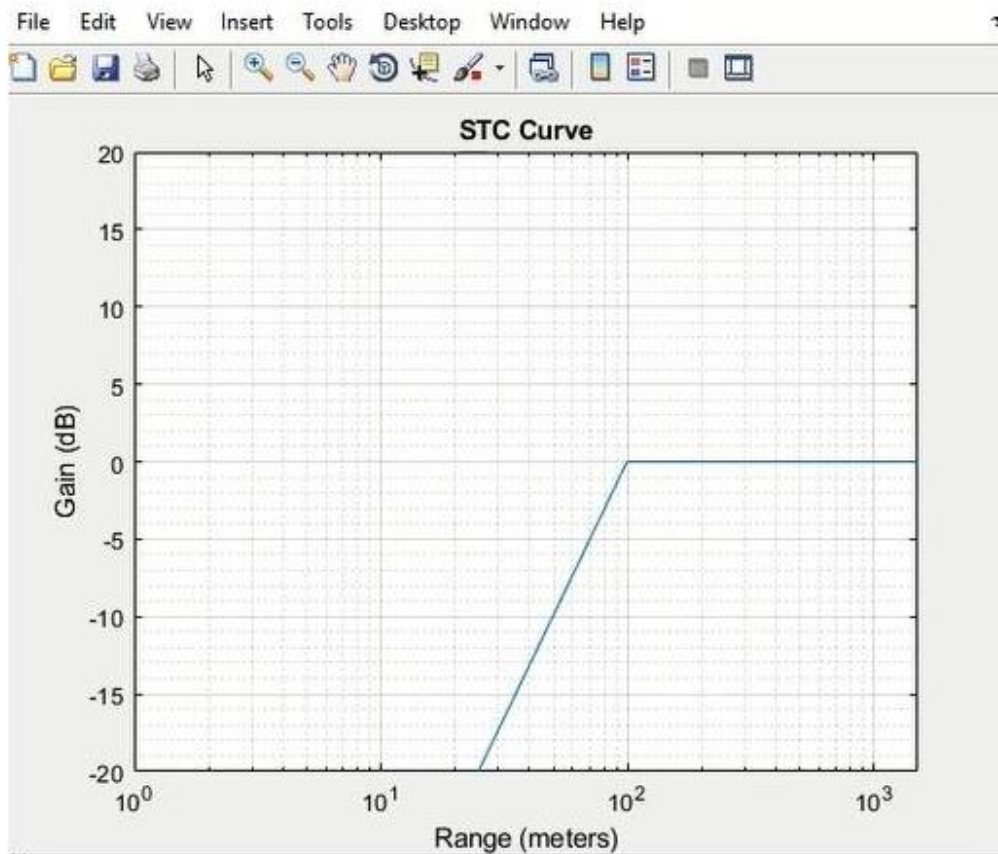


Figure 48. STC visualization panel

## 14 Radar performance

### 14.1 Ground traffic test

The traffic tests were conducted early in our initial ground testing. These tests proved that the radar was able to track and display multiple simultaneous targets.

The following is a sequence of still shots of the radar display and camera image as a set of traffic passed by the radar. The speed limit was 50 miles per hour (MPH) on this road. Note the speed difference and range of cars coming towards and going away from the radar.

The radar was setup so the beam was pointed at an angle with respect to the road. The range display is in range bin number where each range bin was 7.65 meters (25 feet) wide. The targets at low Doppler velocity are static ground targets out to over 1000 feet. Wide Doppler targets at the origin are due to the  $\sin x/x$  rolloff of close strong Doppler targets.

In Figure 49, the red vehicle is traveling away from the radar at about 48 knots (55 MPH).

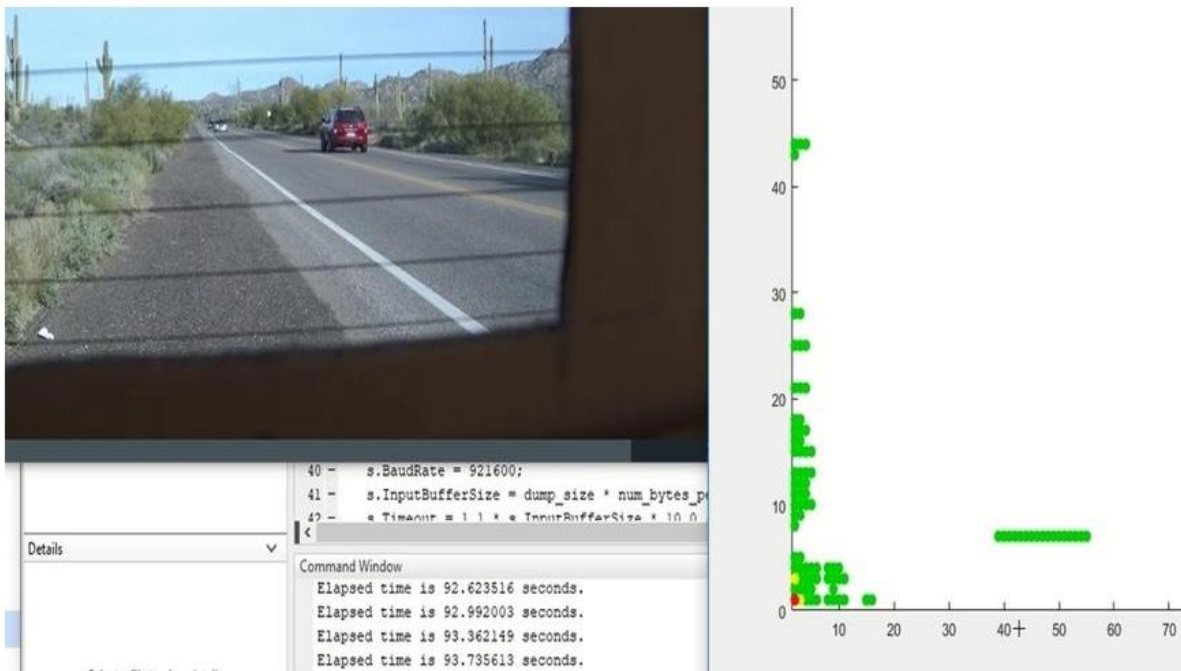


Figure 49. Traffic sequence 1

In Figure 50, the silver vehicle is traveling towards the radar at about 55 knots (63 MPH). The double target is due to the triangular range cross correlation of the radar pulse and target.

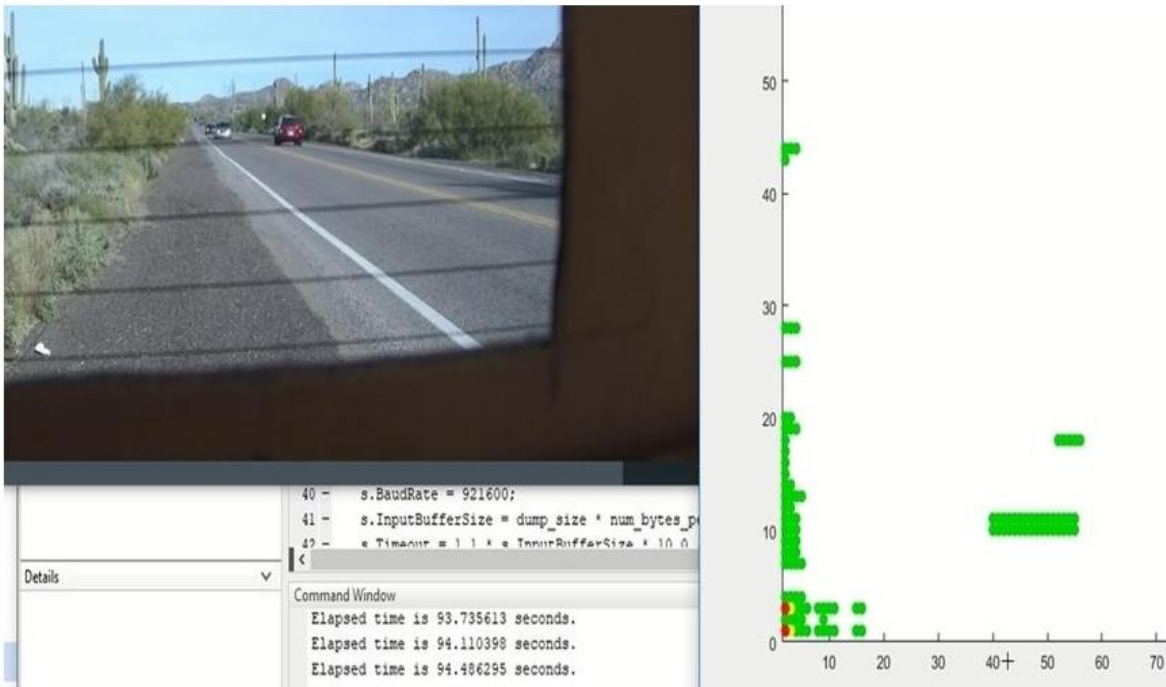


Figure 50. Traffic sequence 2

In Figure 51, the targets are merging.

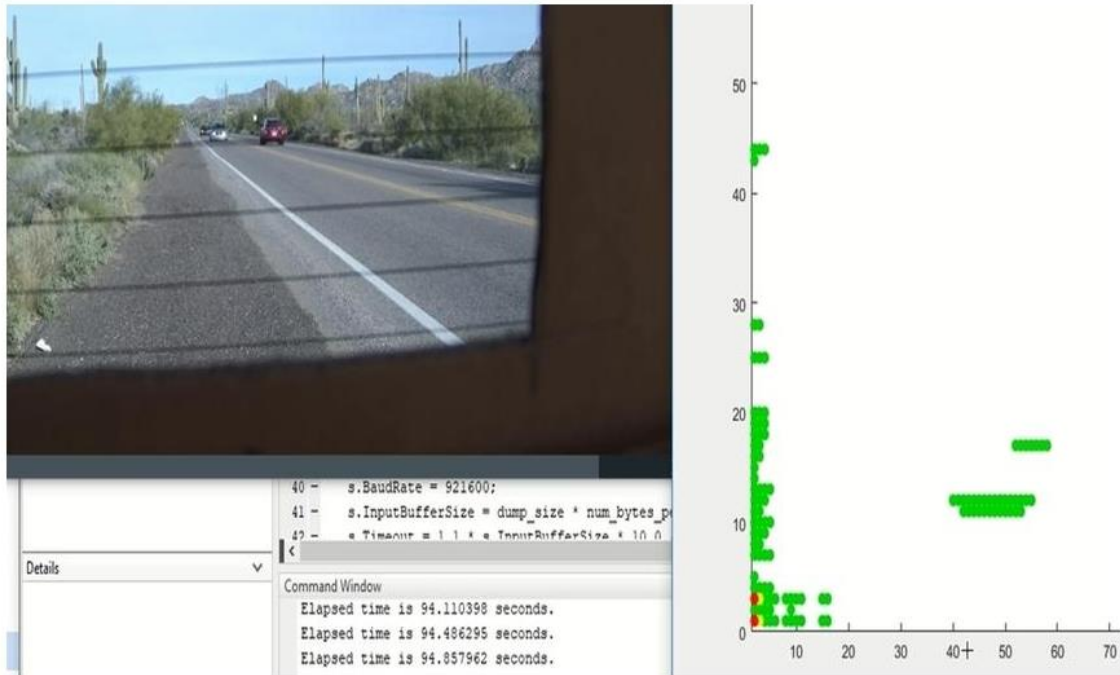


Figure 51. Traffic sequence 3

In Figure 52, the targets are merging.

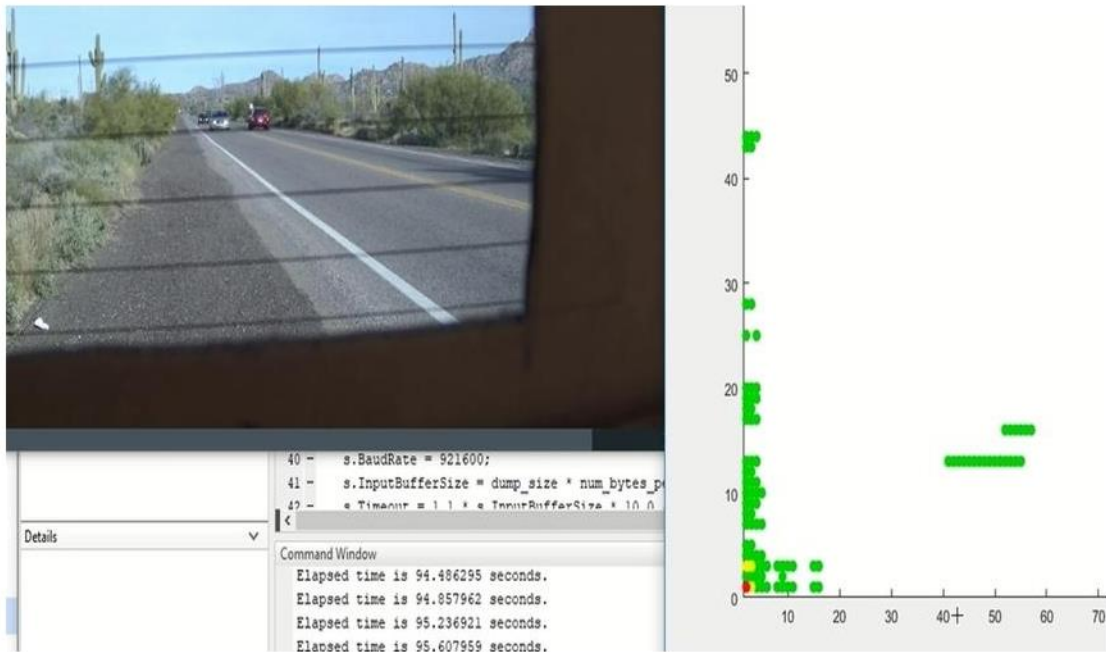


Figure 52. Traffic sequence 4



In Figure 53, the targets have merged.

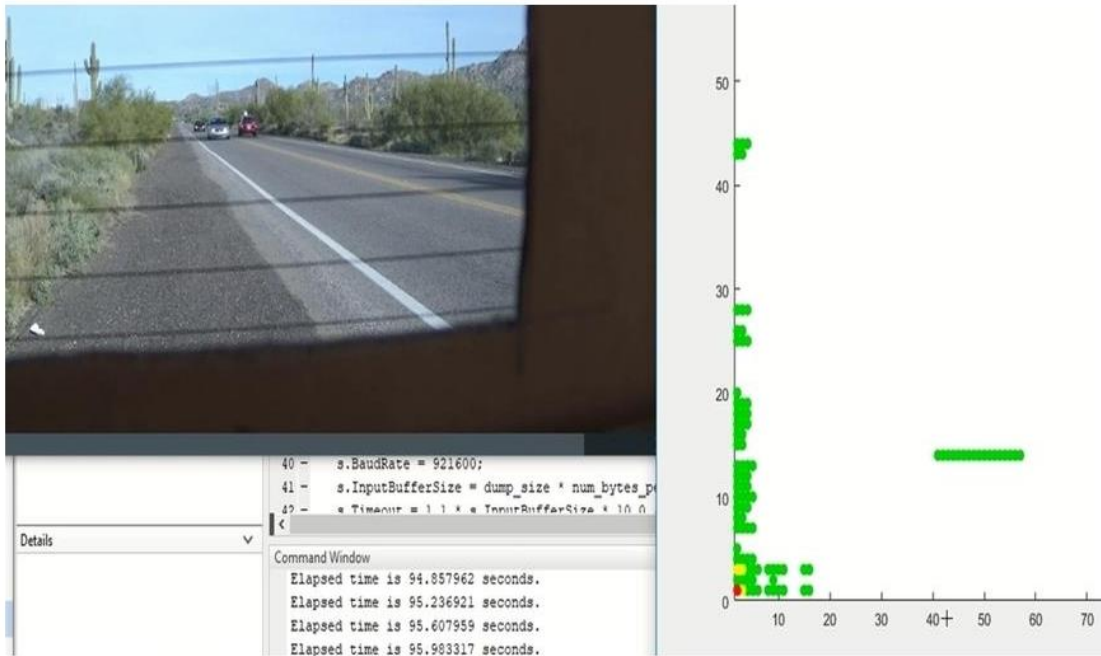


Figure 53. Traffic sequence 5

In Figure 54, the targets are separating again.

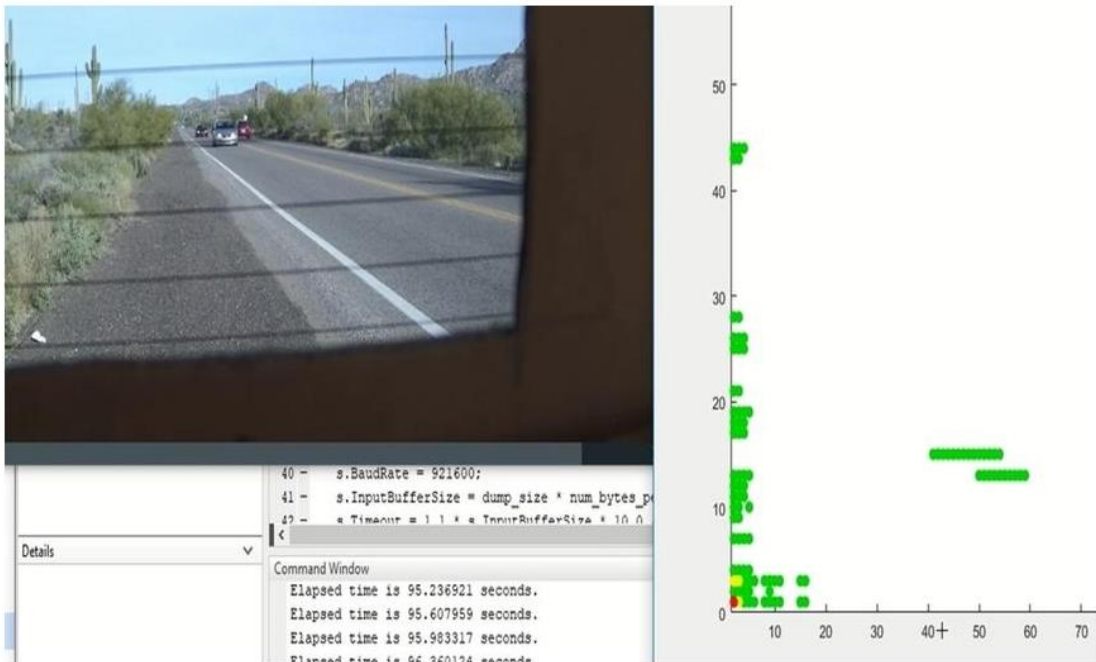


Figure 54. Traffic sequence 6

## 14.2 Drone & conductive balloon test

In this ground test, a Mavic Air drone towing a small conductive balloon was used as targets. The drone was flown straight up. On the way, straight back down, the balloon was caught in an updraft, which caused its tow string to contact and shear off the tip of a propeller blade.

The short range targets are all short range ground clutter.

In Figure 55 frame, the drone starts to fall so the drone and balloon are separated by different velocities as the drone is falling faster than the balloon.

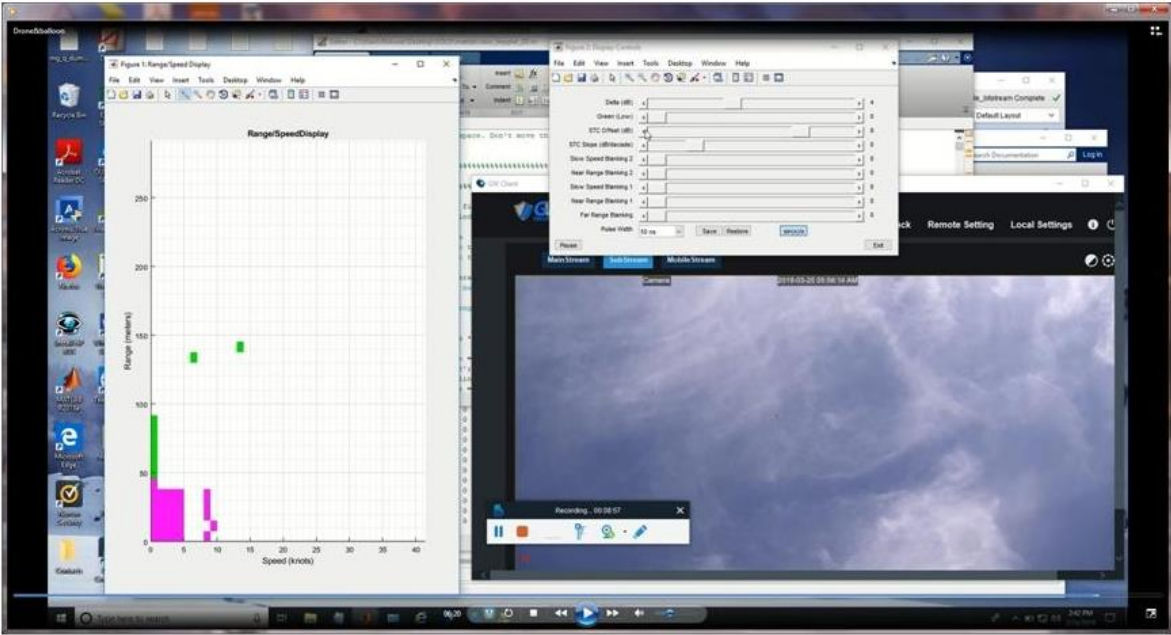


Figure 55. Drone & balloon sequence 1

In Figure 56 frame, the drone is in free fall while the balloon is still drifting down.

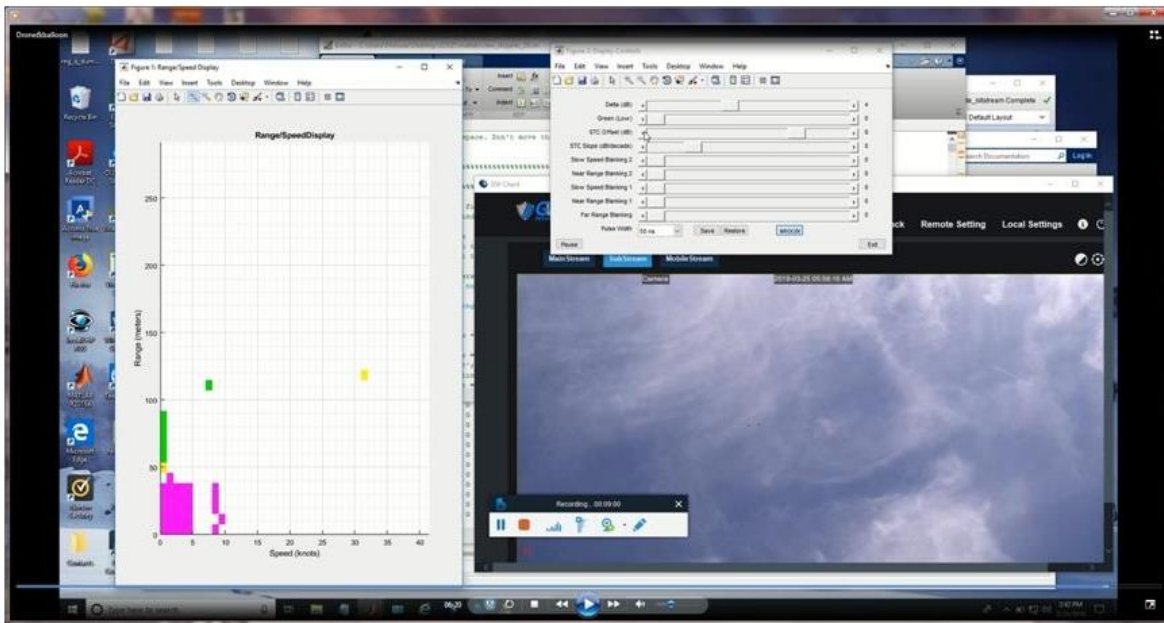


Figure 56. Drone & balloon sequence 2

In Figure 57 frame, the balloon is acting as a parachute, which saved the drone from any damage except for the replacement of the damaged propeller blade.

The RCS of both the drone and balloon are essentially identical.

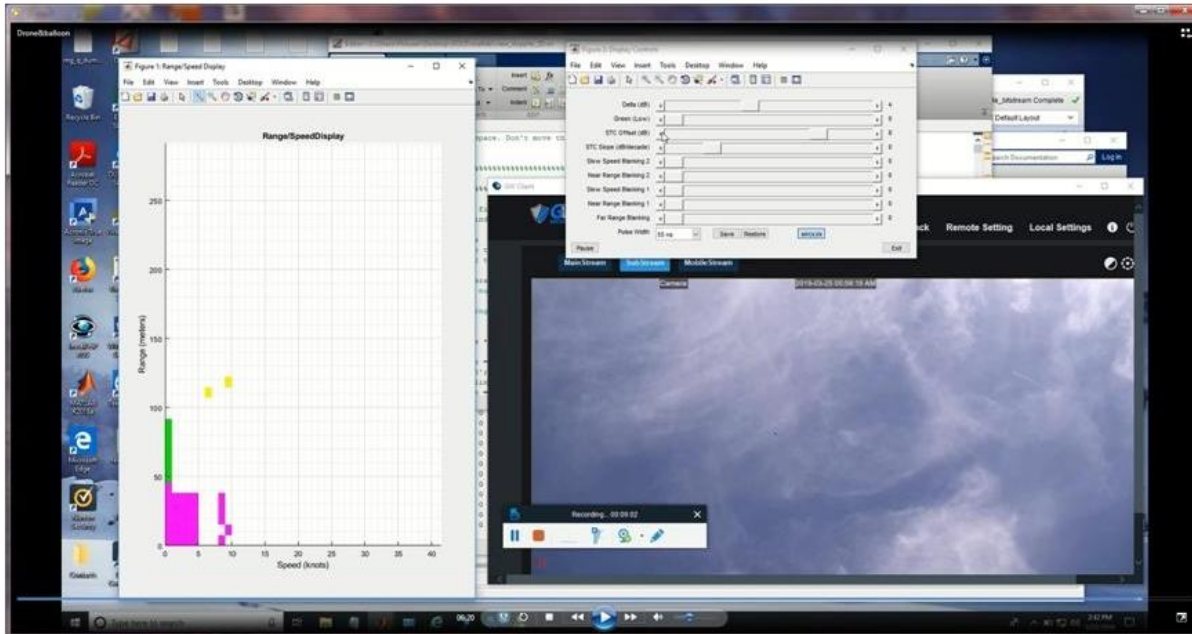


Figure 57. Drone & balloon sequence 3

### 14.3 Drone tests

In this ground test, the Mavic Air drone was flown straight up and straight back down. No STC was used and the test was in an urban environment so there was lots of short range ground clutter (Figure 58).

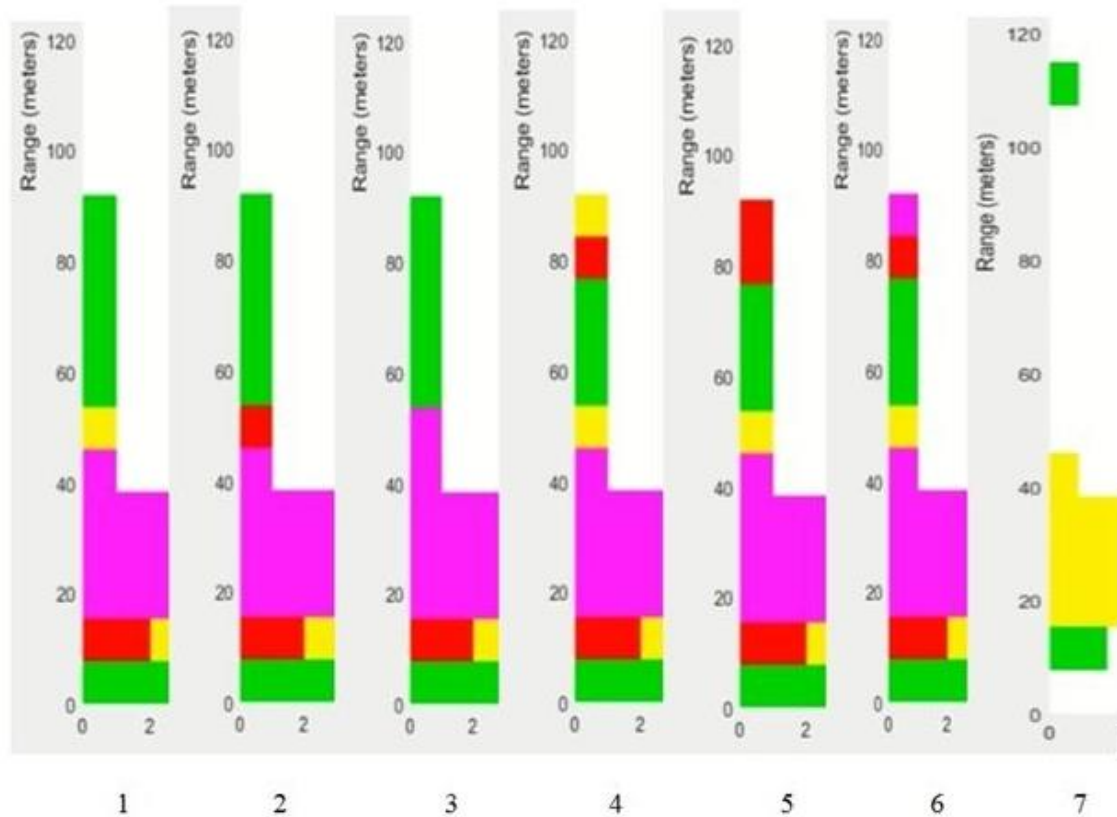


Figure 58. Drone target

The range is in meters. Frame 1 is ground clutter. In frame 2, the drone starts to enter the yellow bin at 50 meters, adds to the clutter, and increases the bin target intensity from yellow to red. In frame 3, the drone fully enters the bin at 50 meters and increases its intensity to magenta.

Later at a higher altitude frame 4, the drone is primarily in the 80-meter bin and is entering the 90-meter bin. In frames 5 & 6, the drone increases the intensity of bin 90 from yellow to red and then to magenta.

In frame 7, STC slope is set to 12 dB per octave out to 100 meters. This eliminates most of the short-range ground clutter, which allows the drone to be separated from the ground clutter at a much shorter range. In frame 7, the drone is at 110 meters.

This test illustrates the triangular cross correlation between the transmit pulsewidth, target, and range bin width. That is, when a target just starts to touch the entrance of a new range bin, bin intensity is zero. When the target touches the exit of the range bin, bin intensity is maximum. When the target totally exits the range bin, bin intensity is zero again.

## 14.4 S76 Flight tests

The original S76 flight test plan assumed that the antenna would be placed on the RTA and both would be placed in the radome in place of the P650 weather radar. When it was discovered insufficient room was available for the RTA, the RT was to be placed in the cabin and connected to the original array antenna in the radome via a medium loss RF cable (~2 dB 2-way loss).

Using the predicted radar range plot in Figure 37, the equivalent MDS for this arrangement would decrease by 6 dB due to reduced prototype radar sensitivity, another 2 dB due to the medium loss antenna RF cable, and another 18 dB due to the reduced 2-way gain of the array antenna with respect to the Alfa antenna, for a total of 26 dB. This would reduce the maximum range on a four-pound bird to around 850 meters on the 50ns resolution range. This range would be increased to around 1500 meters using a light aircraft as a test target.

Using a light aircraft, such as a Cessna 172, for a test target is highly recommended for flight tests. As the RCS of all targets are statistical, there is essentially no difference between a bird, drone, or light aircraft target other than flight path uncertainty. The probability of finding a four-pound bird target during a flight test is minimal. In contrast, numerous approach tests can be devised and their results tested using an aircraft target. It also provides a completely safe target approach as the S76 and Cessna pilots will have each other in sight and know their intentions.

As ground tests have already demonstrated the avian radar works as designed, the main purpose of the S76 flight tests are to obtain information on the impact of ground clutter and urban ISM band interference with respect to altitude. This information would be useful going forward in estimating the ability of any new target track processing algorithms to eliminate interference.

## 15 Conclusions

- The challenge of providing a method of preventing bird strikes on rotorcraft was investigated.
- Avian radar was selected as one of the main technologies to prevent bird strikes day or night in haze, fog, and rain as radar will operate in all these environments.
- A concept was devised to in which a single forward-looking radar antenna could be used to measure target range and Doppler velocity, based on the observation that the intensity and Doppler velocity of on-boresight targets are constant as the aircraft approaches the target. Both these values decrease for off-boresight targets. This fact provides the method by which to determine the collision threat of detected targets.

- Simulations using Matlab were written to investigate and prove that the on/off boresight target detection method of bird strike avoidance was practical and would work.
- Ground clutter was investigated and simulations using Matlab were written to understand its characteristics and magnitude on flights over various terrain. Simulations indicate higher flight altitudes markedly reduce the effect of ground clutter on airborne target threats since the Doppler velocity of dangerous boresight targets will always exceed the lower Doppler velocities of ground clutter. These studies also verify that by implementing a narrow beamwidth yagi antenna that can be tilted up at low altitudes further mitigates the ground clutter problem.
- Possible bird-strike evasion techniques upon target detection were postulated. The most conservative maneuver is to make a short duration course correction upon target detection. The philosophy being that any airborne target ahead of the aircraft is cause for concern.
- The optimum radar frequency for an avian radar was investigated and a search was conducted to find its availability. The ISM band frequency of 2450 MHz was found and selected as no authorization or restrictions (except for out-of-band emissions) were required for Federal use.
- Segmented coherent binary PN coded pulse compression was determined to be the optimum radar signal for this avian radar because it has both superior range and Doppler resolution. This gives the radar the capability to simultaneously separate and display multiple targets of different ranges and Doppler velocities.
- Target range performance based on key radar parameters such as antenna gain, frequency, pulsewidth, pulse power, and processing gain were simulated and plotted to estimate the MDS for various target RCS.
- Top-level hardware and processing block diagrams, to implement the planned avian radar concept, were designed, as were block diagrams for each of the high-level blocks.
- The mechanical structure of the RTA was designed based on the planned substitution of the P650 weather radar in the FAA S76 helicopter radome. Off-the-shelf RF components were selected to fit within the P650 installation space.
- An ADC evaluation board and a FPGA evaluation board were selected. These boards were custom fitted into the ADC/FPGA enclosure, which contained user-controlled toggle switches to power the RTA and select radar resolution pulsewidths.



- A powerful high-end laptop PC was selected to develop the FPGA code and for the radar display using Matlab.
- The required extensive processing and display requirements were successfully implemented in very high-speed integrated circuit (VHSIC) hardware description language (VHDL) code in the FPGA evaluation board and in Matlab code on the laptop PC.
- The avian radar was extensively ground tested both statically and dynamically using live road traffic, a Mavic Air drone, and conductive balloons.
- In conclusion, the design concept of the implemented avian radar worked as expected in that the range and Doppler velocity of multiple targets at different ranges and velocities could be simultaneously measured and displayed.

## 16 Lessons learned

It is always useful to look back on a completed project and examine what might have been done differently. Here are a few things that come to mind.

It is debatable as to whether it was worth the effort to have designed the RTA to fit in a form factor that allowed it to fit in the radome. This is especially true since late in the program it had to be placed in the cabin anyway. On the one hand, the small size of the RTA made it easy to transport to different locations for ground testing. However, placing it in a rectangular multi-shelf equipment rack would have been much easier to construct and tweak the RF components.

In hindsight, it might have been worthwhile to have spent more effort exploring the time and cost required to have a custom pulsed HPA developed. The CW HPA we chose was immediately available, protected from over, under, and reversed voltage, and it tolerated any load impedance so it was nearly indestructible. However, its high noise floor was not anticipated nor specified. Much effort was expended tracking down the source of the initial low radar sensitivity due to HPA noise during the RX period, and finding a solution. The only solution was to insert a high power TX/RX switch prior to the circulator, which dropped the 10+ watt HPA power to about 3 watts into the antenna cable.

Although it worked quite well, designing a 50ns wide pulsed modulator was quite difficult to construct. This would have been another component to have farmed out to a vendor who had access to microwave layout tools, board material, and measuring equipment.

Selecting an equipment rack and pulsed HPA initially would have saved a lot of project time and grief. Although it would have been hard to commit to an expensive custom development of a pulsed HPA early in the project, in the end we would have had an approximately 100-watt RF output instead of a 3-watt output.

Perhaps the lesson going forward for any R&D project is to believe in the paper design, bite the bullet and farm out critical parts, and construct the proof-of-concept hardware as conveniently as possible. The initial hardware will always be modified somewhat prior to production anyway based on prototype experience and performance. Therefore, the goal of the prototype should be to simply verify the overall concept.

## 17 Path to production

Assuming there is a market need/desire for a rotorcraft/aircraft avian radar for birdstrike and drone collision avoidance, here are the necessary design steps required.

1. Select an obtainable radar frequency, which allows a segmented coherent binary PN coded pulse compression transmit pulse. The fact that the average transmitted RF energy is only 0.5% of its peak energy and is spread over a 40 MHz bandwidth might allow it to either remain where it is in the ISM band or in some other slightly higher frequency band. Without very sensitive and specialized equipment, the transmit signal would not even be detectable at altitude. Therefore, interference to others is negligible.
2. The RF components of this prototype (amplifiers, filters, etc.) were implemented using SMA cable connected Mini-Circuits parts. Using their same uncased parts on a custom printed wiring board (PWB) would shrink the size and price of the RF board by an order of magnitude. The same is true for the ADC and FPGA parts with respect to the evaluation boards.
3. Select a display depending on the target aviation market. Send display data to an aircraft data bus for viewing on an electronic flight information system (EFIS) or multifunction display (MFD). For light general aviation aircraft, display targets, and alerts on a smartphone. There are many options for display between these two aircraft extremes.
4. Determine the type and location of the antenna. A yagi antenna has the smallest forward cross section, which could be easily tilted for ground clutter reduction.

In a related Origo project, segmented coherent binary PN coded pulse compression technology is being applied to ground based drone detection in which range/Doppler target data is converted to

X,Y location coordinates. Applying this new technology to avian radar would allow displaying detected targets as range and offset from the aircraft's line of travel, making the display more interpretive.

As aviation and RF emissions are highly regulated, an implementation consensus is the first and most important task of any airborne avian radar.

.

## 18 References

Piesinger, G. H. (2008). *U.S. Patent No. 7382310*.

# A Appendices

## A.1. HIGH-LEVEL VIEW OF THE DOPPLER RADAR PROCESSING

The radar signals are processed by two modules (see Figure A1):

- An FPGA that receives digitized samples of the radar signal from an ADC and produces an  $R \times S$  array of values representing the return signals for targets at each range and speed.
- A PC running a MATLAB program that receives the array over a serial link and generates a two-dimensional display depicting the presence/absence of targets at each range and speed.

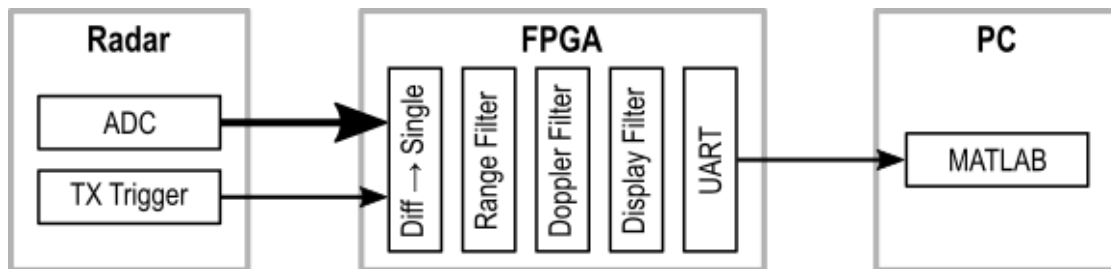


Figure A-1. High-level view of the Doppler radar processing

## A.2. FPGA RADAR PROCESSING

The following sequence of processing steps is performed by the FPGA on the radar signals:

- The differential ADC and TX trigger signals are converted into single-sided signals. Also, a 392 MHz signal is extracted from the ADC data-ready (DRY) signal and used as the clock source for further processing. The range filter processes the ADC values to detect the occurrence of a 98 MHz pulse (I) and its 90°-delayed replica (Q), indicating a return signal from a target. The detection is performed on a window of 20, 40, 80 or 160 ADC samples and quantizes the time of occurrence for the pulse into one of up to 196 range bins that indicate the distance of the target from the radar emitter. The I and Q values for each range bin are passed on to the Doppler filter.
- The downshifter synchronizes the I and Q signals from the range filter clocked at 392 MHz to the lower 98 MHz clock frequency used in the following steps.

- The Doppler filter compares the I and Q range filter outputs to a set of cosine waves with frequencies proportional to various target speeds. The set of  $R$  I and Q values from the range filter will be expanded into an  $R \times S$  array where each element corresponds to the target intensity at a range  $r$  having an approach speed of  $s$ .
- The CORDIC processor calculates the magnitude of each I and Q pair from the Doppler filter.
- The logarithm module computes the base-2 logarithm of the magnitude output by the CORDIC processor.
- The display filter collects the  $R \times S$  values into a *frame of pixels*. It buffers the twenty most-recent frames and outputs another  $R \times S$  frame where each pixel is the best representation of the corresponding pixels across the entire buffer.
- Upon receiving a request from the PC to send a frame of pixels, the gather-dump module retrieves the most-current filtered frame from the display filter and sends  $R \times S$  values to the PC over a UART-driven serial line.

The VHDL code for the FPGA radar processor is distributed across these files:

- `top.vhd`: Top level of FPGA radar processing module.
  - `frontend.vhd`: Converts differential ADC and trigger signals to single-ended signals and generates a 392 MHz clock.
  - `pulse_stretcher.vhd`: Increases the duration of short pulses to make them more visible on an oscilloscope.
  - `processing.vhd`: Main processing block for the radar signals.
    - `range_filter.vhd`: Range filter.
    - `downshift.vhd`: Transfers the filtered data from the faster range filter to the slower Doppler filter.
    - `doppler_filter.vhd`: Doppler filter.
      - `cosine.vhd`: Generates the cosine values for the Doppler filter.
      - `data_distribute.vhd`: Distributes data from the range filter to the Doppler filter.
      - `data_funnel.vhd`: Distributes data from the Doppler filter to the CORDIC processor.

- `cordic/r2p_corproc.vhd`: CORDIC processor for computing the magnitude of the Doppler filter output.
  - `cordic/r2p_pre.vhd`: CORDIC filter preprocessor.
  - `cordic/r2p_cordic.vhd`: Main CORDIC algorithm.
- `log2.vhd`: Computes the logarithm of the Doppler magnitude output by the CORDIC processor.
- `display_filter.vhd`: Buffers twenty frames of range/speed data and outputs the most-significant, least-noisy value for each pixel.
  - `sorter.vhd`: Sorting module for selecting the appropriate pixel from each frame.
- `gather_dump.vhd`: Serializes the display-filtered frames and sends them to the PC.
  - `uart.vhd`: Serial transmit/receive module for communicating with the PC.

The above files make use of the code in these files:

- `common.vhd`: Common definitions/functions.
- `delay.vhd`: General-purpose delay module.
- `edger.vhd`: Generates an output pulse when an edge is detected on its input.
- `parameters.vhd`: Constants for setting the size/performance of the radar processing modules.

The following files are no longer actively used in the FPGA radar processor.

- `activity.vhd`
- `backend.vhd`
- `single_to_diff.vhd`

### A.2.1. FPGA RADAR PROCESSOR FUNCTIONAL BLOCKS

The I/O for the top-level of the FPGA radar processor is shown in Figure A2.

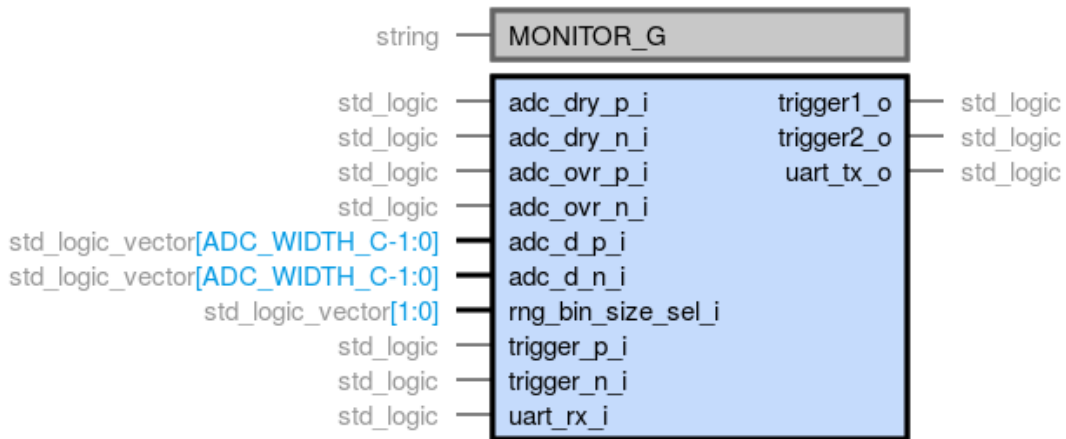


Figure A-2. Top-level of the FPGA radar processor

#### **adc\_dry\_[pn]\_i:**

Differential input that indicates when a sample from the ADC is available.

#### **adc\_ovr\_[pn]\_i:**

Differential input that indicates when the ADC has encountered a signal that is outside the range, which is convertible.

**adc\_d\_[pn]\_i:**

Differential input data bus that carries the digitized sample value from the ADC. The bus width is determined by the `ADC_WIDTH_C` constant that is defined in `parameters.vhd` with a value of 14 in the current implementation.

**rng\_bin\_size\_sel\_i:**

A two-bit input bus driven by two switches that indicates the number of ADC samples accumulated by the range filter. The number of samples for each switch setting is listed in Table A1.

Table A-1. Samples for each switch setting

<i>rng_bin_size_sel_i</i>	<i>#samples</i>
00	20
01	40
10	80
11	160

**trigger\_[pn]\_i:**

Differential input that indicates the start of the TX pulse, thus allowing the calculation of the target distance using the time difference between the ADC samples and this trigger pulse.

**trigger\_1, trigger2\_o:**

Two independent trigger outputs that can be used to monitor the operations of the FPGA.

**uart\_rx\_i, uart\_tx\_o:**

The UART receiver input that gets commands from the PC and the transmitter output that sends the  $R \times S$  frames to the PC.

The submodules in the processing pipeline are shown in Figure A3.



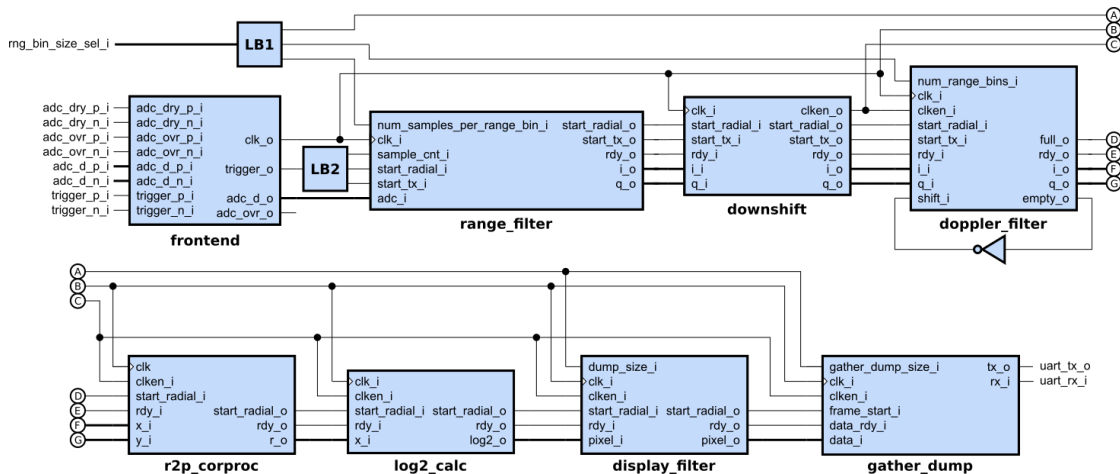


Figure A-3. Submodules in the processing pipeline

Each of these submodules will now be described.

#### A.2.1.1. Front End

The I/O for the frontend is depicted in Figure A4 and described below.

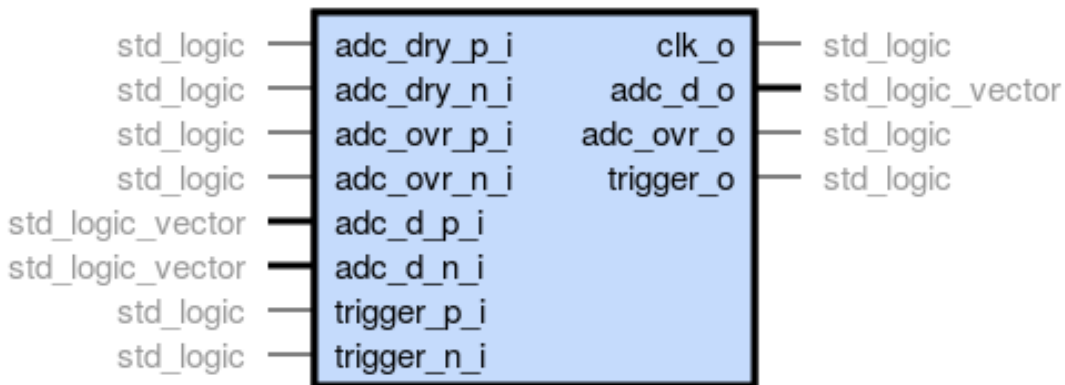


Figure A-4. I/O frontend

#### adc\_dry\_[pn]\_i:

Differential input that indicates when a sample from the ADC is available.

#### adc\_ovr\_[pn]\_i:

Differential input that indicates when the ADC has encountered a signal that is outside the range, which is convertible.

**adc\_d\_[pn]\_i:**

Differential input data bus that carries the digitized sample value from the ADC. The bus width is determined by the `ADC_WIDTH_C` constant that is defined in `parameters.vhd` with a value of 14 in the current implementation.

**trigger\_[pn]\_i:**

Differential input that indicates the start of the TX pulse.

**clk\_o:**

A 392 MHz clock output.

**adc\_d\_o:**

Single-ended output for the ADC sample value. A new sample is output on every rising edge of `clk_o`.

**adc\_ovr\_o:**

Single-ended output for the ADC over-range condition.

**trigger\_o:**

Single-ended output that indicates the start of a TX pulse.

Most of the front-end is composed of `IBUFDS` primitives that convert differential signals to their single-ended equivalents.

In addition, a Digital Clock Manager (DCM) is used to generate a clock from the ADC `DRY` signal (see Figure A5). `DRY` changes polarity every time a new ADC sample is available, so it is a 196 MHz square-wave. The DCM multiplies this frequency by two and shifts it in phase by  $330^\circ$  to create a 392 MHz clock whose rising edge is near the end of the time the ADC sample is valid, thus allowing adequate setup time.

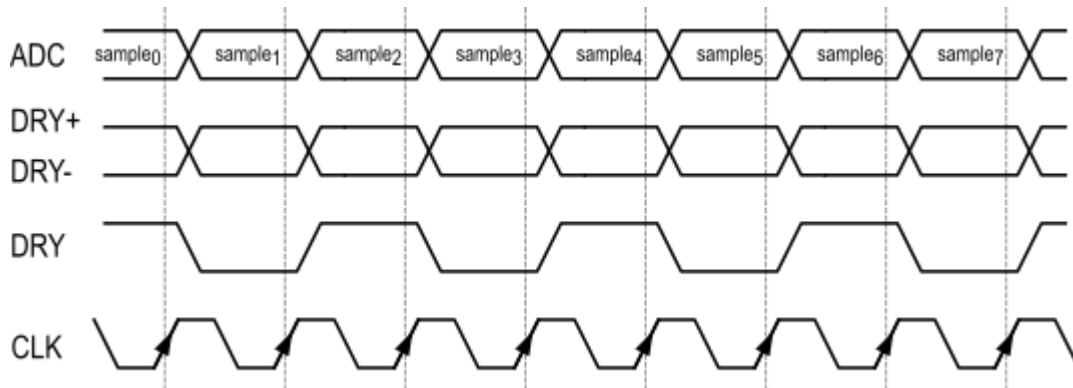


Figure A-5. DCM output.

### A.2.1.2. Range Filter

The range filter I/O is shown below:

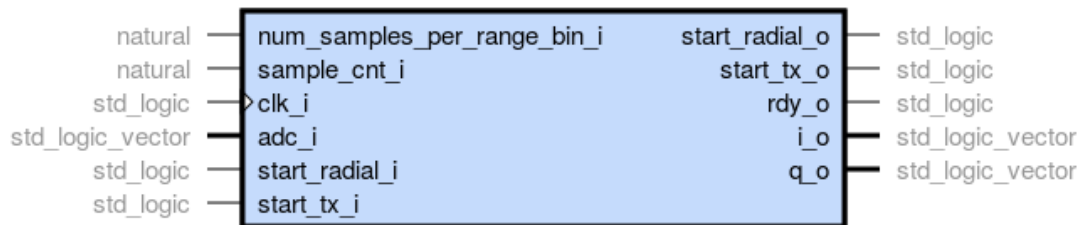


Figure A-6. Range filter I/O

#### **num\_samples\_per\_range\_bin\_i:**

This input bus selects the number of ADC samples that will be accumulated to determine the presence/absence of a target within a range bin that corresponds to a particular distance of the target from the radar transmitter. The allowable values are 20, 40, 80 and 160.

#### **sample\_cnt\_i:**

This input bus accepts the downward-counting index of the current ADC sample within a TX pulse consisting of 3920 total samples.

#### **clk\_i:**

The 392 MHz clock enters through this input.

**adc\_i:**

The ADC sample values enter through this bus.

**start\_radial\_i:**

A pulse with a duration of one clock cycle enters this input whenever a new frame of 1023 TX pulses begins.

**start\_tx\_i:**

A pulse with a duration of one clock cycle enters this input whenever a new TX pulse of 3920 ADC samples begins.

**start\_radial\_o:**

A pulse with a duration of a single clock cycle exits from this output whenever a new frame of filtered I and Q data begins.

**start\_tx\_o:**

A pulse with a duration of one clock cycle exits from this output whenever a new TX pulse of filtered I and Q data begins.

**rdy\_o:**

This output pulses whenever a new I and Q data value is ready.

**i\_o, q\_o:**

These output buses emit the filtered I and Q data from the range filter that indicate the presence/absence of a target in a particular range bin.

The range filter is built from two, nearly-identical kernels (shown below) that independently compute the I and Q values:

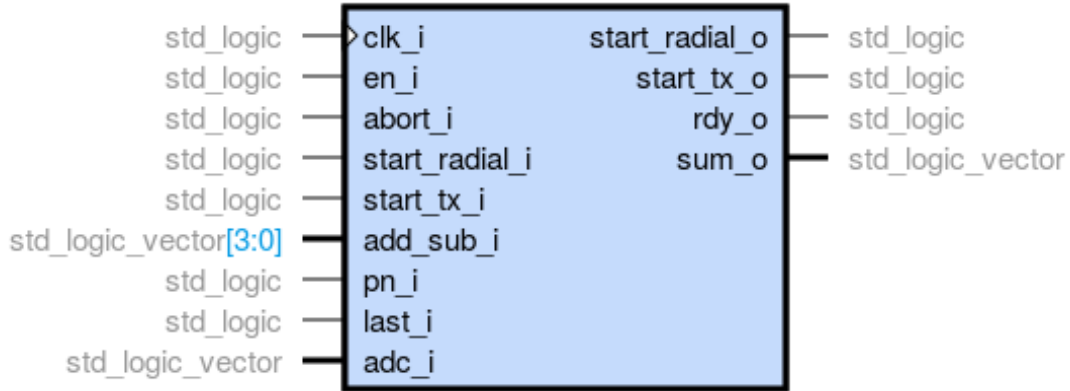


Figure A-7. Range filter kernel

Each kernel is composed of four, identical summation units:

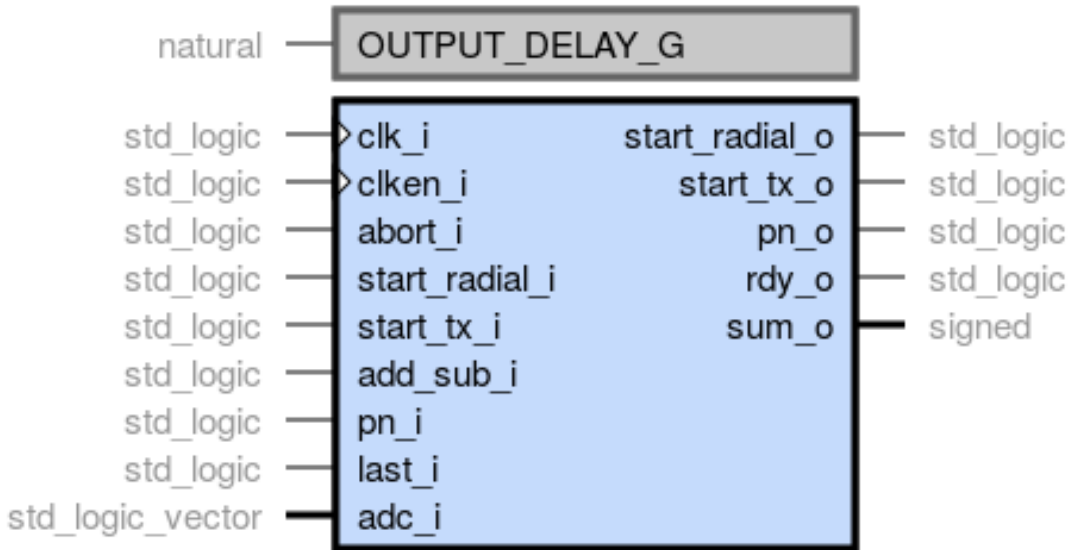


Figure A-8. Kernel summation unit

Below is a more detailed drawing of the kernel and its summation units:

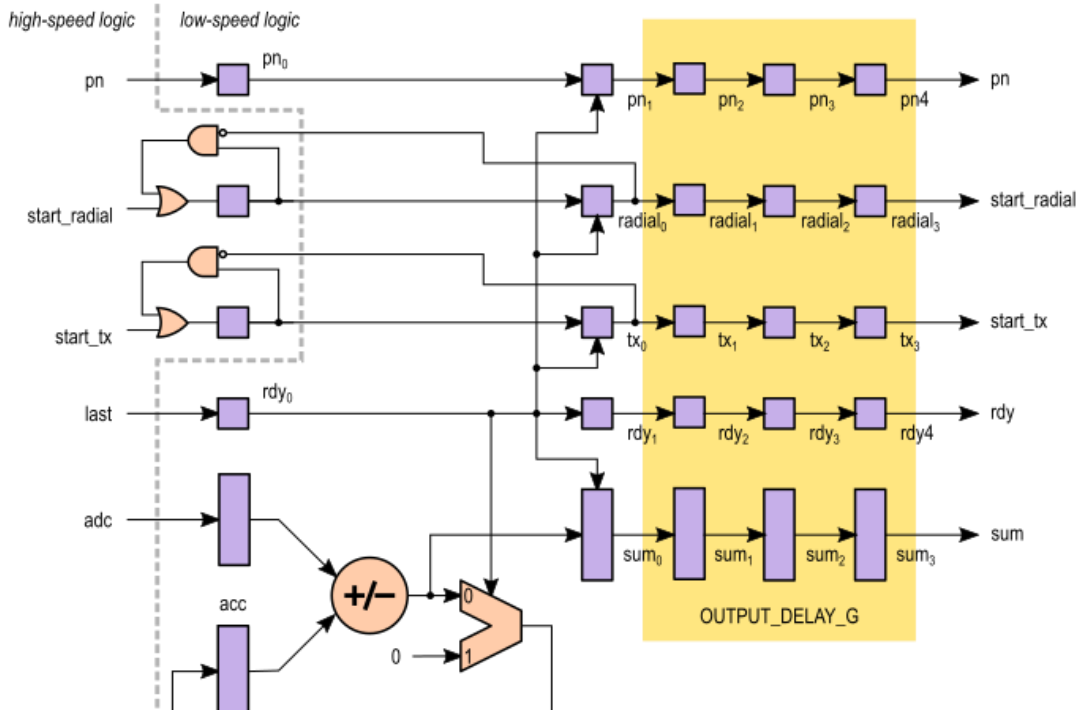
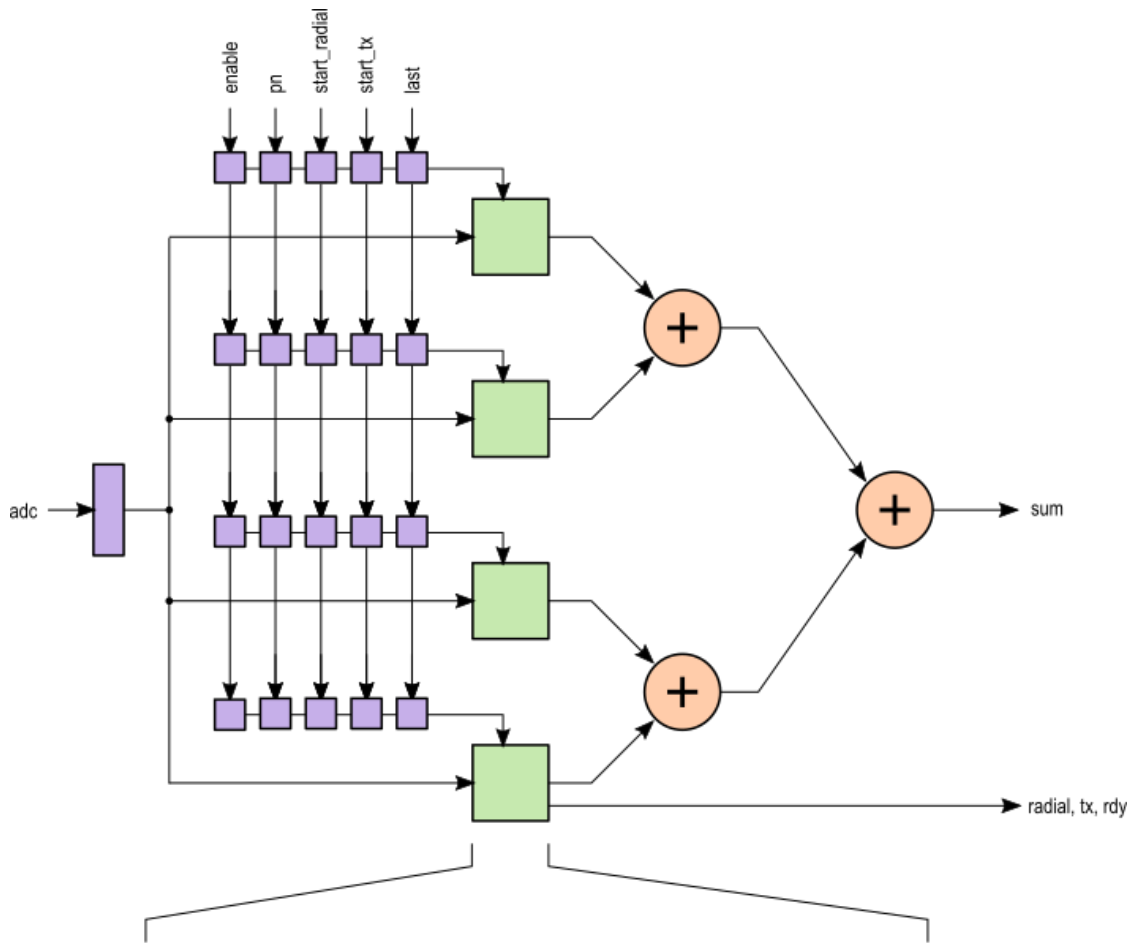


Figure A-9. Detailed kernel drawing

The range filter operates in the following manner:

1. A pulse on the `start_radial_i` input resets a 10-bit pseudorandom number generator (PNG) to the starting seed used by the TX pulse transmitter circuitry. The PNG outputs a new value whenever a pulse arrives on the `start_tx_i` input (i.e., whenever a new TX pulse starts). The least-significant bit (LSB) of the random number is used to set the polarity input (`pn_i`) of the filter kernels so they can scan for target returns with the same phase that was used by the transmitter.
2. A pulse on the `start_tx_i` input sets a counter that emits an enable pulse every four clock cycles. This enable pulse moves through a shift register that sequentially enables the four summation units on successive clock cycles.
3. When enabled, each summation unit accepts the current ADC sample and adds or subtracts it to its accumulator. In this way, the summation units can operate at a slower 98 MHz while handling the 392 MHz stream of ADC samples. The summation unit adds or subtracts based on the value of its `add_sub_i` input. For the kernel that computes the I output, the first two of its summation units add their ADC values to the accumulator, and the last two perform subtractions. Meanwhile, the Q kernel adds the first and fourth samples while subtracting the second and third.
4. When the required number of ADC samples have been accumulated (as determined by the value applied to `num_samples_per_range_bin_i`), the accumulators of the four summation units in each of the I and Q kernels are added together with the sign determined by the `pn_i` input to create the final I and Q outputs. Then the accumulators are cleared (as triggered by the `last_i` input to the summation units) and the summation units repeat the process. The I and Q values will be output at a rate of 19.6 MHz, 9.8 MHz, 4.9 MHz or 2.45 MHz depending upon whether the value of `num_samples_per_range_bin_i` is 20, 40, 80, or 160, respectively.

The following figures show the simulated output of the range filter when a single target travelling at 100 knots (kts) is 750 meters from the transmitter. Both I and Q outputs are sinusoids with a frequency of  $100 \text{ kts} \times 8.4 \text{ kts/Hz} = 840 \text{ Hz}$ .

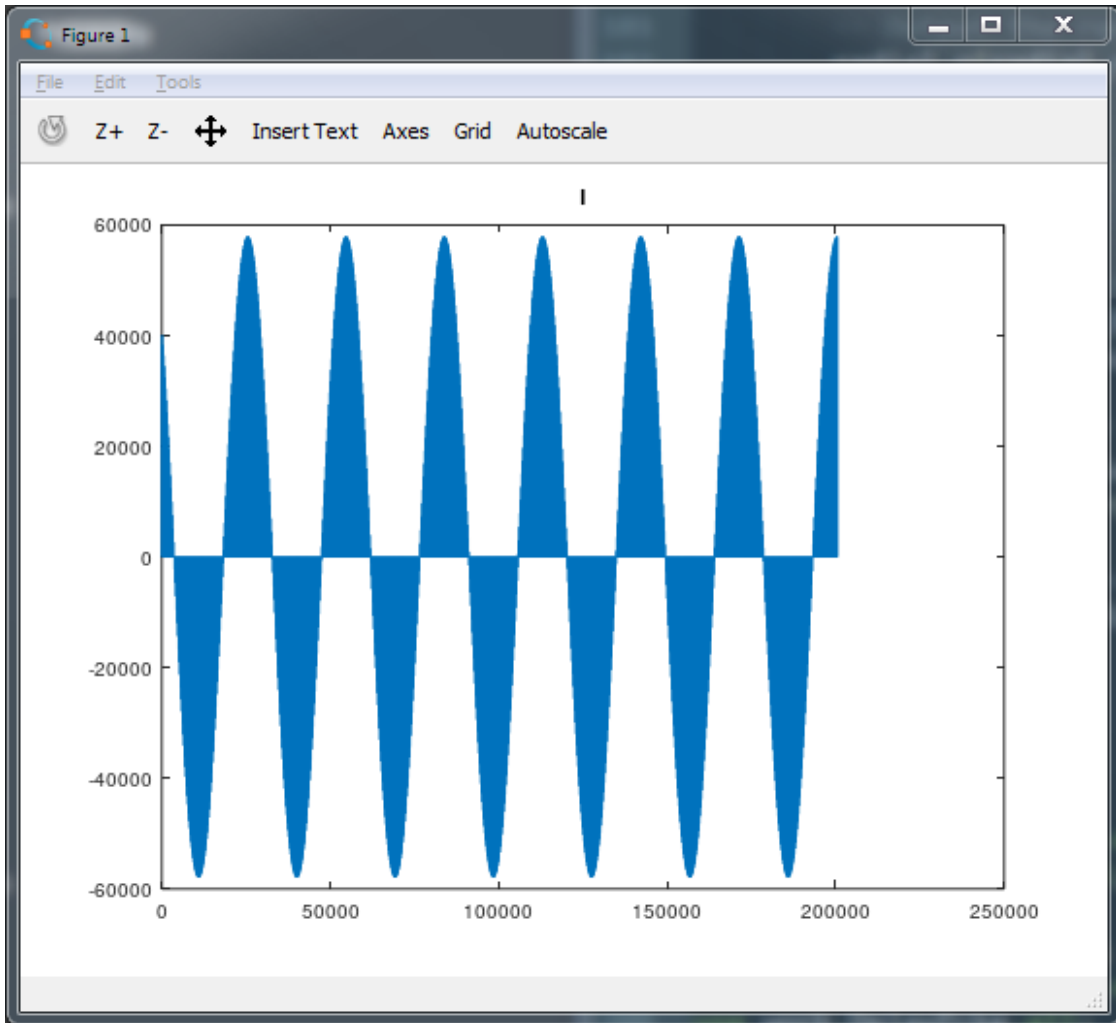


Figure A-10. Simulated output of the range filter



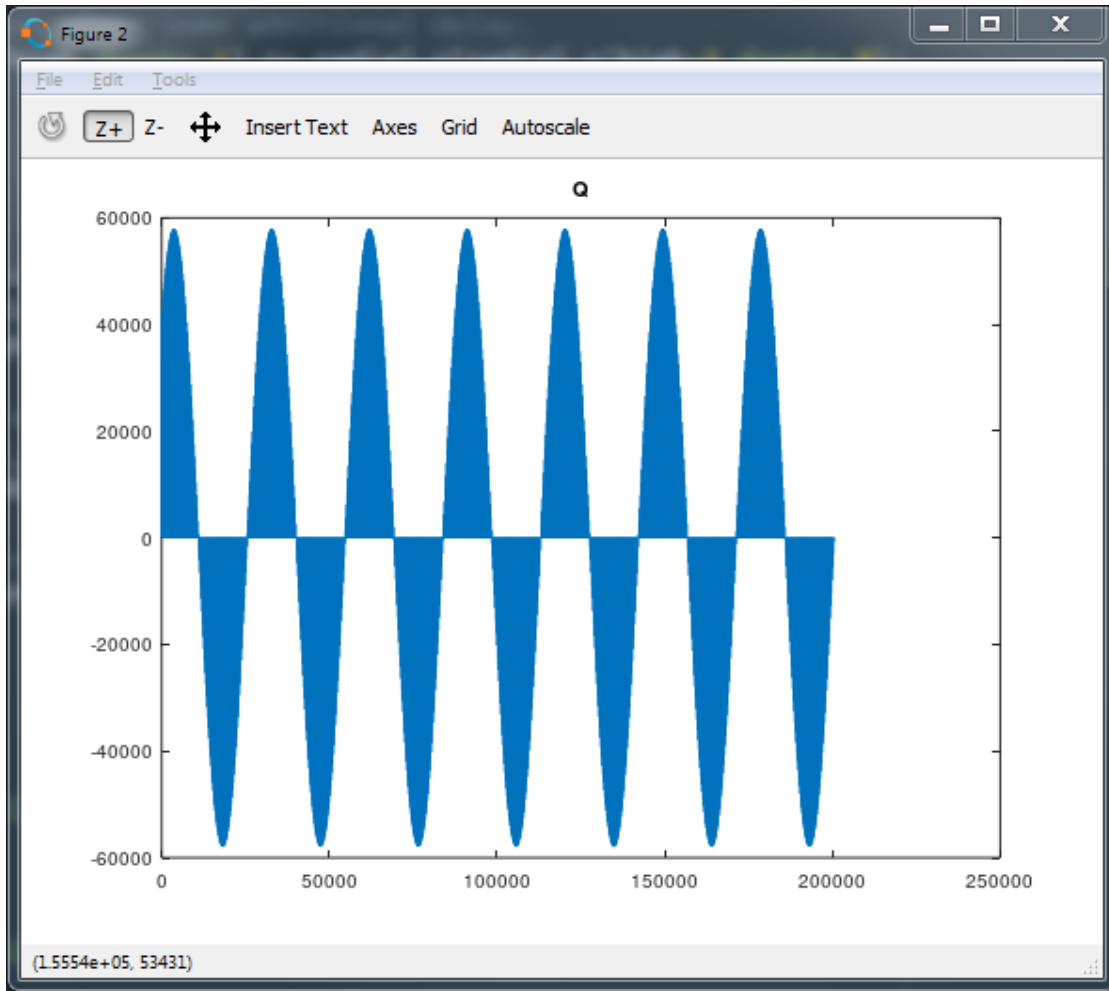


Figure A-11. Simulated output of the range filter

An expanded view of the Q sinusoid shows it is composed of impulses. These are the returns from the target at 750 meters which corresponds to range bin 98 of 196. The other range bin values are zero because no targets exist at those distances.

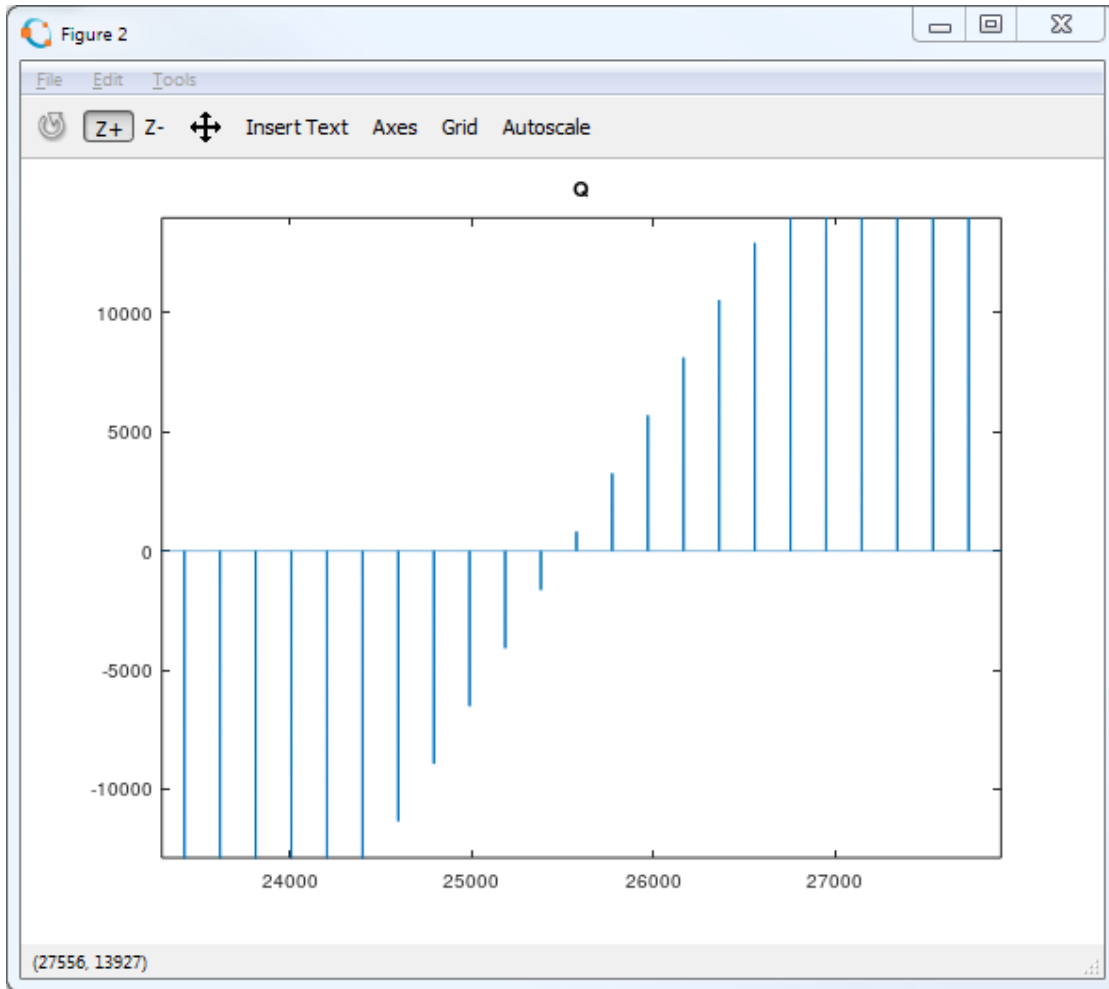


Figure A-12. Expanded view of the Q sinusoid

### A.2.1.3. Downshifter

Figure A-13 shows the I/O for the downshifter.

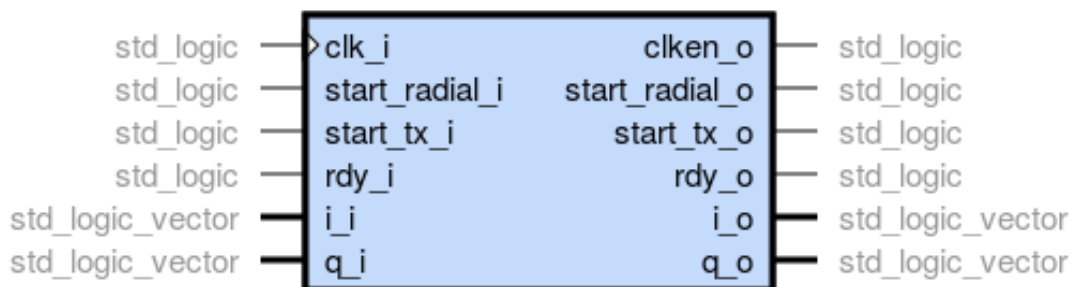


Figure A-13. I/O for downshifter

**clk\_i:**

The 392 MHz clock enters through this input.

**start\_radial\_i:**

A pulse with a duration of one clock cycle enters this input whenever a new frame I and Q data begins.

**start\_tx\_i:**

A pulse with a duration of one clock cycle enters this input whenever a new TX pulse of I and Q begins.

**rdy\_i:**

A pulse with a duration of one clock cycle enters this input whenever a new I and Q data value is ready.

**i\_o, q\_o:**

The I and Q data from the range filter enters through these buses.

**clken\_o:**

A pulse with a duration of one clock cycle appears on this output every DOWNSHIFT\_C clock cycles. DOWNSHIFT\_C is defined in `parameters.vhd` and has a value of 4. This clock enable is used to slow the processing of downstream modules from 392 MHz to 98 MHz.

**start\_radial\_o:**

A pulse exits from this output whenever a new frame of I and Q data exits from the `i_o` and `q_o` buses. This pulse is synchronized to occur when the `clken_o` output is active.

**start\_tx\_o:**

A pulse exits from this output whenever a new TX pulse of I and Q data exits from the `i_o` and `q_o` buses. This pulse is synchronized to occur when the `clken_o` output is active.

**rdy\_o:**

This output pulses whenever data is available on the `i_o` and `q_o` buses. This pulse is synchronized to occur when the `clken_o` output is active.

### **i\_o, q\_o:**

These output buses latch the I and Q data received from the range filter when `rdy_i` pulses.

#### *A.2.1.4. Doppler Filter*

The Doppler filter module has the following I/O:

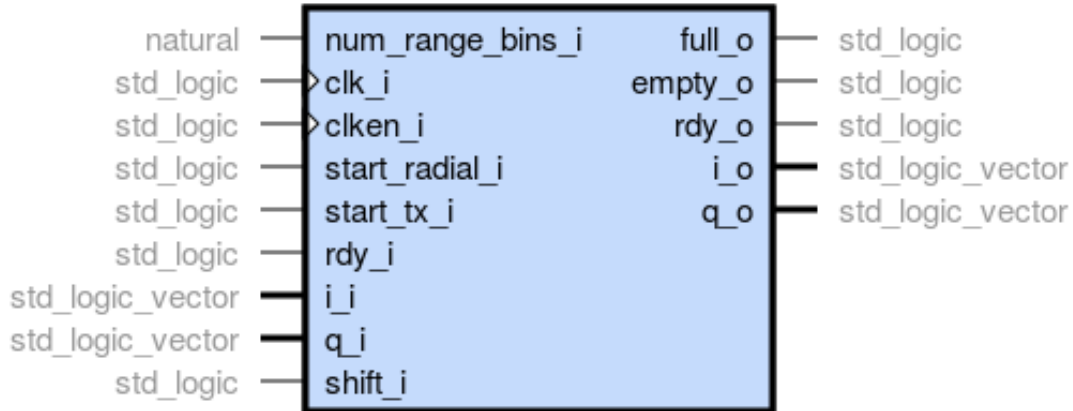


Figure A-14. Doppler filter module I/O

### **num\_range\_bins\_i:**

This input is used to set the number of range bins for a complete TX pulse. The allowable values are 196, 98, 49 and 24.

### **clk\_i:**

The 392 MHz clock enters through this input.

### **clken\_i:**

This input accepts the clock-enable signal that slows the Doppler filter processing to 98 MHz.

### **start\_radial\_i:**

A pulse enters this input to signal the beginning of a radial consisting of 1023 TX pulses.

### **start\_tx\_i:**

This input is driven by a pulse at the beginning of a new set of range bin values for the current TX pulse.

**rdy\_i:**

This input is pulsed when new I and Q values from the range filter are available.

**i\_i, q\_i:**

The I and Q data from the range filter enters through these buses.

**shift\_i:**

When active, this input causes the Doppler filter to transmit an  $R \times S$  array where each element indicates the presence/absence of a target having a given range and speed.

**full\_o:**

This output indicates when the Doppler filter has finished processing a complete  $R \times S$  array.

**empty\_o:**

This output goes active when the Doppler filter has finished transmitting a complete  $R \times S$  array.

**rdy\_o:**

This output is activated as each element from the array appears on the I and Q output buses.

**i\_o, q\_o:**

The I and Q data from the  $R \times S$  array exits the Doppler filter on these buses. The array exits in *column major order* where the entire range bin data from nearest to farthest for speed bin 0 is output, followed by all the range bin data for speed bin 1, etc.

The Doppler filter is built from two, identical processing pipelines (see Figure A-15) that independently compute the I and Q outputs:

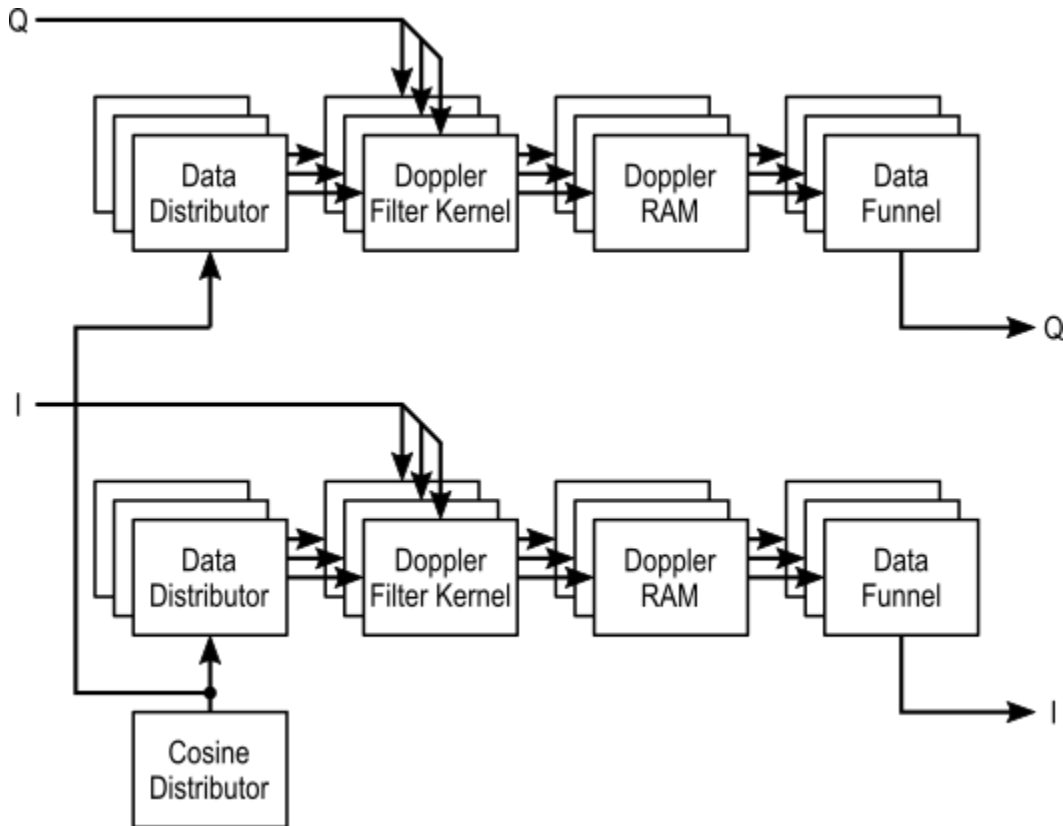


Figure A-15. Doppler filter processing pipelines

Each I and Q pipeline is composed of 160 individual pipelines, one for each possible target *speed bin* from 0 to 159 knots. The individual pipelines are composed of the following units:

- A *data distributor* that loads each pipeline with the value of a cosine wave at the current time and with a frequency related to the target speed associated with the pipeline.
- A *Doppler kernel* that multiplies the incoming I or Q range bin value with its cosine value and adds it to an accumulator for that particular I or Q range bin.
- A *Doppler RAM* that stores all the range bin accumulators.
- A *data distributor* that fetches the values from the RAM when it is full.

A more detailed depiction of the processing in the pipelines is given below in Figure A-16.

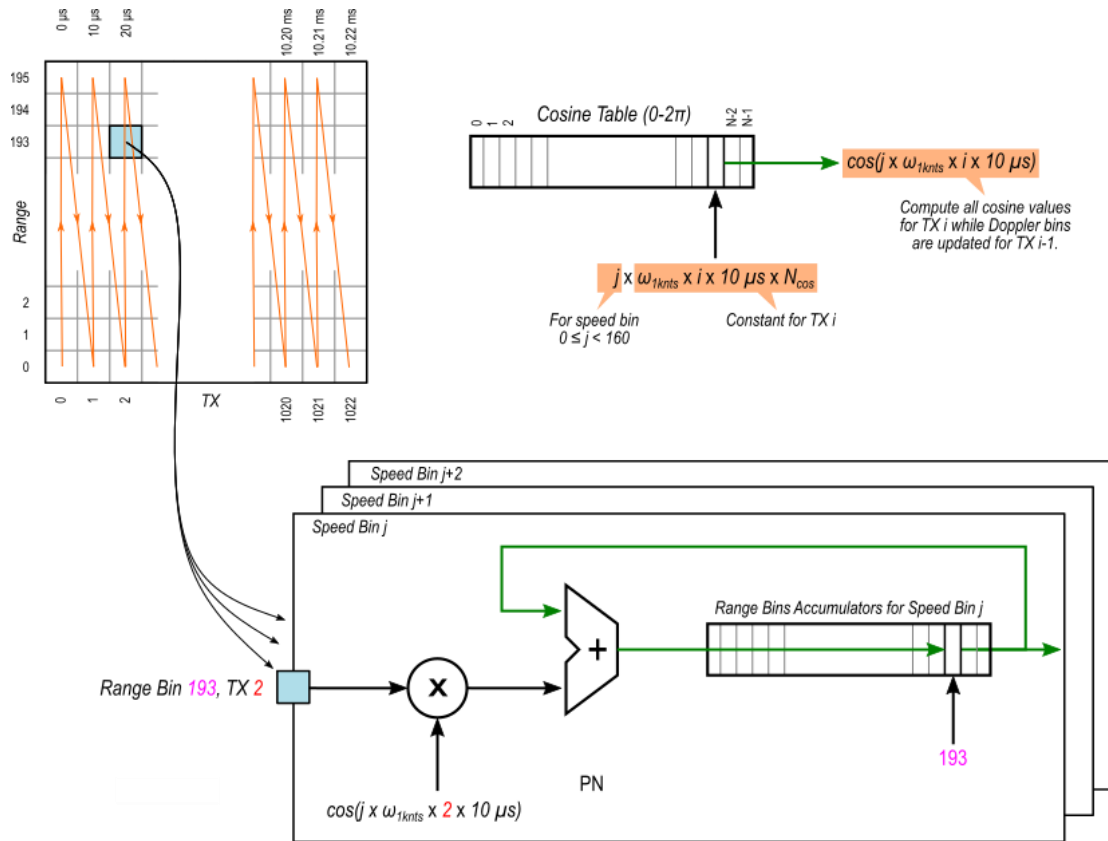


Figure A-16. Processing pipeline - detail

For each TX pulse, the range filter will output 196 values for the I and Q range bins (for the case where 20 ADC samples are processed per range bin). Each TX pulse takes  $10 \mu s$ , so the time for TX pulse  $i$  is  $10 \mu s \times i$ . Each Doppler kernel  $j$  is associated with a speed of  $j$  knots, which corresponds to a radian frequency of  $2\pi \times j \times 8.4 \text{ Hz/knot}$ . Using these values, each Doppler kernel is sent the value of a cosine at the current time for its particular frequency. The kernel will multiply each I or Q range bin sample  $k$  by this cosine value and add it to the accumulator at address  $k$  in the Doppler RAM. Once all 196 accumulators in each kernel are updated from TX  $i$ , then  $i$  is incremented and the process is repeated with TX pulse  $i + 1$ . After all 1023 TX pulses have been processed, the values in the Doppler RAMs are output through the data funnel. This is the  $R \times S$  array of I and Q values where each element corresponds to the target intensity at a range  $r$  having an approach speed of  $s$ .

The Doppler filter implementation discussed above would require 320 kernels, 160 for each of the I and Q signals. Since the range filter outputs data at a maximum rate of 19.6 MHz and the Doppler filter kernels run at 98 MHz, a single kernel can handle the computations for multiple

speed bins just by increasing the size of its connected RAM. The current implementation packs four speed bins in each kernel, reducing the total number of kernels to 80.

In addition, the entire Doppler filter can be sped up by overlapping the computation and distribution of the cosine values for TX  $i$  with the computation the kernels perform on TX  $i - 1$ . The only requirement is an extra register in each kernel to hold the cosine value for TX  $i$  while TX  $i - 1$  is being worked on.

#### A.2.1.5. CORDIC rectangular-to-polar module

The CORDIC module that computes the magnitude of the I and Q Doppler filter outputs has the I/O signals shown below:



Figure A-17. CORDIC module I/O signals

#### **clk:**

The 392 MHz clock enters through this input.

#### **clken\_i:**

This input accepts the clock-enable signal that slows the processing to 98 MHz.

#### **rdy\_i:**

This input is pulsed when new I and Q values from the Doppler filter are available.

#### **x\_i, y\_i:**

The I and Q data from the Doppler filter enters through these buses.

#### **start\_radial\_i:**

A pulse enters this input to signal the beginning of the  $R \times S$  array from the Doppler filter.



**rdy\_o:**

This output pulses when the value on the r\_o bus is available.

**r\_o:**

This bus outputs the magnitude of the values on the x\_i and y\_i buses such that  $r = \sqrt{x^2 + y^2}$ .

**start\_radial\_o:**

This output pulses when the  $R \times S$  array of magnitudes starts to exit on the r\_o output bus.

This module uses a standard CORDIC algorithm to convert rectangular coordinates  $(x, y)$  into polar coordinates  $(r, \theta)$ . Because only the magnitude  $r$  is needed, the  $\theta$  angle is not calculated.

*A.2.1.6. Logarithm module*

The module that computes the base-2 logarithm of the magnitude from the CORDIC module has the I/O shown in Figure A-18.

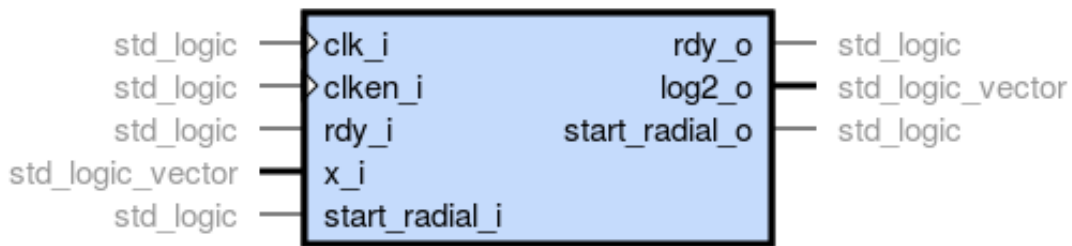


Figure A-18. Base 2 logarithm I/O

**clk:**

The 392 MHz clock enters through this input.

**clken\_i:**

This input accepts the clock-enable signal that slows the processing to 98 MHz.

**rdy\_i:**

This input is pulsed when a new magnitude value from the CORDIC module is available.

**x\_i:**

The magnitude value from the CORDIC module enters through this bus.

**start\_radial\_i:**

A pulse enters this input to signal the beginning of the  $R \times S$  array of magnitude values passing from the CORDIC module.

**rdy\_o:**

This output pulses when the logarithm on the log2\_o bus is available.

**log2\_o:**

This bus outputs an eight-bit, base-2 logarithm of the value on the x\_i bus.

**start\_radial\_o:**

This output pulses when the  $R \times S$  array of magnitude logarithms starts to exit on the log2\_o output bus.

This module uses a two-phase method to compute the logarithm:

1. The position  $p$  of the most-significant 1 bit in  $x_i$  is found. The value of  $p$  is embedded in the most-significant five bits of log2\_o.
2. The  $p - 1$  least-significant bits of  $x_i$  are used as an index into a lookup table that provides the three lower bits of log2\_o.

*A.2.1.7. Display Filter*

The display filter removes anomalously large target returns by comparing the twenty most recent  $R \times S$  frames and selecting the fifth-largest value at each pixel location.

The display filter module has the following I/O:

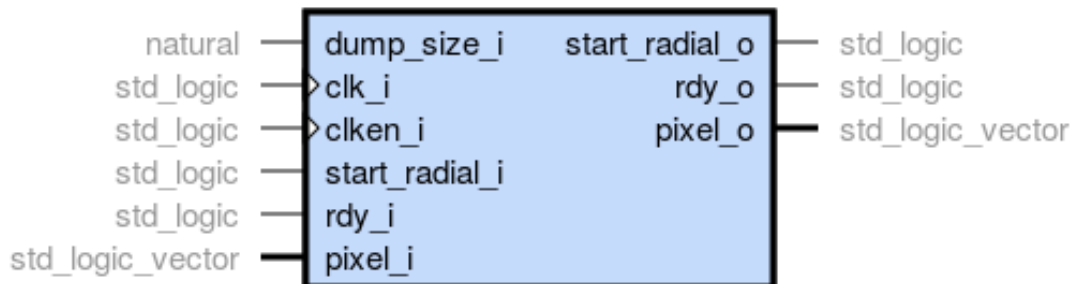


Figure A-19. Display filter module I/O

**dump\_size\_i:**

The number of elements in a  $R \times S$  frame of data enters through this input.

**clk:**

The 392 MHz clock enters through this input.

**clken\_i:**

This input accepts the clock-enable signal that slows the processing to 98 MHz.

**start\_radial\_i:**

A pulse enters this input to signal the beginning of the  $R \times S$  array of values passing from the logarithm module.

**rdy\_i:**

This input is pulsed when a new value from the logarithm module is available.

**pixel\_i:**

The value from the logarithm module enters here.

**start\_radial\_o:**

This output pulses when a filtered  $R \times S$  array of logarithms starts to exit on the `pixel_o` output bus.

**rdy\_o:**

This output is activated as each element from the array appears on the `pixel_o` bus.

**pixel\_o:**

The elements of the filtered  $R \times S$  array exit on this bus.

The display filter is built with two, linked finite state machines (FSMs):

- The first FSM maintains a set of the twenty most-recent  $R \times S$  arrays. As a new array enters from the logarithm module, it replaces the oldest array in the set.
- The second FSM is triggered whenever the first FSM finishes loading a new array into the set. Then the second FSM accesses pixel  $(i, j)$  from each array and sends them to a sorting circuit that selects the five largest values. The smallest of these five values is output on the `pixel_o` bus. This is repeated for every combination of  $i$  and  $j$ . The pixels

exit in column major order where the entire range bin data from nearest to farthest for speed bin 0 is output, followed by all the range bin data for speed bin 1, etc.

#### A.2.1.8. Gather-Dump

The gather-dump module I/O is as follows:

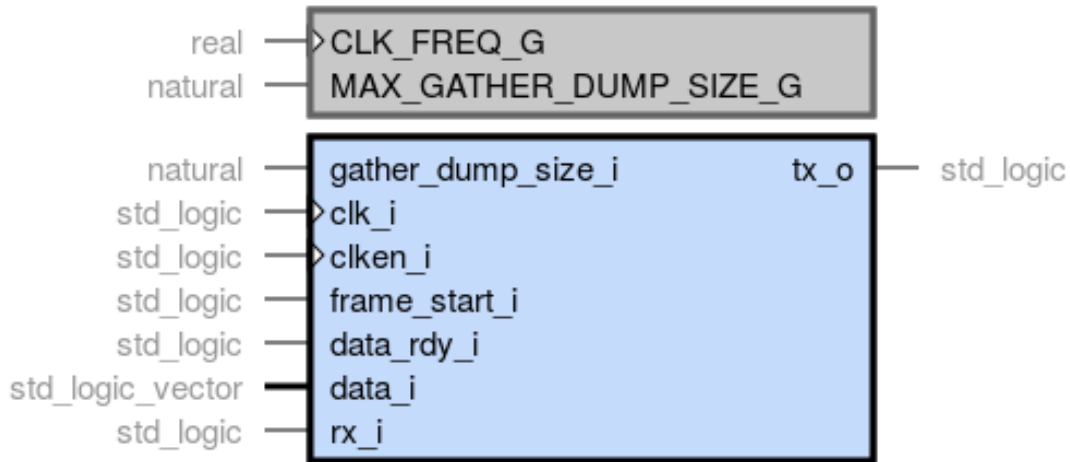


Figure A-20. Gather-dump I/O module

#### **CLK\_FREQ\_G:**

The effective clock frequency enters here and is used to set the timing for the UART that communicates with the PC. This value is typically the 392 MHz master clock frequency divided by the downshift factor.

#### **MAX\_GATHER\_DUMP\_SIZE\_G:**

The maximum size of the  $R \times S$  array is passed in here and is used to set the size of the RAM buffer.

#### **gather\_dump\_size\_i:**

The currently active size of the  $R \times S$  array enters this input and is used to determine when all the elements of a complete array have been received from the display filter.

#### **clk:**

The 392 MHz clock enters through this input.

**clken\_i:**

This input accepts the clock-enable signal that slows the processing to 98 MHz.

**frame\_start\_i:**

A pulse enters this input to signal the beginning of the  $R \times S$  array of values passing from the display filter.

**data\_rdy\_i:**

This input is pulsed when a new value from the display filter is available.

**data\_i:**

Pixels from the display filter enter through this bus.

**rx\_i:**

Serial commands from the PC enters through this input.

**tx\_o:**

Serialized element values from the RAM buffer are sent to the PC through this output.

The gather-dump module employs two FSMs to control a common RAM buffer and a UART:

1. When the gather FSM receives a “G” command sent from the PC over the serial link, it waits for the dump FSM (see below) to finish sending any data to the PC. After that, it waits for the display filter to pulse its `start_radial_o` output. Then the FSM gathers the values output by the display filter and stores them at sequential addresses in the RAM buffer until the count equals the value on the `gather_dump_size_i` input.
2. When the dump FSM receives a “D” command sent from the PC over the serial link, it waits for the gather FSM to finish collecting a complete array from the display filter. Then the FSM reads the data from sequential addresses of the RAM buffer and sends them to the PC through the UART.

### A.2.3. FPGA radar processor parameters

The following parameters defined in `parameters.vhd` control the configuration of the radar processing blocks:

**SAMPLING\_FREQ\_C:**

Sets the sampling frequency of the ADC (392 MHz).

**ADC\_WIDTH\_C:**

Sets the number of bits for the ADC samples (14 bits).

**F\_1KNT\_C:**

Stores the frequency shift caused by an object moving at 1 knot (8.402593 Hz/knt).

**DOWNSHIFT\_C:**

Sets the divider by which the downshift module reduces the processing rate for modules following the range filter (4).

**NUM\_TXS\_PER\_RADIAL\_C:**

This is the number of radar transmitter pulses that comprise a complete radial (1023).

**NUM\_SAMPLES\_PER\_TX\_C:**

This is the number of ADC samples taken during each transmit pulse (3920).

**MIN\_NUM\_SAMPLES\_PER\_RANGE\_BIN\_C:**

This is the minimum number of ADC samples contained in a range bin (20).

**MAX\_NUM\_SAMPLES\_PER\_RANGE\_BIN\_C:**

This is the maximum number of ADC samples contained in a range bin (160).

**MAX\_NUM\_RANGE\_BINS\_C:**

This is the maximum number of range bins within a single transmit pulse ( $\text{NUM\_SAMPLES\_PER\_TX\_C} / \text{MIN\_NUM\_SAMPLES\_PER\_RANGE\_BIN\_C}$ ).

**NUM\_DOPPLER\_BINS\_C:**

This is the number of distinct speeds the radar can distinguish (160).

**NUM\_DOPPLERS\_PER\_KERNEL\_C:**

This sets the number of speed bins computed by each Doppler kernel module (4). The total number of Doppler kernels will be  $2 \times 160 \text{ NUM\_DOPPLERS\_PER\_KERNEL\_C}$  since both I and Q channels must be processed. In addition, the maximum number of speed bins that

can be computed by a single kernel module within the interval between range filter outputs is  $\text{MIN\_NUM\_SAMPLES\_PER\_RANGE\_BIN\_C} / \text{DOWNSHIFT\_C}$ .

**RNG\_OUT\_WIDTH\_C:**

This is the number of bits in the range filter I and Q output buses. It is automatically set to be wide enough to hold the summation of ADC samples for the maximum number of samples within a range bin.

**COSINE\_WIDTH\_C:**

This is the resolution of the cosine values used in the Doppler filter (10 bits).

**DOPPLER\_OUT\_WIDTH\_C:**

This is the number of bits in the Doppler filter I and Q output buses. It is automatically set to be wide enough to hold the summation of range filter outputs for an entire radial of  $\text{NUM\_TXS\_PER\_RADIAL\_C}$  TX pulses.

**CORDIC\_OUT\_WIDTH\_C:**

This is the number of bits in the CORDIC processor output bus. It is automatically set to be the width of the Doppler module output plus two.

**LOG2\_OUT\_WIDTH\_C:**

This is the number of bits in the output bus of the logarithm module. It is set to eight bits to give enough resolution for target return intensities while being small enough to transmit serially and still meet the display refresh rate that was desired.

**DISPLAY\_PIXEL\_WIDTH\_C:**

This is the width of the pixels stored in the  $R \times S$  frames of the display filter. It is the same width as the output of the logarithm module.

**NUM\_DISPLAY\_RADIALS\_C:**

This sets the number of radials (frames) the display filter buffers (20).

**DISPLAY\_RANK\_C:**

This sets the rank of the selected pixel in the sorting output. A setting of 5 means the fifth-largest pixel will be output from the set of twenty pixels at the same  $(i, j)$  position across all twenty frames in the buffer.

**MAX\_DISPLAY\_SIZE\_C:**

This sets the number of words of RAM that are allocated for storing the display filter buffer. It is automatically calculated from the product of the number of range bins, Doppler bins, and display filter frames.

**DISPLAY\_ADDR\_LEN\_C:**

This sets the number of bits in the address register for the display filter frame buffer. It is automatically calculated from the base-2 logarithm of the MAX\_DISPLAY\_SIZE\_C parameter.

**MAX\_DUMP\_SIZE\_C:**

This sets the size of the dump buffer that will be transferred over the serial link to the PC.

**DUMP\_ADDR\_LEN\_C:**

This sets the number of bits in the address register for the dump buffer. It is automatically calculated from the base-2 logarithm of the MAX\_DUMP\_SIZE\_C parameter.

**GATHER\_CMD\_C:**

This sets the received character that will initiate the gathering of a frame from the display filter into the dump buffer (“G”).

**DUMP\_CMD\_C:**

This sets the received character that will initiate the transmission of the dump buffer through the serial link to the PC (“D”).

**DATA\_RATE\_C:**

This sets the transmission rate for the serial link to the PC (921600 bps).

## A.3. MATLAB radar processing

The MATLAB script in the `view_doppler_2D.m` file displays the  $R \times S$  array received from the FPGA as a two-dimensional [pseudocolor plot](#) where each rectangular cell is assigned a color based on the target return intensity at that point.

### A.3.1. Script Processing

The following steps describe the overall operation of the MATLAB script:



1. The plotting area and interactive controls are initialized before the main loop begins.
2. To start the loop, the script sends a “G” character to the FPGA over the serial link to initiate a “grab” of the current range/speed returns.
3. Then the script sends a “D” to begin a “dump” of the  $R \times S$  array from the FPGA through the serial link. The array is received as a linear vector where the range bins for speed bin 0 are received first, then the range bins for speed bin 1, and so on until speed bin 159 is completed. Then the vector is reshaped into an array with  $R$  rows where each row corresponds to a specific target distance from the radar transmitter, and  $S$  columns where each column represents a specific target speed.
4. User-configurable masks are applied to the  $R \times S$  array to remove target returns at ranges and speeds that are considered irrelevant. Additional masks are also applied to amplify or attenuate the returns.
5. If enabled, a peak detector is applied that zeroes every element of the array except for the maximum return found in each range bin.
6. The pseudocolor plot window is updated with the transformed array and the loop is repeated. A configurable colormap determines the color according to the intensity of each target return.

#### *A.3.1. Initialization*

Upon initiation, the script does the following:

1. The various constants and data vectors/arrays are initialized
2. The GUI controls are instantiated and set to their default values.
3. A single  $R \times S$  array is read from the FPGA and the maximum value is used to set the range for the colormap axis.

#### *A.3.2. Array processing*

In the main loop of the script, each  $R \times S$  array undergoes these operations:

1. If a transmitter pulse width greater than 50 ns is used, the size of the received array will be  $N \times S$  where  $N < R$  because each range bin will be larger, thus reducing the total number of range bins in each transmission. Therefore, each range bin will be replicated several times to expand the array to the full  $R \times S$  size that occurs when the pulse width is 50 ns ( $196 \times 160$  for this particular combination of hardware/software).

2. The logarithmic values received from the FPGA are converted into linear values.
3.  $R \times S$  array is filled with the radar gain and distance-dependent STC gain values. Another  $R \times S$  array is filled with ones which are overwritten with zeroes depending upon the settings for the blanking regions. Then the received values are multiplied by these two matrices to apply the gain and blanking operations.
4. If the  $\sin x/x$  option is active, the maximum value in each row of the matrix is retained and all the other values are zero'ed.

### *A.3.3. Colormapping*

The colormap for coloring the target returns according to their intensities is derived as follows:

1. The threshold separating the white/green bands is held constant at 20%.
2. The threshold for each succeeding transition is increased by  $X$  dB where  $X$  is set interactively by the script user.
3. A 500-entry colormap is created. The initial 100 entries (20%) contain the RGB combination for the color white. The next  $n$  entries are loaded with green depending upon the difference between the white/green and green/yellow thresholds. And this process is repeated for each successive color band.

By loading a large colormap as described above, it ensures rapid color transitions from one band to another because the colors between adjacent map entries are only different at four locations. Since MATLAB does color interpolation for data that lands between colormap entries, this means that most colors will be strictly white, green, yellow, red or magenta (rather than some combination) because the adjacent entries will contain the same colors.

## A.4. Interactive controls

The behavior of the script is changed interactively using the following graphical controls.

### *A.4.1. Blanking Controls*

There are various sliders to blank areas of the pseudocolor plot, which may contain extraneous signals. See Figure A-21.

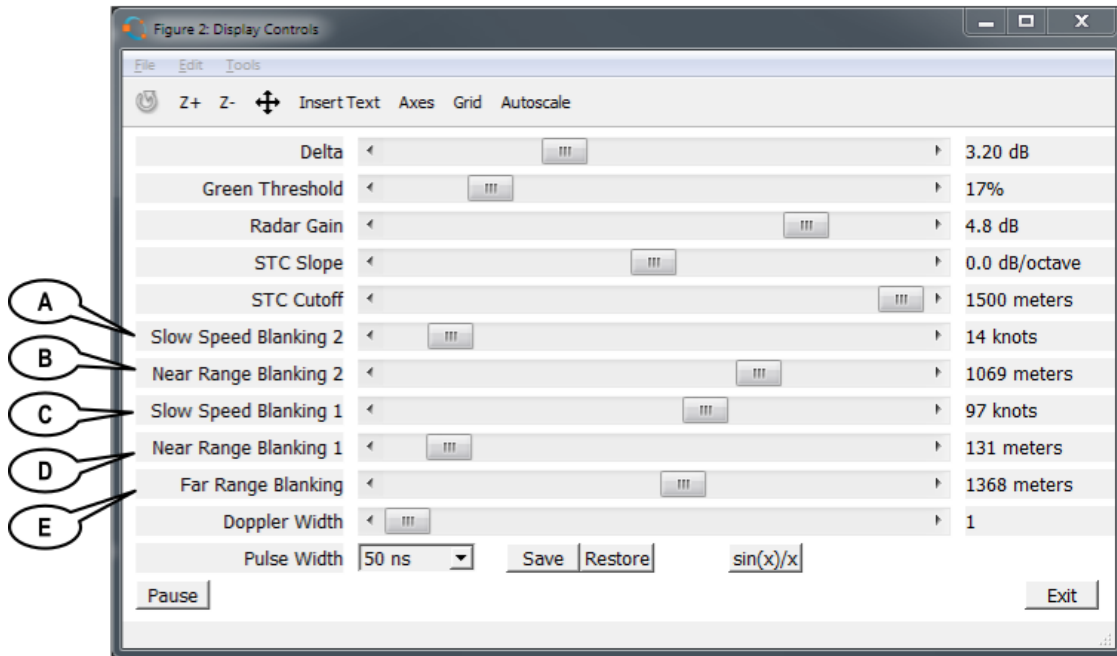
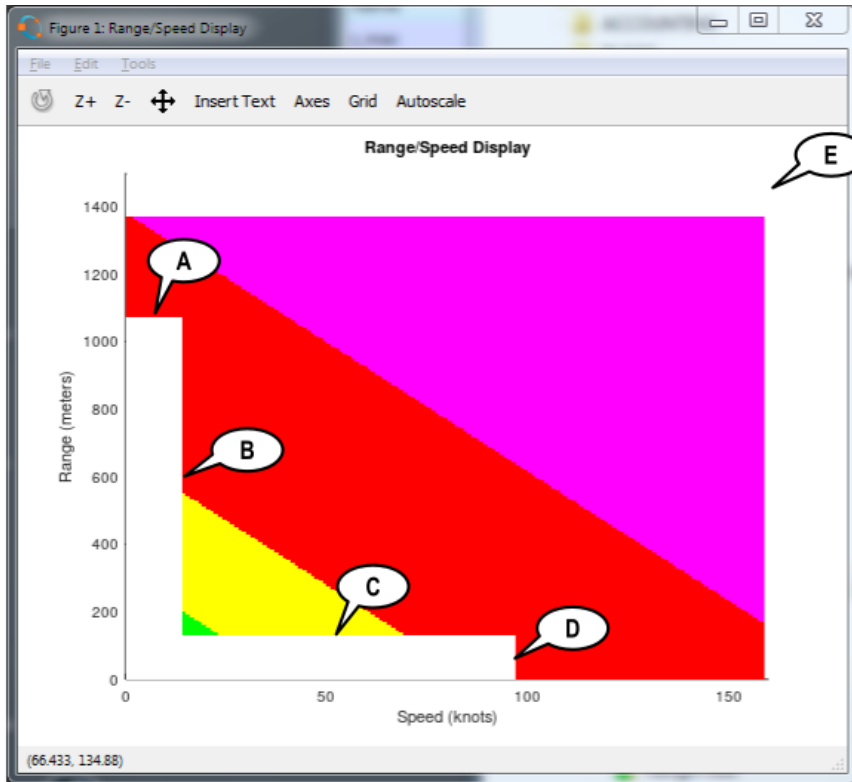


Figure A-21. Sliders controlling colorplot

**A, B:**

These sliders affect the width (A) and height (B) of a region that blanks targets moving slower than A meters/second at distances less than B meters. This is primarily intended to blank slow-moving targets.

**C, D:**

These sliders affect the width (C) and height (D) of a region that blanks targets closer than D meters and moving less than C meters/second. This is primarily intended to blank targets close to the transmitter.

**E:**

This slider affects the distance (E) at which targets will be ignored. This is intended to blank ground clutter at large distances.

*A.4.2. STC controls*

These sliders control the overall gain of the radar receiver as well as amplifying/attenuating the received signal at closer distances.

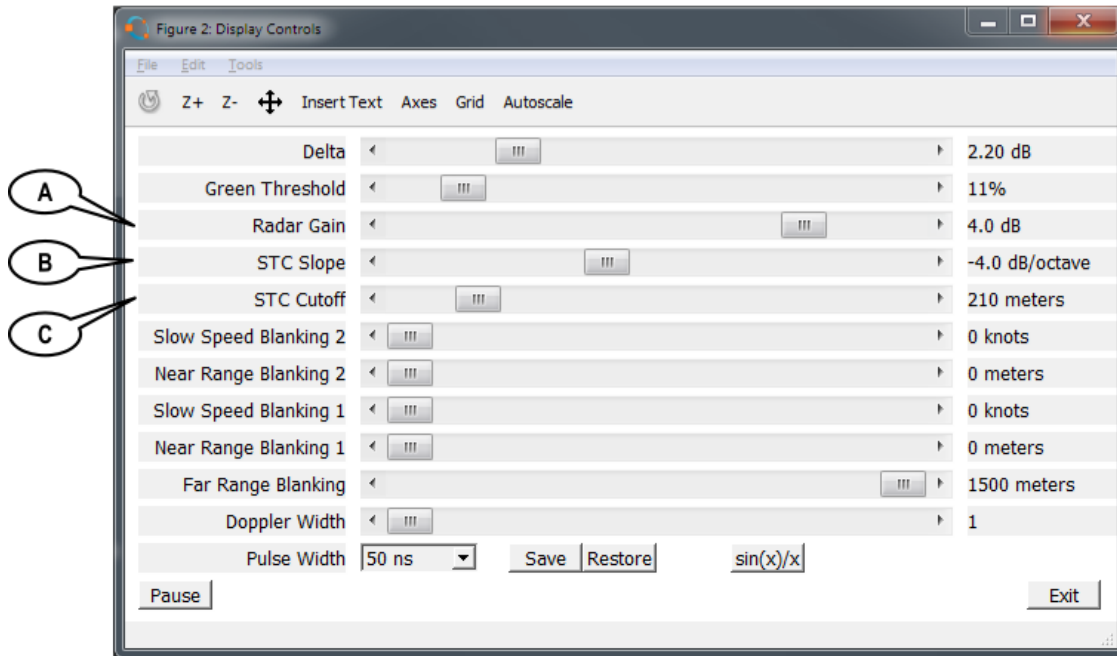
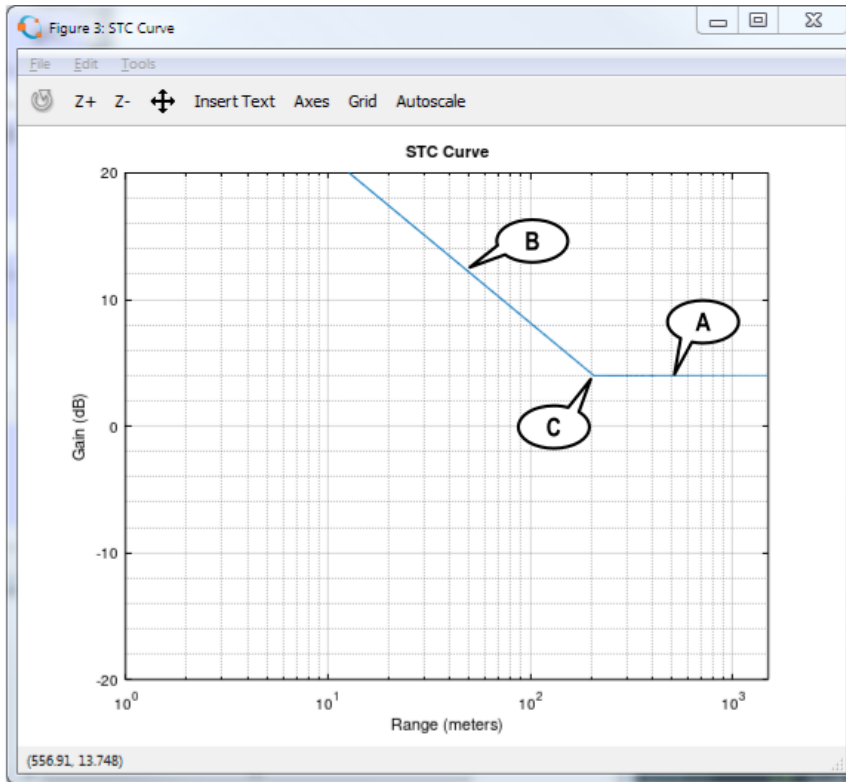


Figure A-22. STC controls

**A:**

This slider sets the overall gain of the radar to A dB. Higher values amplify received target signals, while lower values attenuate them.

**B:**

This slider controls a distance-dependent gain to received target signals. Positive slopes (B dB/decade) will cause increased attenuation the closer the target is, while negative slopes will apply increased amplification to closer targets.

**C:**

This slider controls the distance-dependent gain so that it is applied to all targets closer than C meters. At distances greater than C meters, all target signals are amplified by the overall gain (A).

*A.4.3. Color thresholds controls*

These sliders control color assignment for the level of received signals.

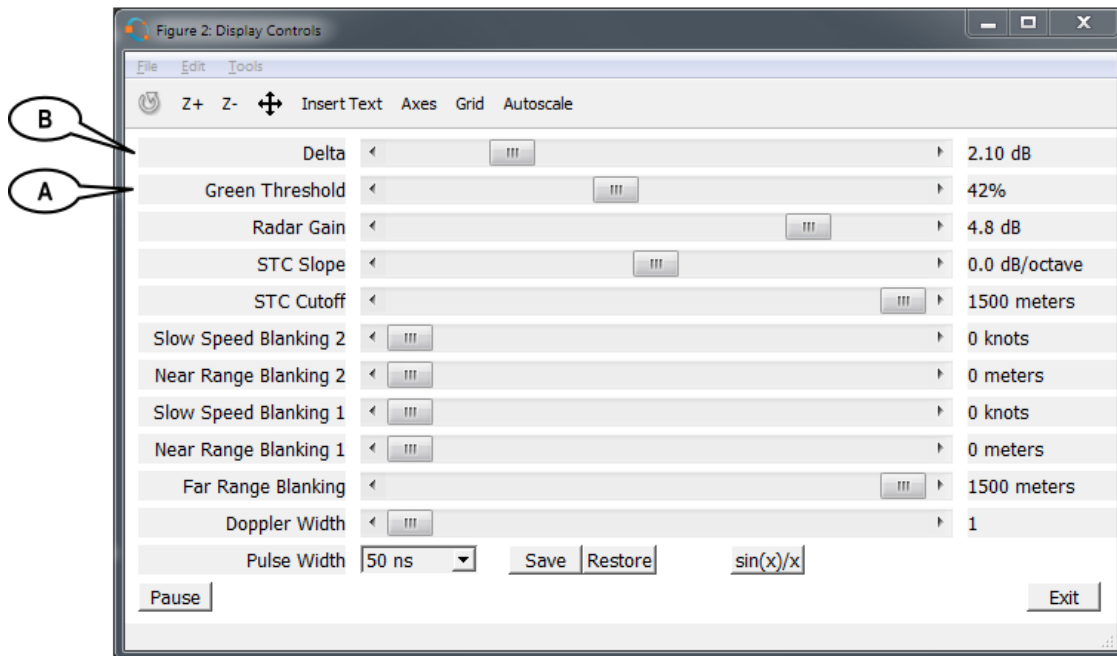
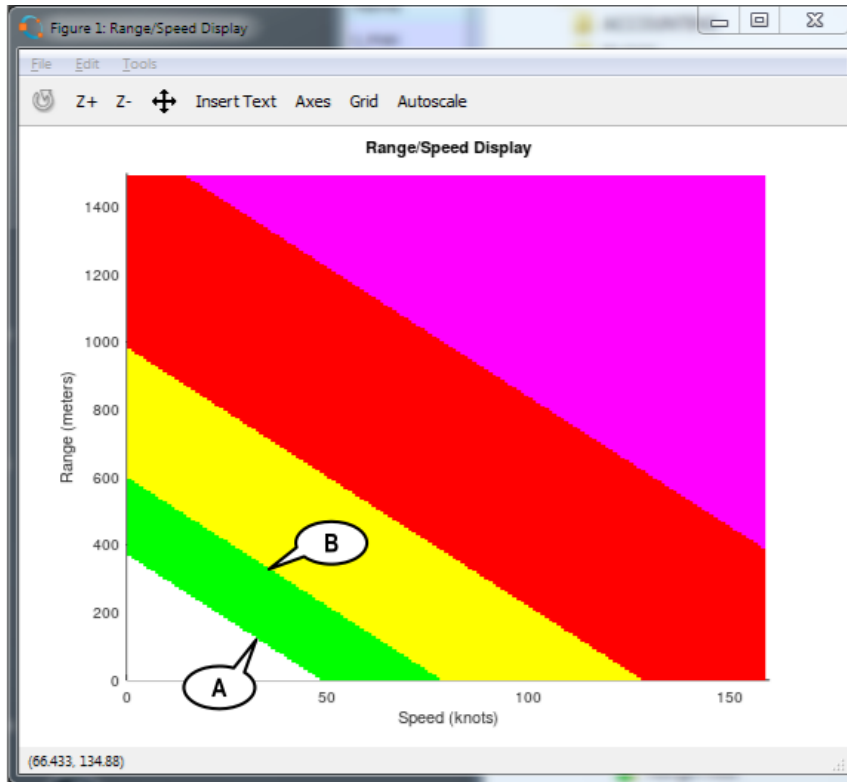


Figure A-23. Color threshold controls

**A:**

This slider sets the minimal threshold for target detection as a percentage (A) of the full-strength signal amplitude. Any received signal less than this will be colored white and will not be visible.

**B:**

This slider sets the change in threshold between the green, yellow, red and magenta color bands. The change in signal level between each color band will be approximately B dB.

*A.4.4. Sin(x)/x removal controls*

When the  $\sin x/x$  button (A) is off, the return signal from a real target will display a  $\sin(x)/x$  across  $x$  Doppler bins at the target distance. This leads to a maximum peak within a particular Doppler bin surrounded by lower levels in nearby bins.



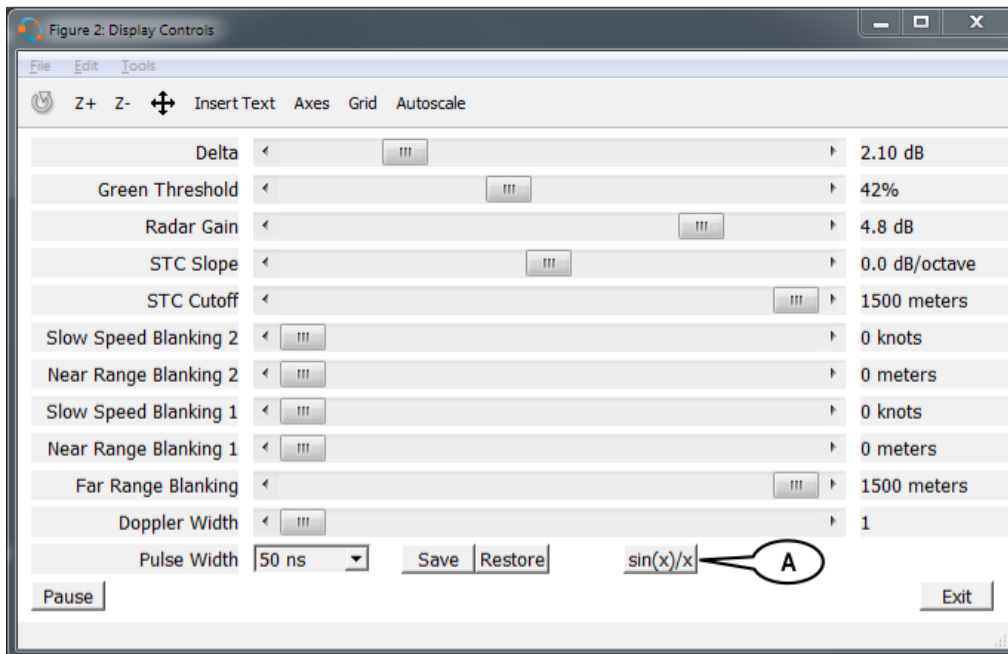
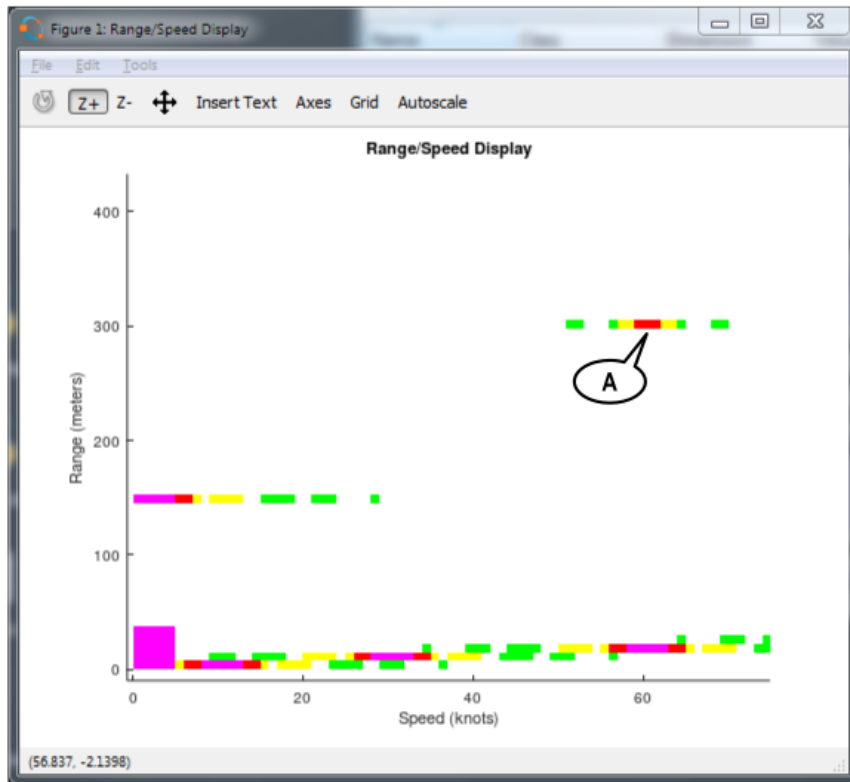


Figure A-24. Sin(x)/x removal controls

When the  $\sin x/x$  button is on (Figure A-25), every Doppler bin at each distance is zero'ed *except* for the bin with the maximum value. This tightens the target returns to a single bin as can be seen below.

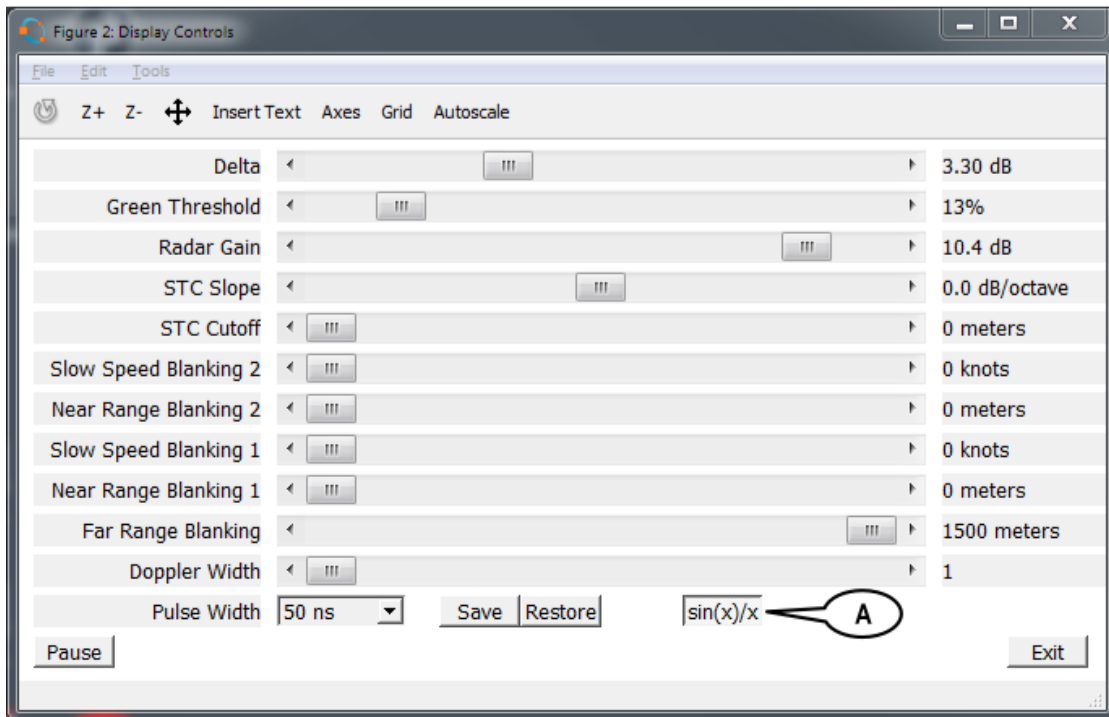
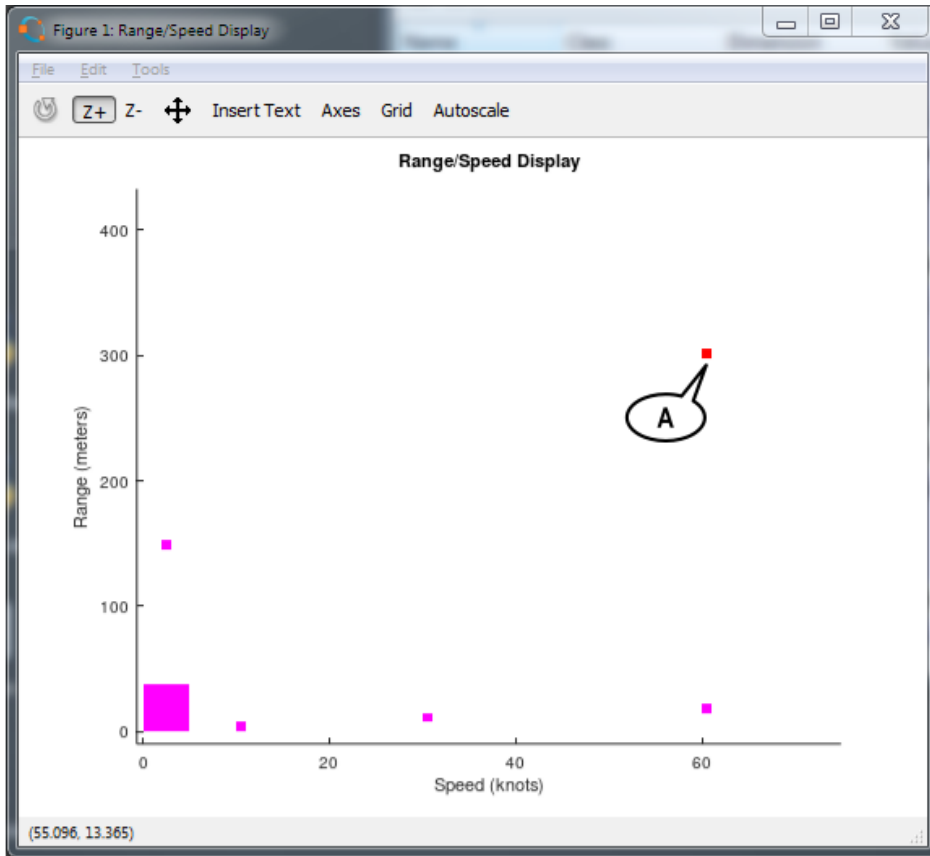


Figure A-25. Display when  $\sin(x)/x$  button is on

A target return restricted to a single Doppler bin can be difficult to discern (especially if it is colored yellow). The Doppler Width slider (A) increases the number of Doppler bins taken up by each target return, thus making them more visible (Figure A-26).

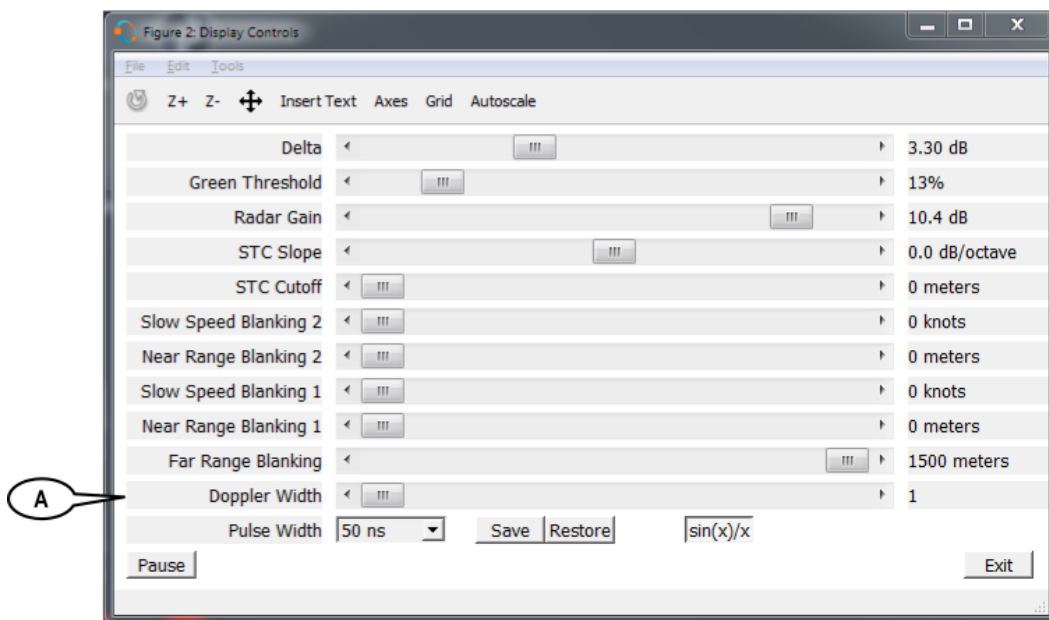
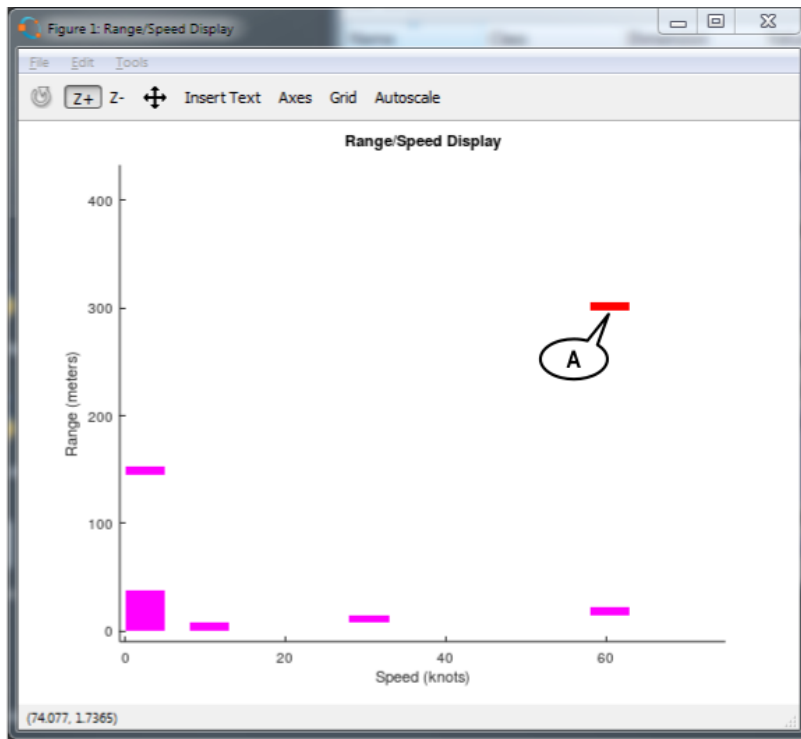


Figure A-26. Doppler width slider59.

#### A.4.5. Radar transmitter pulse width controls

The radar transmitter can output pulses with durations of 50, 100, 200, and 400 nanoseconds. The Pulse Width drop-down menu (A) is used to match the MATLAB script software with the behavior of the hardware.

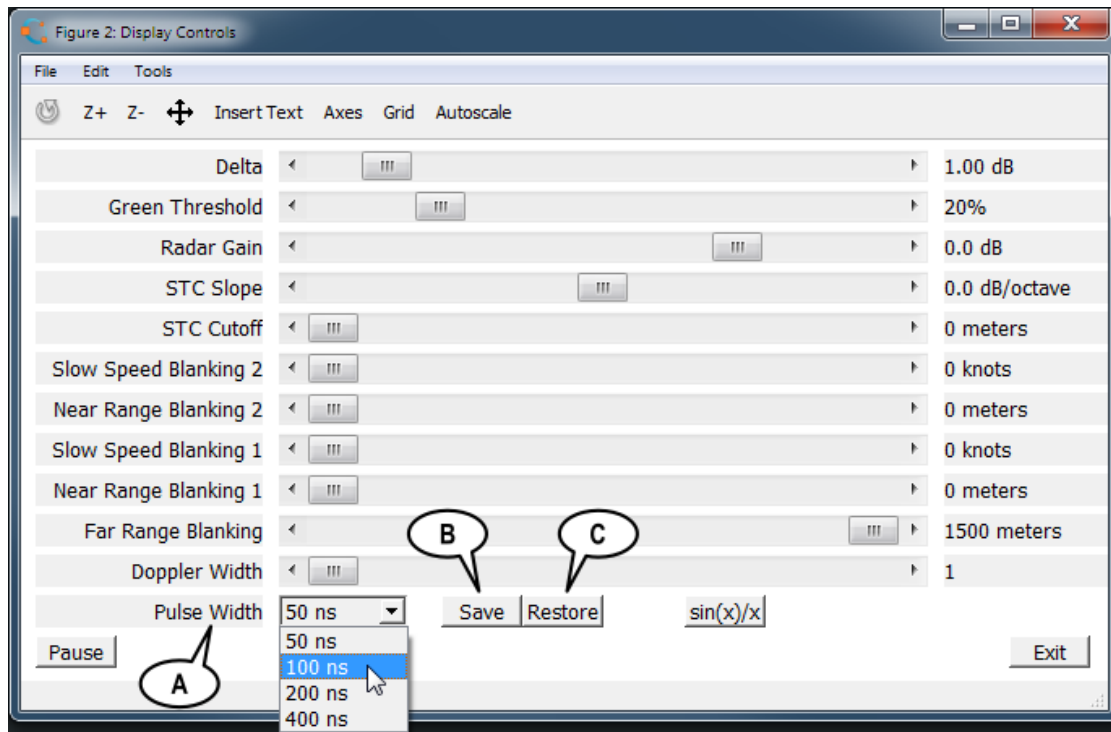


Figure A-27. Radar transmitter pulse width controls

Note: The parameters of the software may need adjustment depending upon the transmitter pulse width, so the save button (b) will save the slider settings for the currently-active pulse width in a file named `ctrl_set_<pulse width>_ns.txt`. The restore button (c) will recall the slider.